GEOPHYSICAL MAPPING OF BURIED RIVER CHANNELS AND OTHER SHALLOW STRUCTURES RECHARGING MAJOR AQUIFERS IN THE LAKE NAKURU BASIN, KENYA RIFT: CASE STUDY FROM KABATINI AQUIFER.

By
AARON WASWA KUTUKHULU
I56/70439/2008

Dissertation submitted in partial fulfilment for the degree of Master of Science in Geology (Applied Geophysics) in the University of Nairobi
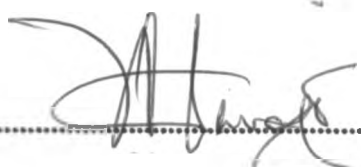
August 2010

DECLARATION

This is my original work and has not been submitted for a degree in any other University.

Signed 6/9/2010

Aaron Waswa Kutukhulu

This dissertation has been submitted for examination with my knowledge as University supervisor

Signed 6/9/2010

Professor Justus O. Barongo

Abstract

The project covered the geophysical mapping of buried river channels and other shallow structures recharging major aquifers in the upper Nakuru basin of Kenya rift and in particular the Kabatini area. The project aimed at unveiling scientific knowledge of the subsurface geology using resistivity and magnetic geophysical methods. It also aims at solving water shortages and improvement of livelihood of the people of Nakuru and its neighbor hood through proper and more precise geophysical ground water exploration methods. The ultimate goal of the report is to provide guidance to policy makers in decision making especially for ground water extraction in Kabatini aquifer. Geology and hydrogeology of the area have been discussed in the report. The methods used in the research and the expected outputs have also been mentioned in the report. These field methods include vertical electrical sounding, electrical resistivity tomography and magnetic survey. Data processing was done using Earth imager software, RES2DINV, and Euler. The findings of the research ascertain that Kabatini area has underground river channel that flows in the north – south direction. The research also shows that the area has some shallow structures which contain low resistivity materials in different locations. It has also been ascertained that the thickness of kabatini aquifer is more than 150 m.

Acknowledgement

I wish to thank my almighty God for the care, knowledge and wisdom He granted me during this research. He is a wonderful God.

I am greatly indebted to Professor Justus Barongo, who constantly followed this work, and for his invaluable advice, encouragement, useful criticisms, and for sparing his time to read this dissertation and suggesting useful comments, and above all his sense of humour and understanding. I also express my profound gratitude to the Chairman of the department of geology and the entire teaching staff for their support during my masters program.

It is with pleasure and gratitude that I thank the University of Nairobi and in particular the Board of post graduate studies to have given me the scholarship for two years. I also appreciate the hospitality and effective services of the staff without singling any, of the Department of Geology at the University of Nairobi. I am grateful to my fellow students and friends who in many ways assisted me during the period of study.

I wish to acknowledge my Parents for their encouragement and prayers. As ever, the major inspiration and encouragement comes from my daughters Miriam, Grace, and Martha, who cannot be thanked adequately. Their encouragement, understanding, and patience, even during hard times, is appreciated.

My God bless whoever participated directly or indirectly to the success of this dissertation.

CONTENTS

List of figures

Tables

CHAPTER ONE

1.0 Introduction

1.1 Background

Buried river channels are increasing becoming the target for groundwater exploration due to the unreliability of surface river channels that have been affected by climate changes. Areas located in urban centers like Nakuru town have high population that dictates the higher demand of water. Nakuru is located in an environmentally sensitive area, sandwiched between Mau escarpment to the south west and the Menengai crater and its associated volcanic landscapes to the north. To the north-east of the town is the Bahati escarpment which forms the western fringe of the Aberdares escarpment. Lake Nakuru is the lowest point in the region, at only 1,758 meters above sea level, and all rivers in the region drain into it. Statistics suggest the population of Nakuru has increased and its municipality expanded tremendously. Large population increase implies a much increased demand for urban services such as water. Increased population has further strained the existing water supply from the available sources. The major economic sectors in Nakuru's urban economy are commerce, industry, tourism, agriculture and tertiary services. The commercial sector in Nakuru contributes about 19 per cent to the economy of the town. In the recent past, the water supply in Nakuru has been characterized by chronic shortages affecting mainly residential and industrial functions. The town has been getting its water from both surface and underground water sources. Current climate changes have made surface water to be unreliable. Surface water in Nakuru basin includes; River Njoro, Larmudiac, Makalia and Enderit (see fig 1.2) which drain from Mau escarpment towards Lake Nakuru. Stream channels give a connotation of ground water flow. The Ngosur River and several minor streams flow from the Bahati forest towards the lake Nakuru, although none of them reaches the lake. The streams that originate from Menengai disappear to become subsurface in the upper slopes of the crater. McCall, 1967 postulated that Ngosur River is controlled by the slope of piedmont –plain bounding the very straight north – west trending Bahati escarpment while other scientist who have worked in this area suggest that buried rivers area controlled by the fault system .This phenomenon of conflicting information regarding disappearance of rivers in Menengai and Bahati plains called for integrated geophysical methods to determine the existence of the river channels in Kabatini area.

Geoelectrical resistivity techniques are popular and successful geophysical exploration for study groundwater conditions in areas with complex geology. The resistivity of material depends on many factors such as groundwater, salinity, saturation, aquifer lithology and porosity. For example, the resistivity of an aquifer is related to Electrical Conductivity (EC) of its water. When the groundwater EC is high, the resistivity of the aquifer could reach the same range as a clayey medium and the resistivity parameter is no longer useful to determine the aquifer (Vouillamoz *et al.*, 2002). However, this method has been carried out successfully for exploration of groundwater. This technique is widely used to determine depth and nature of an alluvium, boundaries and location of an aquifer. The resistivity method has been used to solve more problems of groundwater in the alluvium, karstic and volcanic aquifers as an inexpensive and useful method. Some uses of this method in groundwater are: determination of depth, thickness and boundary of an aquifer (Zohdy, 1969; and Young *et al.* 1998), determination of interface saline water and fresh water (El-Waheidi, 1992; Yechieli, 2000; and Choudhury *et al.*, 2001), porosity of aquifer (Jackson *et al.*, 1978), and water content in aquifer (Kessels*et al.*, 1985), hydraulic conductivity of aquifer (Yadav and Abolfazli, 1998; Troisi *et al.* 2000), transmissivity of aquifer (Kosinski and Kelly, 1981), specific yield of aquifer (Frohlich and Kelly, 1987), contamination of groundwater (Kelly, 1976; and Kaya, 2001). Contamination usually reduces the electrical resistivity of pore water due to increase of the ion concentration (Frohlich and Urish, 2002). However, when resistivity methods are used, limitation can be expected if ground inhomogeneties and anisotropy are present (Matias, 2002). Investigations of the subsurface water channels and other structures using integrated geophysics remain the reliable solution to water shortages in Nakuru area.

1.2 Nakuru Basin

1.2.1 Location

Nakuru basin is located in central part of the Kenya rift valley which forms part of the great rift that passes through Ethiopia, Tanzania, Malawi and then to Uganda. The basin is bounded by longitudes $32^0 21'20''$ on the east $36^0 10'$ on the west and latitudes $0^0 13'15''$ on the north, $0^0 2830'$. The Nairobi – Eldoret and Nairobi Kisumu roads pass through the basin.
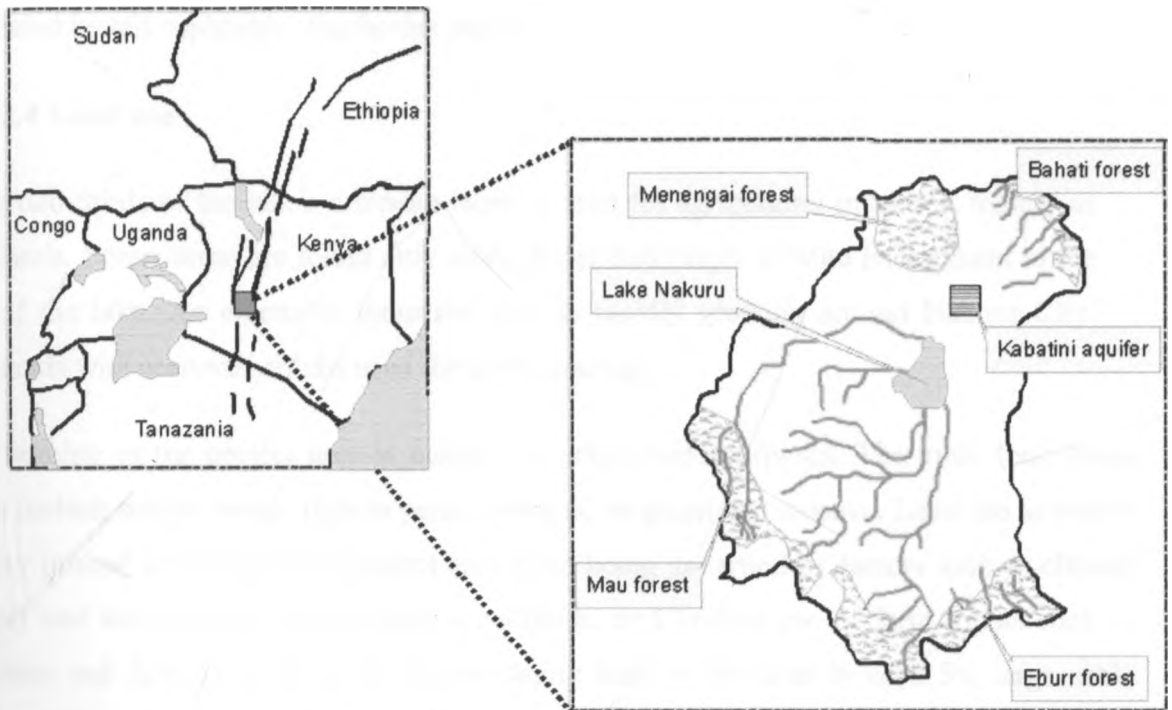
Figure 1.1: Location map for Nakuru Basin in relation to the map of East Africa

1.2.2 Climate

Nakuru basin is generally hot and dry, with two rainy seasons; the long and the short rains. The long rains start at the end of March and continue to the end of May, and the short rains start at the end of October and continue to the end of December. The average rainfall varies from 500 to 1300 mm with high altitude areas receiving more rain. The area is classified as semi-humid to semi-arid. The mean average maximum temperature is 25°C and the average minimum temperature is 12.3°C. The coldest months being July to August, while October and March are the hottest as observed in Agro-climatic Zone Map of Kenya of 1980.

1.2.3 Vegetation

The forested areas of the catchment basin consist of the eastern Mau, northern Eburru, and Bahati forests. The eastern Mau forest forms part of a national watershed (the Mau complex), being the largest of these forest blocks. The vegetation surrounding the lake consists of a narrow belt of fringing forest dominated by *Acacia xanthophloes* , scrub communities on steep cliff encircling the southern part of the lake (in some places dominated by tall euphorbia, *Euphorbis ingens*)

1.2.4 Land use

About two-thirds of the lake's drainage basin is used for agricultural purposes, mainly as rangelands. Forest areas are found only along watershed ridges of Mau Escarpment to the west of the lake. An extensive industrial area is rapidly growing around Nakuru City. Grasslands with scattered shrubs used for cattle grazing.

Crop farming in the project area is mainly for subsistence purposes. The main food crops grown include maize, beans, pigeon peas, cowpeas, sorghum and cassava. Land use activities are very limited and vary in the project area these being governed by factors such as climate (rainfall and temperature), soil conditions, altitude, and limited use of farm inputs such as pesticides and fertilizers. Most of the remaining land in the area is used for large scale commercial ranches (beef and dairy cattle). Dairy and beef cattle populations have increased steadily over the years due to increased local demand from Nakuru town. Other livestock reared in the district include sheep, goats, rabbits, pigs and bees.

1.2.5 Drainage

Nakuru basin lies within the Rift valley floor on the general nprthern slope of the central dome. Lake Nakuru is a basin of internal drainage which is separated from lake Elementaita by a low topographical devide. Lake Nakuru lies in a graben between Isirkon 2097m to the east and Mau escarpment to the west, (Kuria, 1999). The Menengai crater (2280 meters above sea level) on the northern part of the basin and to the south lies the high ground of Mau and Eburr forest. Lake Nakuru is alkaline and saline a result of evaporation and is recharged by rainfall, surface runoff and groundwater. Drainage of the basin is characterized by poor surface runoff caused by existence of highly porous and unsorted pumice rocks. River Njoro, Larmudiac, Makalia and Enderit (see fig.1.2) drain from Mau escarpment towards Lake

Nakuru. The Ngosur river and several minor streams flow from the Bahati forest towards the lake Nakuru, although non of them reaches the lake. The streams that originate from Menengai disappear to become subsurface in the upper slopes of the crater. The drainage in Nakuru basin is controlled by the faults. This is noted by sudden changes in the direction of the water courses which respond to the general orientation of the Rift valley faulting.
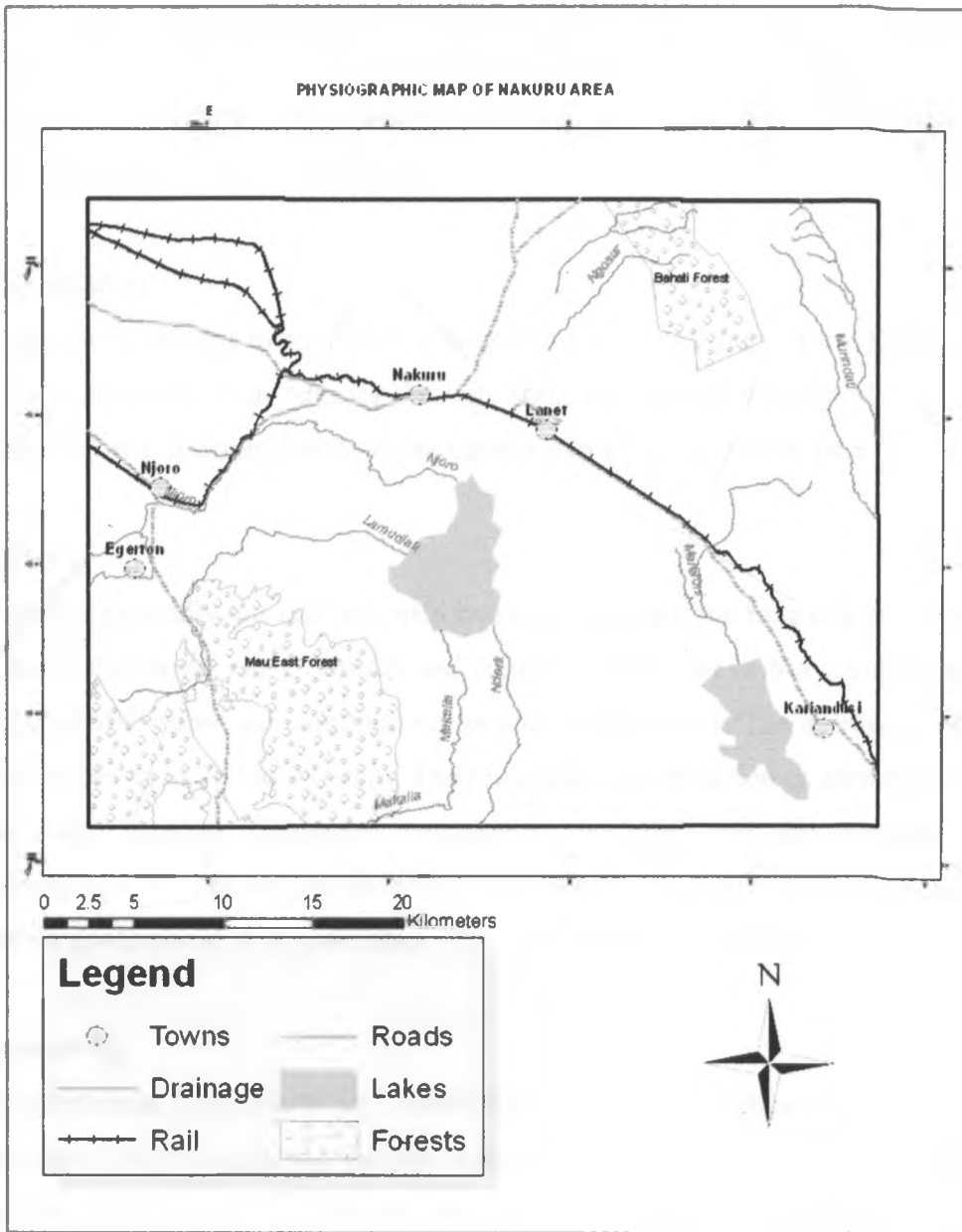
Figure 1.2: The Physiography of the Nakuru basin and its drainage system

1.3 Kabatini Aquifer

1.3.1 Location

The study area lies in Nakuru district of rift valley province in the Republic of Kenya. It is covered by Nakuru topographical map sheet 119/3 of scale 1:50,000. Kabatini aquifer can be located by coordinates S $0^0$15'36.6'/E $36^0$8'00.0" on the sheet 119/3 of Nakuru. It is located on the north eastern part of Nakuru town. Nakuru town can be accessed by a tarmac road and a railway line which forms part Trans Africa railway and road network from Nairobi. Nakuru - Solai tarmac road passes on the western part of the project area. A good earth road connects to Nakuru – Solai road to the project area

1.3.2 Accessibility

Kabatini aquifer is Nakuru town which is found in the central part of the Kenyan rift. The aquifer can be accessed from Nairobi through Solai road which connect Nairobi – Nakuru road in Nakuru town. It occurs on the north eastern part of Nakuru town (see fig 1.3).

1.3.3 Climate

Kabatini area is generally hot and dry, with two rainy seasons; the long and short rains. The long rains start at the end of March and continue to the end of May, and the short rains start at the end of October and continue to the end of December. The average rainfall in the project area varies from 700 to 981 mm. The project area is classified as semi-humid to semi-arid. The mean average maximum temperature is 25°C and the average minimum temperature is 12.3°C. The coldest months being July to August, while October and March are the hottest as observed in Agro-climatic Zone Map of Kenya (1980).

1.3.4 Vegetation

The vegetation found in Kabatini well field consists mainly of indigenous shrubs and grass and exotic trees. The trees planted include *Eucalyptus, Pinus patula, Grevillea robusta* and kei-apples (see fig.1.3a and 1.5). Farmers also find the trees useful as windbreaks, for fencing and, in the long run, for fuel-wood or timber. There have been other motivators for farmers to plant trees. The type of vegetation cover is predominantly of the exotic family since most of the indigenous trees have been destroyed.

6
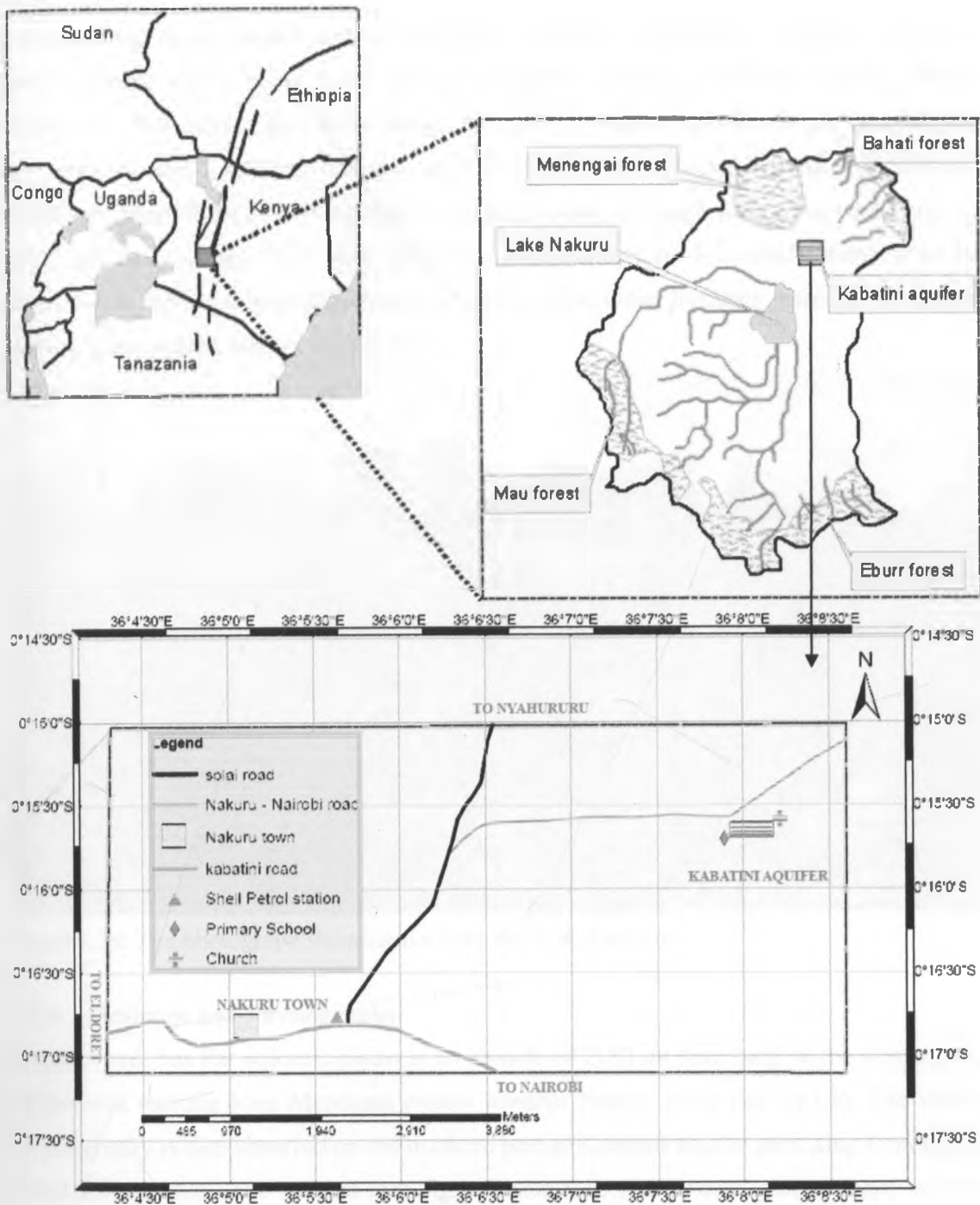
Figure 1.3: location map of Kabatini aquifer north – eastern part of Nakuru town.

1.3.5 Land use

Crop farming in the project area is mainly for subsistence purposes. The main food crops grown include maize, beans, pigeon peas and potatoes. Land use activities are very limited and vary in the project area these being governed by factors such as climate (rainfall and temperature), soil conditions, altitude, and limited use of farm inputs such as pesticides and fertilizers. Most of the remaining land in the area is used for large scale commercial ranches (beef and dairy cattle). Dairy and beef cattle populations have increased steadily over the years due to increased local demand from Nakuru town. Other livestock reared in the district include sheep, goats, rabbits, pigs and bees.

Figure1.3a: The photograph showing the land use in Kabatini area

1.3.6 Drainage and Physiography

Kabatini area has flat volcanic plains at an altitude of 2180 mt stretching on the western part of the area running from Menengai creator towards Nakuru town (see fig1.5). The similar Physiography is also observed on the northern part of Kabatini aquifer stretching from Bahati forest towards the Lake Nakuru (see fig.1. 2 and 1.7), and a more gently sloppy country formed by the volcanic rocks system varying from 1837 m to 2040 m on the southern part of the project area. Generally Kabatini area is characterized by rolling terrain, with a notable Menengai crater on the north western part (see fig 1.8). The terrain can be described as generally flat to rolling; the highlands being the Menengai crater and Bahati escarpment.There are two rivers in the northern part of Kabatini aquifer. These rivers are

river Ngosur and Menengai River. Menengai River flows towards the Menengai crater where it disappears underground. Ngosur River flows in the south west direction and disappears underground in Bahati plains.

Figure 1.4: The photograph of general Physiography of Kabatini area, see Bahati hills in the background. The photograph is taken facing in the Northern direction.

Figure1.5 The photograph shows the general Physiography of the project area, see Menengai crater at the background. The photograph was taken facing north western direction.

Figure 1.6 Vegetation (Grevillea robusta trees) in project area, the photograph was taken facing towards the south of the project area
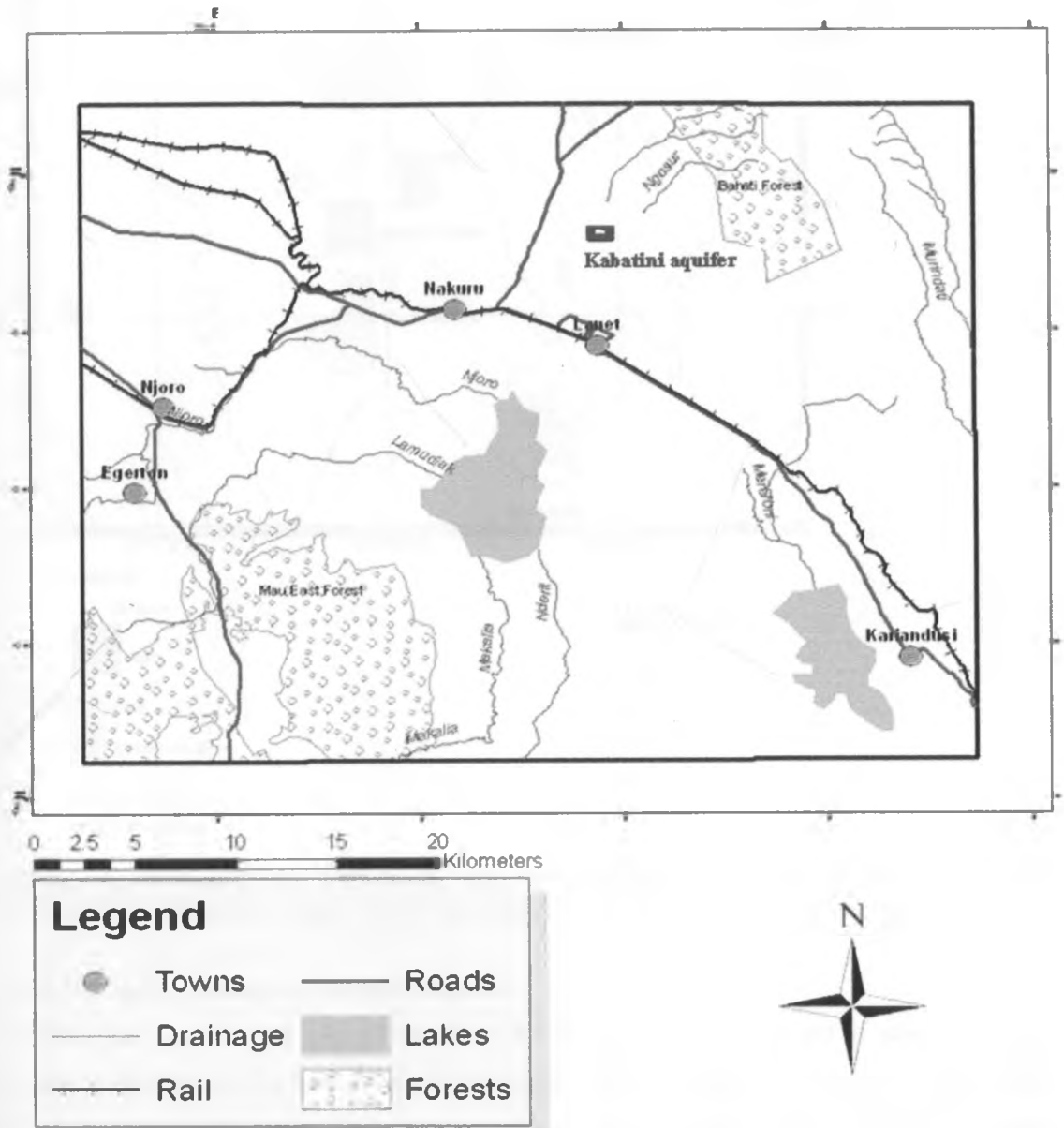
Figure 1.7 Drainage map of Nakuru basin.
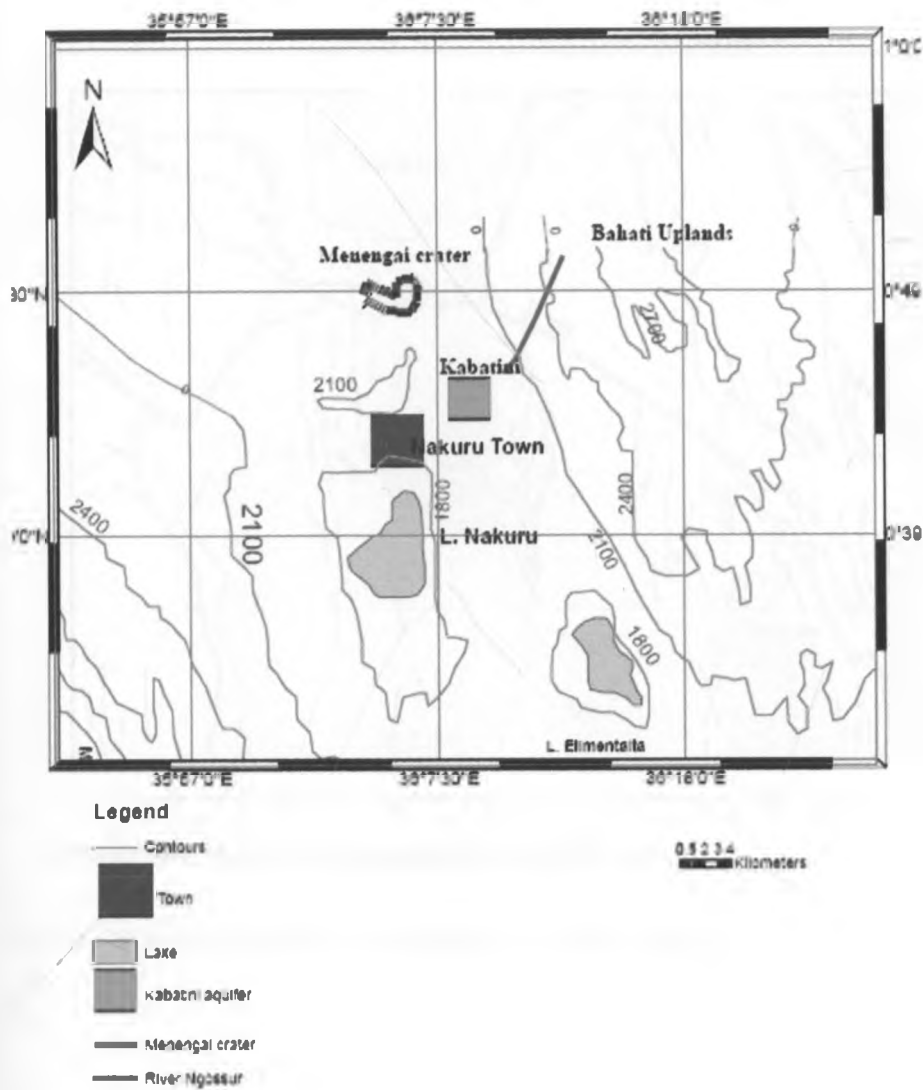
Figure 1.8 Physiographical map of the area surrounding Kabatini aquifer in Nakuru basin. The contours are seen to decrease towards the Lake Nakuru.

1.3.7 Geological setting of Kabatini aquifer

Kabatini has complex geological structures which have been subjected to several tectonic processes leading to the formation of varying structural features. To northern side occurs Menengai crater while to Bahati uplands occurs on the eastern part. The area is mainly occupied by volcanic rocks which consist of Vitric pumice tuff, ashes, agglomerates and trachytes. The lake beds on the southern part of the area are composed mainly of volcanic material and subsequently deposited pyroclastics. The sediments are composed of sand, pebbles as well as gravels made up of rounded pumice, (MacCall, 1967).

11
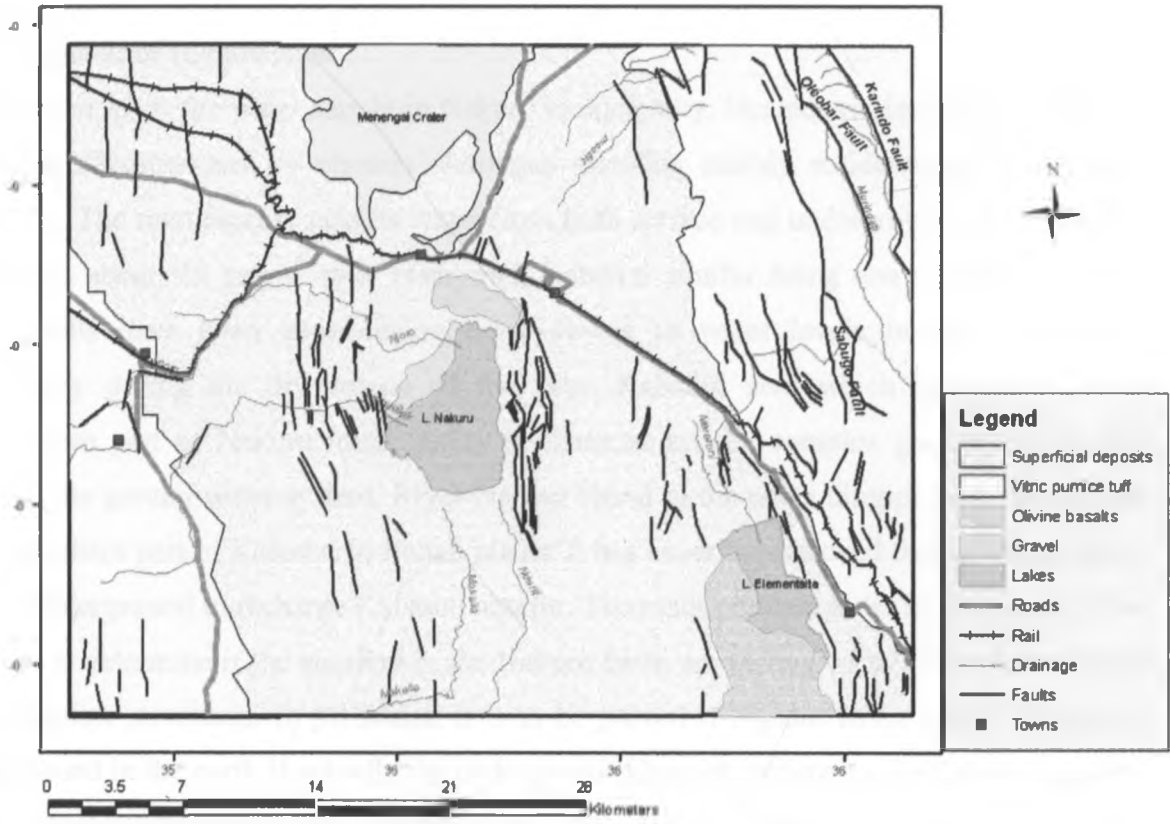
Figure 1.9: Geological and structural map of Nakuru basin

1.4 Statement of the problem

In the recent past, the water supply in Nakuru municipality, located within the Nakuru basin, has been characterized by chronic shortages affecting mainly residential and industrial functions. The municipality gets its water from both surface and underground water sources, and it has about six major water reservoirs, Kabatini aquifer being one of them. Kabatini water wells have been experiencing draw downs in water levels in the recent past, particularly during the dry season of the year. Kabatini area which is located in the northeastern part of Nakuru municipality is characterized by complex geology which has affected the ground water system. River Ngosur found to the north disappears in the ground in the northern part of Kabatini in Bahati plains. It has never been proved that the river cannel passes underground to recharge Kabatini aquifer. The main problem to be investigated in this study is to determine if the aquifers in the Nakuru basin are recharged by river channels and other shallow structures. In particular, it is to be proved if Ngosur River which disappears underground in the north is actually the underground channel recharging the Kabatini aquifer. The geological condition in the Kabatini area is complex and intricately related to the nature of the groundwater regime, a fact that could be attributed to the difficulty to fully assess the aquifer with the conventional hydrogeological methods alone. The entire area is covered by volcano-sedimentary materials, intercalated lava flows. The exact distribution and depth of the lava has not been mapped.

1.5. Aim of the research and its objective

The aim of this research is to map the buried river channels and other structures that sustain constant recharge of the main aquifers in the Nakuru basin using geophysics.

The objectives of this research are;

1. To delineate the geometry of any river channel(s) and other structures contributing to the recharge of the aquifers in Nakuru basin with the main focus on Kabatini.

2. To determine the depths of the Kabatini aquifer and relate it to the number of channels/structures recharging it.

1.6 Justification and significance of the research

Groundwater becomes the readily available option for exploitation in areas where surface water shortages exist like the Nakuru basin. However, the over-exploitation of this resource has moved groundwater research to the forefront of the geosciences in trying to answer the questions of groundwater recharge and discharge in aquifers. These questions become increasingly relevant as we continue to test the limits of groundwater resource sustainability in areas of complex geology like Kabatini area. Whereas other researchers have worked in the area, none of them has addressed the existence or non - existence of the buried river channels and other shallow underground structures that may be controlling groundwater flow systems. The structures such as faults may form channels through which water flow and recharge the aquifer. Geophysical methods are used to obtain accurate information about subsurface structures like faults and buried river channels. The marginal rift faulting and the system of grid faulting on the Rift floor have a substantial effect on the groundwater flow systems of the area. In general faults are considered to have effects on groundwater flow. They may facilitate flow by providing channels of high permeability, or they may prove to be barriers to flow by offsetting zones of relatively high permeability. The methods used have proved to be efficient tools in groundwater exploration. Not only have they been used in the direct detection of the presence of water but also in the estimation of aquifer size, properties and mapping of buried valleys and rivers even in areas of complex geology for direct drilling . The cost of drilling large-scale water-supply boreholes like in the Kabatini area almost demands that the risk of drilling a poorly yielding borehole should be lessened through the proper use of geophysics. The results in this research will be used to identify potential drilling locations, decreasing the risk of drilling in unproductive areas that may waste the resources. This complex nature of the geology and the groundwater system in the upper Nakuru basin makes a detailed and a systematic geophysical study, the appropriate alternative, as the conventional hydrological approach so far has proved its inability to exhaustively deal with the problem alone. Geophysical mapping in the area consists of Electrical Resistivity Imaging, Vertical Electrical Sounding and Proton Precession Magnetic Survey. These methods are bound to reveal aspects that were not known in the project area.

Geophysical mapping of buried rivers and other underground structures is one of the tools that will readily present conceptualized real-life situations and therefore provide quick answers to some of the questions that policymakers, researchers, environmentalists, investors and other relevant authorities require before they make sound decisions within Nakuru and elsewhere in the world.

CHAPTER TWO

2.0 Literature Review

2.1 Geology and structures

Review of the previous geological and structural work was undertaken in order to understand the origin of Kabatini aquifer. The terrain under study is part of a section of the central Kenya Rift Valley. The rift Valley is a Cainozoic intercontinental rift system separating the Somalia sub – plate from the rest of Africa (Smith and Mosley, 1993). The Rift valley system has a north – south geographic trend delineated by faults with individual faults oriented at diverse angles (Onywere, 1997). Step scarps mark flanks along fault lines, while the intervening smaller faults are places marked by low, narrow hoist graben structures (Baker et al., 1972). Part of the Rift valley in the study area is bordered on the eastern shoulder by an abrupt topographic break, which is a surface trace of the rift bounding Sattima fault. Mau escarpment forms the boundary of the basin on the western shoulder. The Kabatini aquifer lies on the north eastern part of the Nakuru basin within the Kenya rift Valley. The geology of the area consists of volcanic rocks which include basalts, phonolites, tuffs, and trachytes. Rocks and structures within the rift valley where the project area is located have been generated during the past 4 million years, (Clarke et al 1990). They are associated with the full graben and inner trough stages of the development of the rift valley. The Rift margins expose an older sequence of trachytic, often ignimbritic, pyroclastics (the Mau and Kinangop Tuff formations to the west and east respectively), and a younger thick sequence of trachytic flood lavas. Subsequent faulting produced the stepped escarpment which has an effect on the drainage pattern and groundwater flow. Lake sediments form a large part of the floor of the rift and are exposed in gullies, road sections and small quarries. Sand and pebble beds dominate exposures of lake sediments around the northern side of the Olkaria Volcanic Complex. Deposition in a high energy, possibly fluvial, environment is indicated by well-bedded sand dominated sequences which show large-scale cross-bedding and channel development.

Table 2.1 Main stages of Kenya rift valley development, (Clarke et al 1990)

STAGE	PRE-RIFT DEPRESSION	HALF GRABEN	FULL GRABEN	INNER TROUGH
AGE TECTONIC STYLE	25-12 Ma Bp Broad shallow depressions (warping) in the Turkana region	12-4Ma Faulting in western part of Turkana, extending S-wards by 7 Ma	4-1.7Ma Commencement of faulting on Eastern side of rift. Grid faulting.	1.7-0Ma Deepening of axial zone of rift. Extensional tectonics in narrow zones.
VOLCANISM	Alkali Basalts and basanites erupted over wide areas in the north. Carbonatite-nephelinite volcanism in west Kenya and the southern rift, especially on the south and west flanks of the Kenya Dome.	Alkali basalts and flood phonolites e.g. Uasin-gishu and Yatta plateau, then transitional basalts and Basalts/Trachyte shield volcanoes having marked Daly gaps.	Basalt/Trachyte volcanism in central sector characterized by very large pyroclastics eruptions. Basalts less but Trachytes very widespread in south and extending east over Nairobi area mainly.	Eruption of flood Trachytes followed by grid faulting(<0.8 Ma). Building of a chain of dominantly Trachytic caldera volcanoes with alkali-rhyolite prominent in the central sector.
SUMMARY	BASALT and NEPHELINITE	PHONOLITE. BASALT and TRACHYTE.	TRACHYTE often as large as large ash flows	TRACHYTE and BASALT in north. TRACHYTE, RHOYOLITE and minor BASALT in south.

Bahati area is composed of well-rounded gravel and pebble-sized pumice and other pyroclastic material which form the aquifer in that area. Many of the gullies that have dissected parts of the rift floor have smooth floors as a result of the deposition of alluvial sediments. Renewed down cutting in gullies on River Njoro in Nakuru has revealed that these alluvial deposits are dominated by sand and gravel in the Basin.
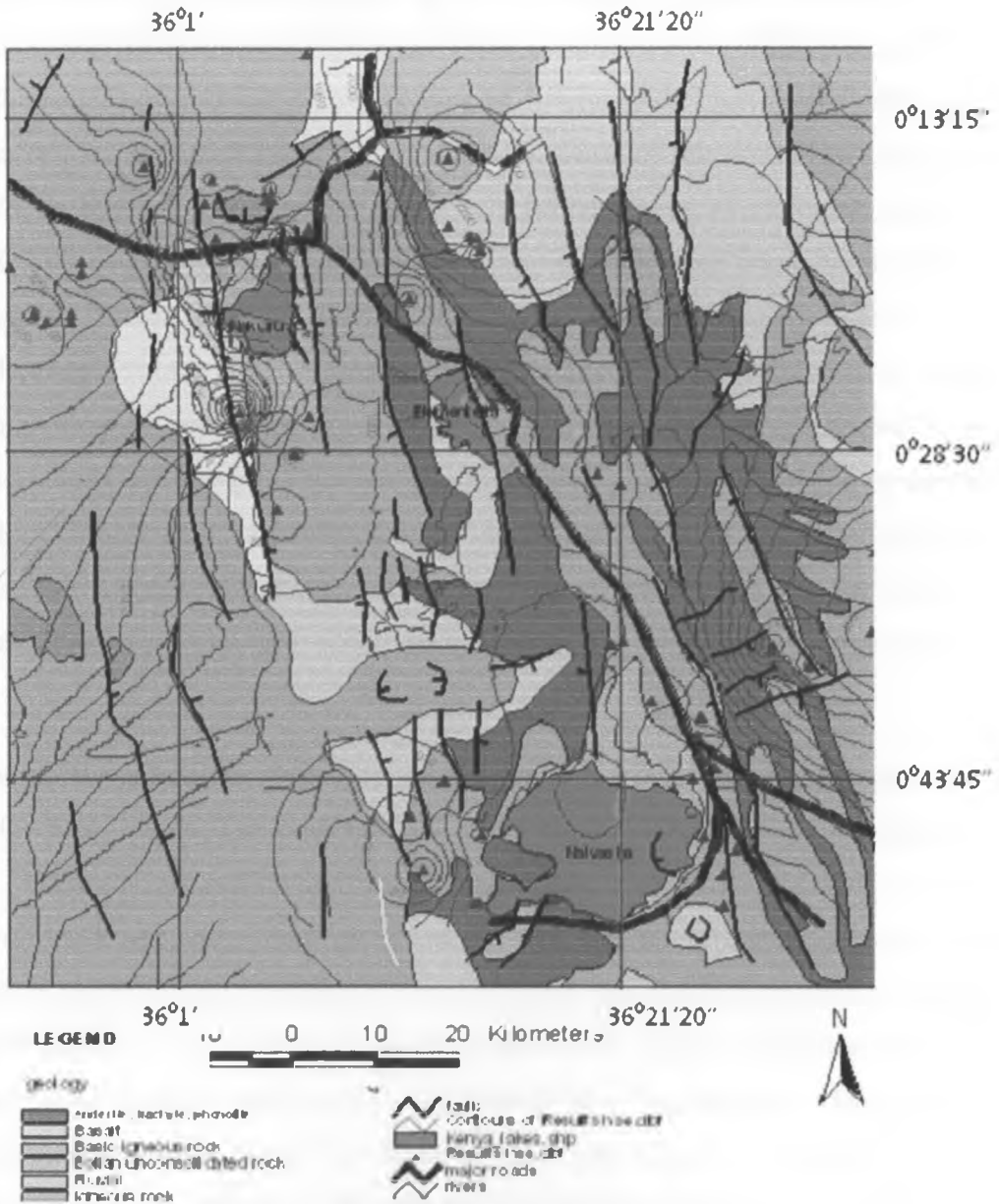
Figure 2.1: Geology and faults in the rift from Clarke, *et al* 1990.

17

2.2 Geophysics

There have been some geophysical studies in the past in the area on geothermal prospects. These include regional gravity, aeromagnetic and resistivity soundings. Airborne Magnetic survey data can provide vital information about regional structural features such as faults, intrusions and basement rocks (that can be associated with an aquifer). The distribution of magnetic properties in rocks can also give rise to a complex magnetic anomaly pattern or signature which may be associated with a particular assemblage of rocks. This pattern may differ from the pattern over an adjacent rock type of different lithology in amplitude level, in number of anomalies and in shape of the anomalies. Criteria of this sort allow many hidden boundaries to be mapped out between often only limited areas of exposure suitable for conventional field mapping. Magnetic data covering the study area come from part of the African Database, Pastor, (2001). Barritt, 1993, contains the original source of African Magnetic Mapping Project (AMMP) results. The database is a compilation of regional magnetic anomalies of several African countries that have been re-processed (upward continued to 1000m) and merged together. The magnetic field intensity of the study area is 34000 nT, at an inclination of approximately $-5°$ and a declination of $-1°$. The first presents the gross magnetic intensity differences caused by different rock types like the mafic rocks like the basalt outcrops and the felsic counterparts like the trachytes, rhyolites and pyroclastics.

Measurement of the electrical resistivity of the earth has been a tool for groundwater exploration for many years. The conventional direct current (DC) surveys are designed to discriminate between anomalies reflecting subsurface electrical resistivity contrasts associated with lithologic and hydrologic characteristics. The interpretation of the resistivity sounding data is usually made assuming a stratified earth and can only provide the apparent resistivity parameters of a horizontally layered model with limited resolution (Keller and Frischknecht, 1966). Spatial variations of earth materials or topographic effects, however, invalidate such assumptions. Some DC Schlumberger soundings were carried out in the north-eastern part of Lake Nakuru in the past by organizations like the Kenyan Ministry of irrigation and Water services, Ministry of Energy, Kenya and Groundwater Survey (Kenya) Ltd, a consulting company. Some of the data collected by the Ministry of irrigation and water services obtained from their archives. The location of the soundings is not indicated precisely except for some relative locations, and more so, the quality of most of data was low and therefore cannot be used for location of the fault, aquifer boundary, River Ngosur which

disappears from the surface river channel in Bahati plains in the north and any other serious study. The causes of irregularities in DC resistivity data could be due to several factors such as; faults or abrupt lateral changes in properties, faulty equipment and current leakage. Therefore exact location and azimuth of a DC Sounding survey of River Ngosur is of paramount importance in this research.

2.3 Hydrogeology

The Kabatini area is hydro-geologically complex due to the rift floor geometry and tectonics (Clarke et al., 1990). The volcanic ash with lapili forms the main aquifer in the area. The superficial deposits are made of variable materials, including clay, fine sand, cemented sand, pebbles and gravels of trachyte and pumice, pyroclastics (Kuria,1999). Groundwater is encountered at depths of 57-60m below-ground-level in the boreholes drilled in the Kabatini aquifer by Nakuru water and Sewerage Company. Recharge of the aquifer is postulated to be River Ngosur found in the north eastern part of the Kabatini aquifer. The information supporting this ideology is not available. McCall, 1967 states that River Ngosur disappears underground in Bahati plains to feed the water table under Lake Nakuru. He further states that the course of this river is controlled by the slope of piedmont-plain bounding the very straight north – west trending Bahati escarpment. The overall surface geometry of the rift valley in the project area is in the form of a wide trough (drainage basin) Kuria, 1999. Piezometric map (fig 2.3) shows that ground water flow from elevated areas to low lying discharge areas.

In general, the permeability of rocks in the rift valley is low, although there is considerable local variation. Aquifers are normally found in fractured volcanics, or along the weathered contacts between different lithological units. These aquifers are confined or semi confined and storage coefficients are likely to vary. In addition, aquifers with relatively high permeability are found in sediments. Values of more than 10,000m^3/day have been derived from pumping tests (Becht, *et al.*, 2005). Tectonic movements of the rift valley have important effects on aquifer properties, both on a small scale by creating the local fracture systems which comprise many aquifers, and on large scale by forming regional hydraulic barriers or shatter zones of enhanced permeability (Nabidi, 2002). The study area has a total of 8 eight productive boreholes which supply water to Nakuru municipality (see fig. 4.2).

2.4 Groundwater flow systems

The marginal rift faults and the system of grid faulting on the Rift floor have a substantial effect on the groundwater flow systems of the area. In general faults are considered to have two effects on fluid flow. They may facilitate flow by providing channels of high permeability, or they may prove to be barriers to flow by offsetting zones of relatively high permeability. The hydraulic role of faults is a subject which is poorly understood because there is often little direct evidence that a particular fault behaves in a particular way. In the rift valley, the main direction of faulting is along the axis of the rift (N-S), and this has a significant effect on flows across the rift (fig 2.2). It is apparent from the high hydraulic gradients which are developed across the rift escarpment that the effect of the major faults is to act as zones of low permeability, Kuria, 1999. This is caused by displaced fault lines that occurred during the rapid occurrence of the faults hence filling water pores. This is particularly true of the Bahati escarpment where river Ngosur originates.
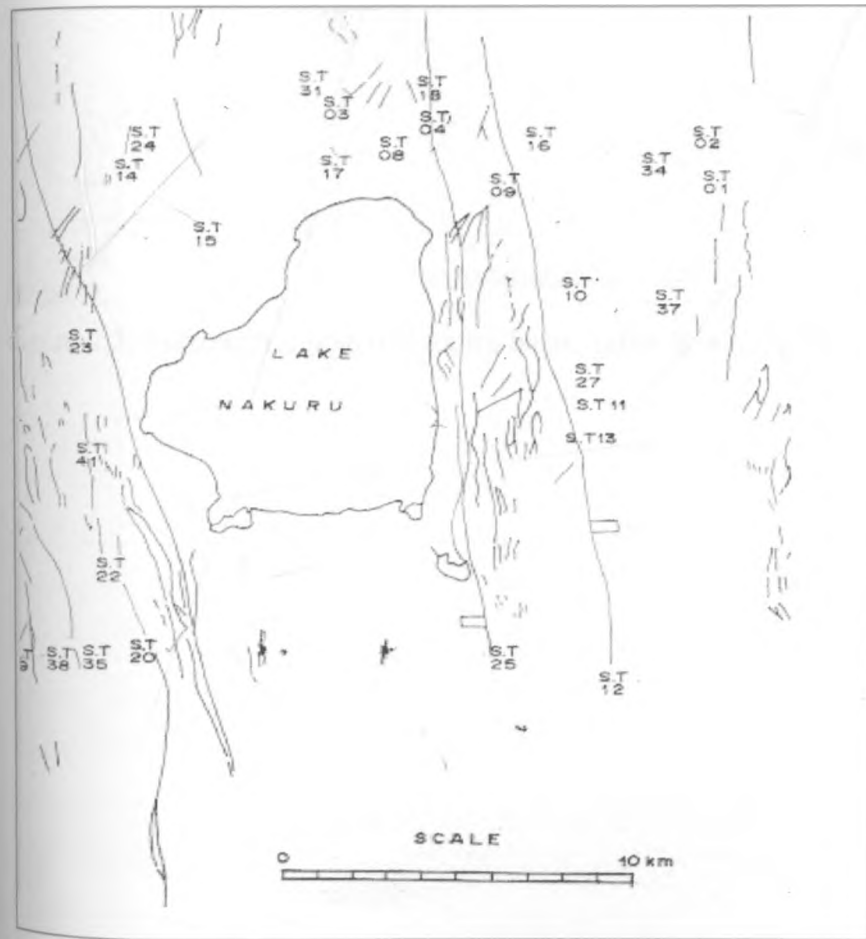
Figure 2.2: The map showing geological structures according to Kuria, 1999
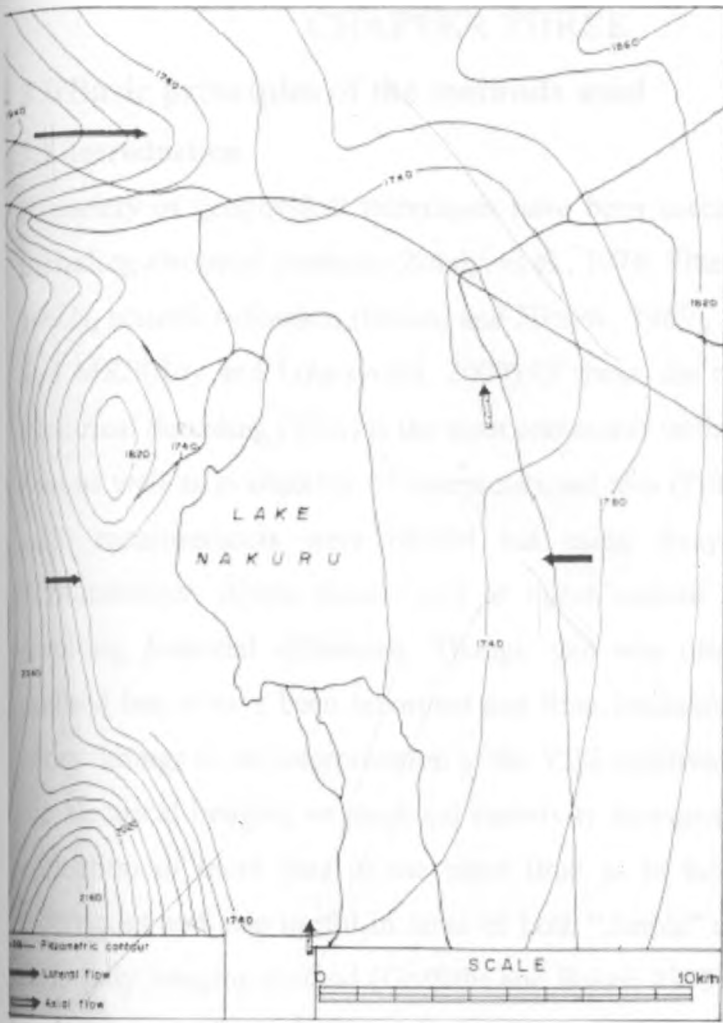
Figure 2.3: Piezometric map of Nakuru basin, (after Kuria, 1999)

CHAPTER THREE

3.0 Basic principles of the methods used

3.1 Introduction

A variety of geophysical techniques have been successfully used for groundwater studies, including electrical methods (Zohdy, et al., 1974; Fitterman and Stewart, 1986; Taylor, et al., 1992), seismic refraction (Bonini and Hickok, 1969), gravity (Carmichael and Henry, 1977) and MRS(Roy and Lubczynski, 2000).Of these, the electrical method (particularly Vertical Electrical Sounding (VES) is the most commonly utilized because of its user friendliness, low cost as well as availability of interpretational aids (Fitterman and Stewart, 1986). In the past, such measurements were carried out using arrays of grounded electrodes (Wenner, Schlumberger, dipole-dipole, etc) to inject current into the ground and to measure the resulting potential difference. Though this was often successful, the conventional VES method has always been laborious and time consuming. Addressing these issues and other shortcomings in the interpretation of the VES resistivity data led to the recent development of the electrical imaging or electrical resistivity tomography technique (ERT). It allows for the collection of more data in the same time as in the "traditional" profiling and sounding techniques and also useful in areas of both "simple" and "complex" geology. The electrical resistivity imaging method (Griffiths and Baker, 1993) differs from the VES survey in using a multi-electrode array system and in recording the maximum number of independent measurements on the array (Michel, et al. 1999).

Geoelectrical resistivity techniques, has been extensively used for a wide variety of geotechnical and groundwater exploration problems (Zohdy, 1969; Bernard and Valla, 1991; Nowroozi *et al.*, 1999; Mousa, 2003, Ibrahim, *et al.*, 2004; Youssef, *et al.*, 2004; Al-Abaseiry *et al.*, 2005; Hosny, *et al.*, 2005; Alotaibi and Al-Amri, 2007; Nigm, *et al.*, 2008). This is due to the fact that, the electrical resistivity survey is one of the simplest and less costly geophysical surveys employed. Moreover, it can be used either in the form of vertical electrical soundings (VES's) or horizontal profiling to search for groundwater in both porous and fissured media (Barker, 1980; Van Overmeeren, 1989; Abd El-Rahman, A. and Khaled, M.A., 2005).

In the present study geo-electric resistivity field survey was carried out by applying the vertical electrical sounding (VES) technique which measures the electrical resistivity

variation with depth. It is worth mentioning here that the electric resistivity of a rock formation varies according to the rock nature of material (density, porosity, pore size and shape), water content and its quality and temperature. Hence, there are no sharp limits for electric resistivity of porous formations. The resistivity is more controlled by the water contents and its quality within the matrix of the formation than by the solid granular resistivity value itself. Therefore, the geological unit may be subdivided into different geoelectrical units according to the different percentage of humidity within it, (Parasnis, 1997).

3.2 Basic theory of electrical resistivity method

The fundamental physical law used in resistivity surveys is Ohm's Law that governs the flow of current in the ground. The equation for Ohm's Law in vector form for current flow in a continuous medium is given by

$$J = \sigma E \tag{3.0}$$

Where σ is the conductivity of the medium, J is the current density and E is the electric field intensity. In practice, what is measured is the electric field potential. We note that in geophysical surveys the medium resistivity ρ, which is equals to the reciprocal of the conductivity ($\rho = 1/\sigma$), is more commonly used. The relationship between the electric potential and the field intensity is given by

$$E = -\nabla \phi \tag{3.1}$$

Combining equations (3.0) and (3.1), we get

$$J = -\sigma \nabla \phi \tag{3.2}$$

In almost all surveys, the current sources are in the form of point sources. In this case, over an elemental volume ΔV surrounding the a current source I, located at (xs,ys,zs) the relationship between the current density and the current (Dey and Morrison 1979a) is given by ;

$$\nabla . J = \left(\frac{I}{\Delta V}\right) \delta(x - xs)\delta(y - ys)\delta(z - zs) \tag{3.3}$$

Where δ is the Dirac delta function, Equation (3) can then be written as

$$-\nabla . [\sigma(x,y,z)\nabla \Phi(x,y,z)] = \left(\frac{I}{\Delta V}\right) \delta(x - xs)\delta(y - ys)\delta(z - zs) \tag{3.4}$$

This is the basic equation that gives the potential distribution in the ground due to a point current source. A large number of techniques have been developed to solve this equation. This is the "forward" modeling problem that determines the potential that would be observed over a given subsurface structure. Fully analytical methods have been used for simple cases, such as a sphere in a homogenous medium or a vertical fault between two areas each with a constant resistivity. For an arbitrary resistivity distribution, numerical techniques are more commonly used. For the 1-D case, where the subsurface is restricted to a number of horizontal layers, the linear filter method is commonly used (Koefoed, 1979). For 2-D and 3-D cases, the finite-difference and finite-element methods are the most versatile. We consider the simplest case of a homogeneous subsurface and a single point current source on the ground surface (Figure 3.1). In this case, the current flows radially away from the source, and the potential varies inversely with distance from the current source. The equipotential surfaces have a hemisphere shape, and the current flow is perpendicular to the equipotential surface. The potential in this case is given by

$$\Phi = \frac{\rho I}{2\pi r} \qquad (3.5)$$

where r is the distance of a point in the medium (including the ground surface) from the electrode. In practice, all resistivity surveys use at least two current electrodes, a positive current and a negative current source. Figure 3.2 show the potential distribution caused by a pair of electrodes. The potential values have a symmetrical pattern about the vertical place at the mid-point between the two electrodes. The potential value in the medium from such a pair is given by

$$\Phi = \rho I/2\pi \left(\frac{1}{rc_1} - \frac{1}{rc_2} \right) \qquad (3.6)$$

where rc_1 and rc_2 are distances of the point from the first and second current electrodes.

In practically all surveys, the potential difference between two points (normally on the ground surface) is measured. A typical arrangement with 4 electrodes is shown in Figure 3.3. The potential difference is then given by

$$\Delta\Phi = \frac{\rho}{2\pi} \left(\frac{1}{rc_1p_1} - \frac{1}{rc_2p_1} - \frac{1}{rc_1p_2} + \frac{1}{rc_2p_2} \right) \qquad (3.7)$$

The above equation gives the potential that would be measured over a homogenous half space with a 4 electrodes array. Actual field surveys are invariably conducted over an inhomogenous medium where the subsurface resistivity has a 3-D distribution. The resistivity measurements are still made by injecting current into the ground through the two current electrodes (C_1 and C_2 in Figure 3.4), and measuring the resulting voltage difference at two potential electrodes (P_1 and P_2). From the current (I) and potential ($\Delta\Phi$) values, an apparent resistivity (ρa) value is calculated.

$$\rho a = k \, \frac{\Delta\phi}{I} \tag{3.8}$$

$$\text{where} \quad k = \frac{2\pi}{\left(\dfrac{1}{r_{C_1 P_1}} - \dfrac{1}{r_{C_2 P_1}} - \dfrac{1}{r_{C_1 P_2}} + \dfrac{1}{r_{C_2 P_2}}\right)} \tag{3.9}$$

k is a geometric factor that depends on the arrangement of the four electrodes. Resistivity measuring instruments normally give a resistance value $R = \Delta\phi/I$, so in practice the apparent resistivity value is calculated by

$$\rho a = kR \tag{3.10}$$

The calculated resistivity value is not the true resistivity of the subsurface, but an "apparent" value that is the resistivity of a homogeneous ground that will give the same resistance value for the same electrode arrangement. The relationship between the "apparent" resistivity and the "true" resistivity is a complex relationship. To determine the true subsurface resistivity from the apparent resistivity values is the "inversion" problem. Different patterns of electrode arrangement can be used during the survey. Some of these patterns are shown in fig 3.5.
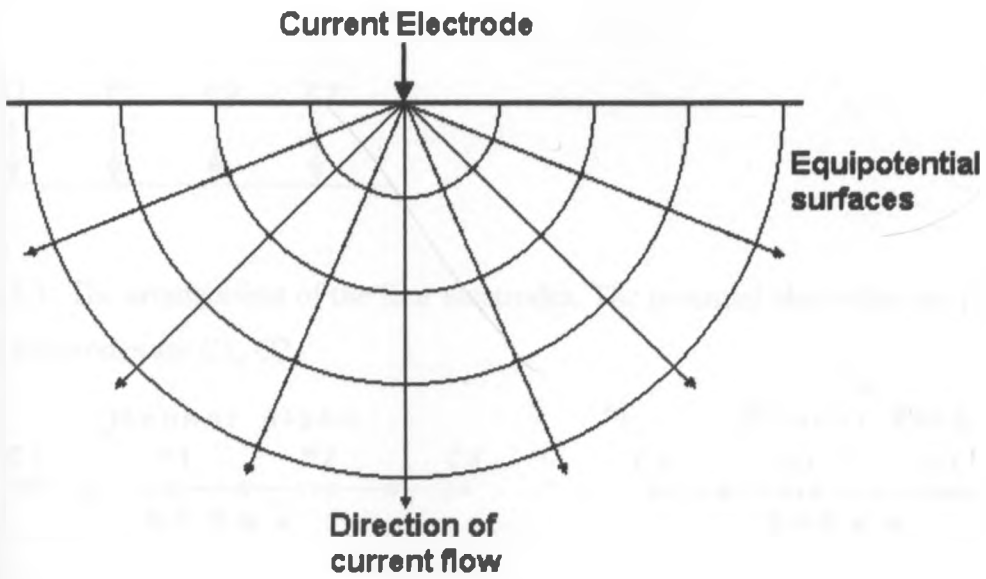
Figure 3.1: Single current electrode in homogeneous ground showing equipotential surfaces and current direction
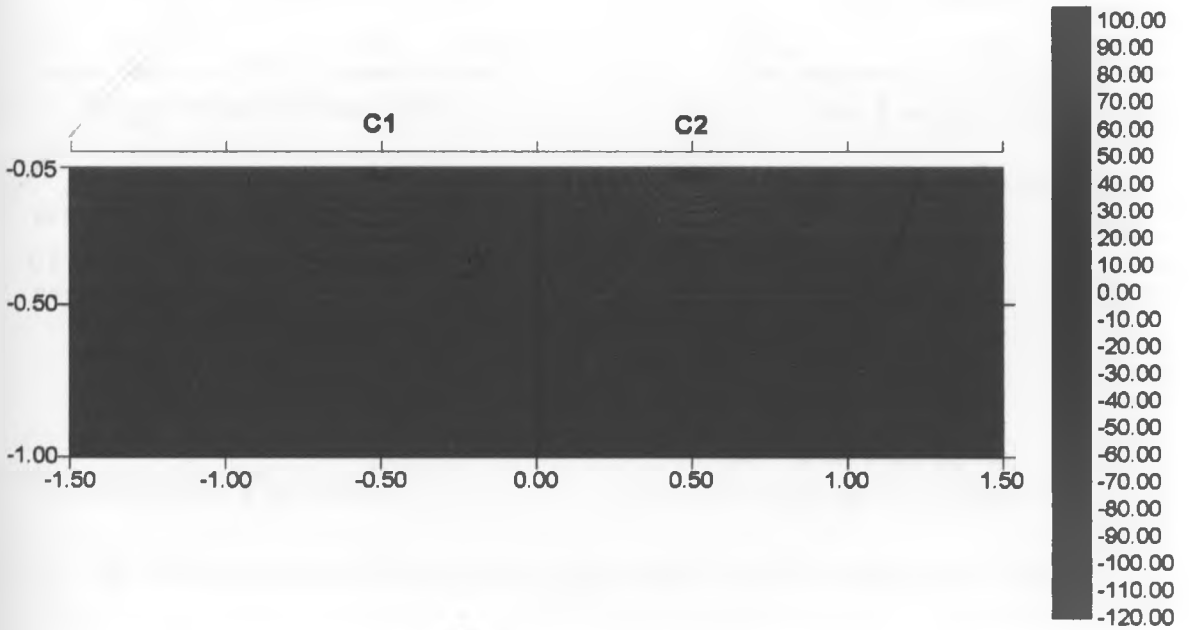
Figure 3.2: Two current electrodes in homogeneous ground showing potential distribution

```
C1      P1      P2      C2
 |       |       |       |
 v       v       v       v
_____
```
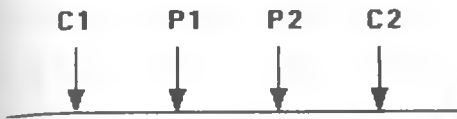
Figure 3.3: The arrangement of the four electrodes. The potential electrodes are P1, P2 while current electrodes are C1, C2.

a).

Wenner Alpha

C1   P1   P2   C2
•←—a—→•←—a—→•←—a—→•
$k = 2 \pi a$

b).

Wenner Beta

C2   C1   P1   P2
•←—a—→•←—a—→•←—a—→•
$k = 6 \pi a$

c).

Wenner Gamma

C1   P1   C2   P2
•←—a—→•←—a—→•←—a—→•
$k = 3 \pi a$

d).

Pole - Pole

C1   P1
•←—a—→•
$k = 2 \pi a$

e).

Dipole - Dipole

C2   C1   P1   P2
•←a→•←———na———→•←a→•
$k = \pi n(n+1)(n+2) a$

f).

Pole - Dipole

C1   P1   P2
•←———na———→•←a→•
$k = 2 \pi n(n+1) a$

g).

Wenner - Schlumberger

C1   P1   P2   C2
•←——na——→•←a→•←——na——→•
$k = \pi n(n+1) a$

h).

Equatorial Dipole - Dipole

C2   P2
 ↑   b   ↑
 a ←———————na———————→ a
 ↓   ↓
 •   •
C1   P1

$b = na$
$k = 2 \pi b L / (L - b)$
$L = (a * a + b * b)^{0.5}$

k = Geometric Factor
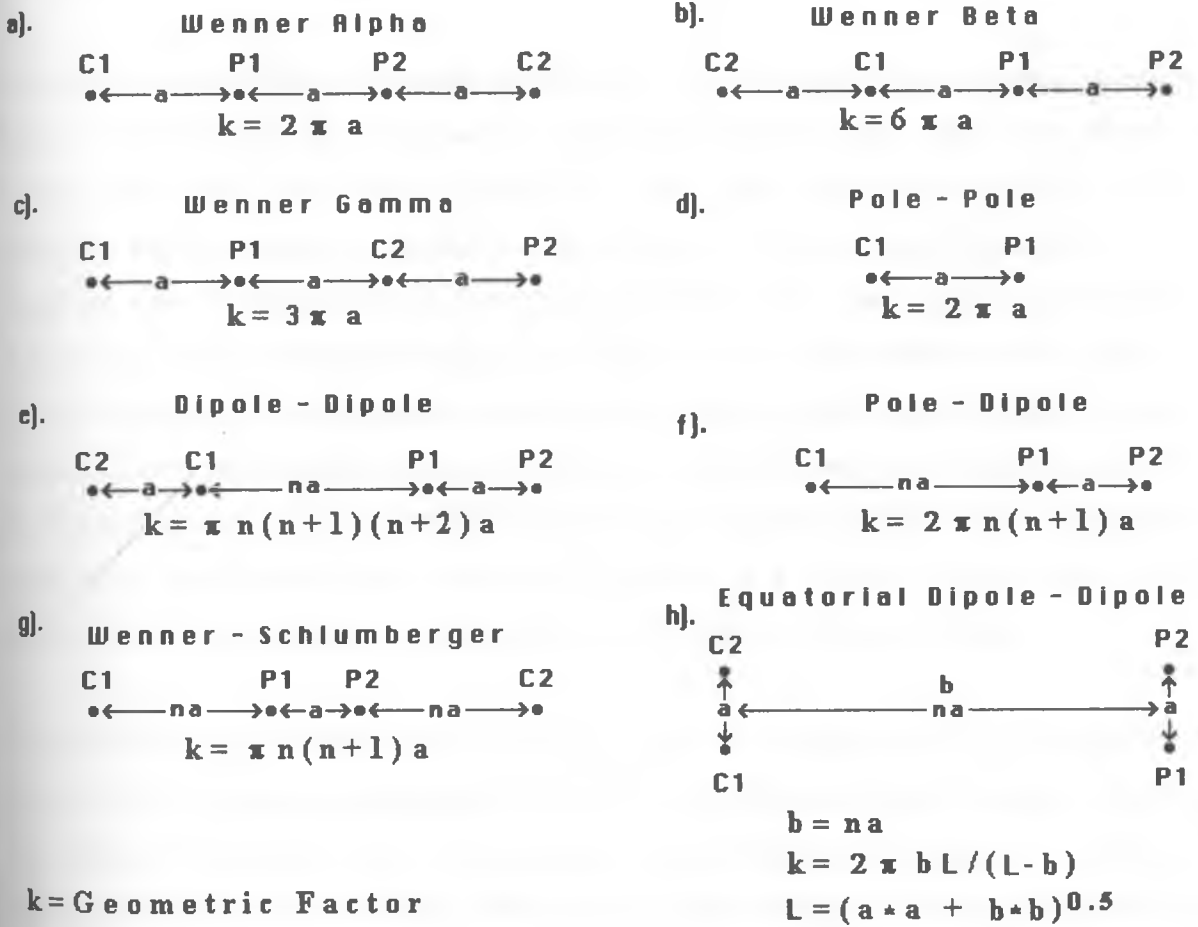
Figure 3.4: The figure showing different patterns that may be used in geophysical survey

3.2.1 Electrical properties of earth materials

Electric current flows in earth materials at shallow depths through two main methods. They are electronic conduction and electrolytic conduction. In electronic conduction, the current flow is via free electrons, such as in metals. In electrolytic conduction, the current flow is via the movement of ions in groundwater. In environmental and engineering surveys, electrolytic conduction is probably the more common mechanism. Electronic conduction is important when conductive minerals are present, such metal sulfides and graphite in mineral surveys.

The resistivity of common rocks, soil materials and chemicals (Keller and Frischknecht 1966, Daniels and Alberty, 1966) is shown in Figure 3.5. Igneous and metamorphic rocks typically have high resistivity values. The resistivity of these rocks is greatly dependent on the degree of fracturing, and the percentage of the fractures filled with ground water. Thus a given rock type can have a large range of resistivity, from about 1000 to 10 million $\Omega.m$, depending on whether it is wet or dry. This characteristic is useful in the detection of fracture zones and other weathering features, such as in engineering and groundwater surveys.

Sedimentary rocks, which are usually more porous and have higher water content, normally have lower resistivity values compared to igneous and metamorphic rocks. The resistivity values range from 10 to about 10000 $\Omega.m$, with most values below 1000 $\Omega.m$. The resistivity values are largely dependent on the porosity of the rocks, and the salinity of the contained water. Unconsolidated sediments generally have even lower resistivity values than sedimentary rocks, with values ranging from about 10 to less than 1000$\Omega.m$. The resistivity value is dependent on the porosity (assuming all the pores are saturated) as well as the clay content. Clayey soil normally has a lower resistivity value than sandy soil. However, note the overlap in the resistivity values of the different classes of rocks and soils. This is because the resistivity of a particular rock or soil sample depends on a number of factors such as the porosity, the degree of water saturation and the concentration of dissolved salts.

The resistivity of groundwater varies from 10 to 100 $\Omega.m$ depending on the concentration of dissolved salts. Note the low resistivity (about 0.2 $\Omega.m$) of seawater due to the relatively high salt content. This makes the resistivity method an ideal technique for mapping the saline and fresh water interface in coastal areas. One simple equation that gives the relationship between the resistivity of a porous rock and the fluid saturation factor is Archie's Law. It is applicable for certain types of rocks and sediments, particularly those that have low clay content. The electrical conduction is assumed to be through the fluids filling the pores of the rock. Archie's Law is given by

$$\rho = a\rho_{\omega}\phi^{-m} \tag{3.11}$$

where ρ is the rock resistivity, ρ_{ω} is fluid resistivity, ϕ is the fraction of the rock filled with the fluid, while a and m are two empirical parameters (Keller and Frischknecht 1966). For most rocks, a is about 1 while m is about 2. For sediments with significant clay

content, other more complex equations have been proposed (Olivar et al. 1990). The resistivities of several types of ores are also shown. Metallic sulfides (such as pyrrhotite, galena and pyrite) have typically low resistivity values of less than $1\ \Omega.m$. Note that the resistivity value of a particular ore body can differ greatly from the resistivity of the individual crystals. Other factors, such as the nature of the ore body (massive or disseminated) have a significant effect. Note that graphitic slate has a low resistivity value, similar to the metallic sulfides, which can give rise to problems in mineral surveys. Most oxides, such as hematite, do not have a significantly low resistivity value. One exception is magnetite.
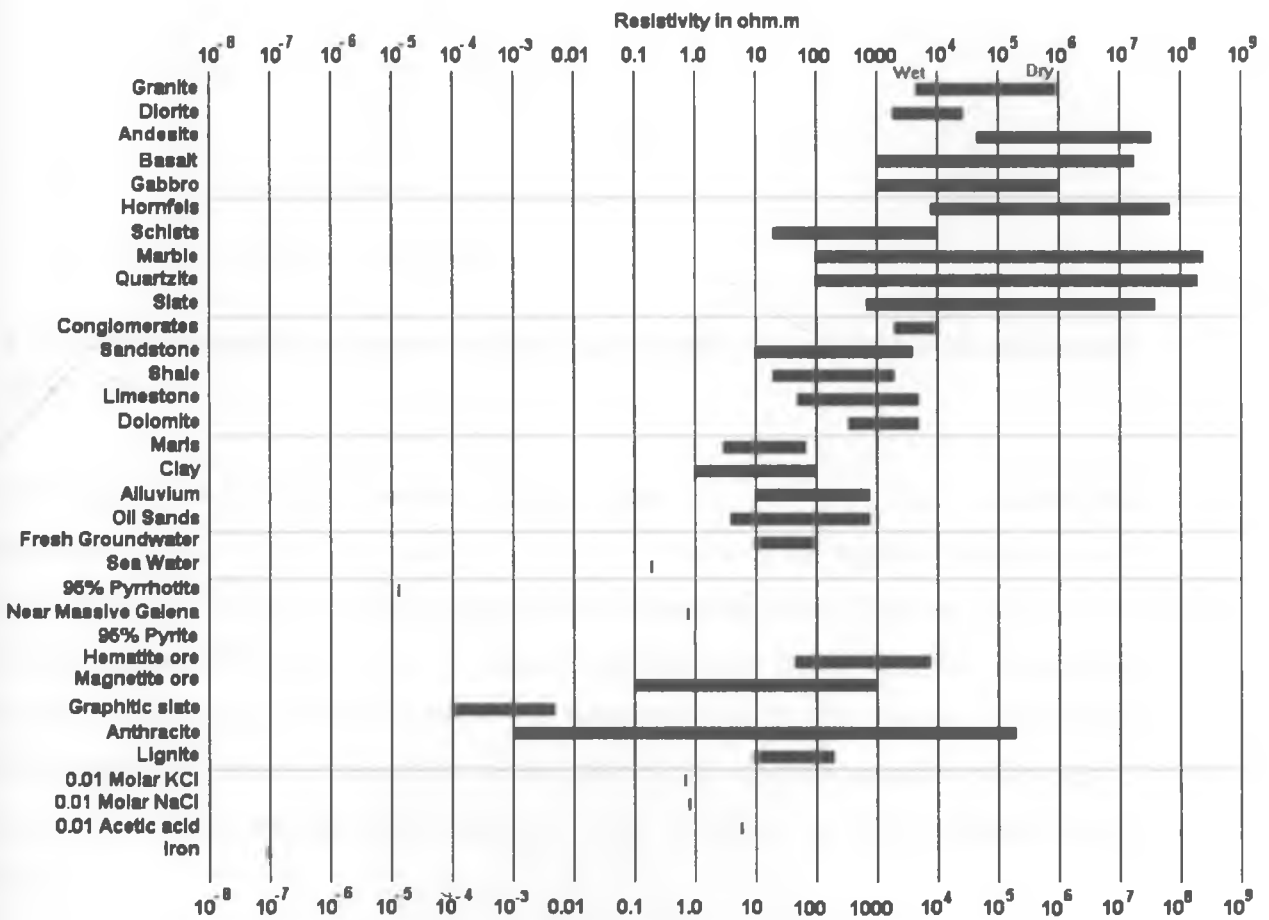
Figure 3.5: Resistivity of common rocks, minerals and chemicals (after Keller and Frischknecht, 1966)

3.2.2 Geoelectrical Sections

The vertical distribution of resistivities within a particular volume of earth is known as geoelectrical section. The sub-surface data can often be approximately determined by a geoelectrical section. The vertical electrical sounding procedure is best for this type of section.
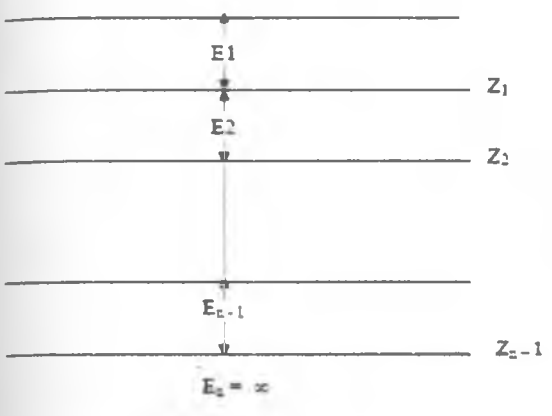
Figure 3.6:The figure showing a vertical section depicting thickness of layers that may be experienced in Schlumberger array.

The above figure 3.6 represents vertical sections where E1, E2 …….. En-1 indicate the thickness $Z1 = E1$, $Z2 = E1+E2$ …. $Zn-1 = E1 + ……+ En-1$ is the depth of the bottom of successive layers and is the true resistivities of the respective layers. The last nth layer is taken to have a great thickness, i.e. En $=\infty$. Geoelectrical sections can be classified depending on the number of layers n. For two layers $n = 2$: three layers, $n=3$: four layers, $n = 4$ and so on. Each category is classified according to the pattern of resistivity variation with depth. Two types of two layer sections are possible i.e., $\rho1 > \rho2$ and $\rho1 < \rho2$ as shown in the figure 3.7.
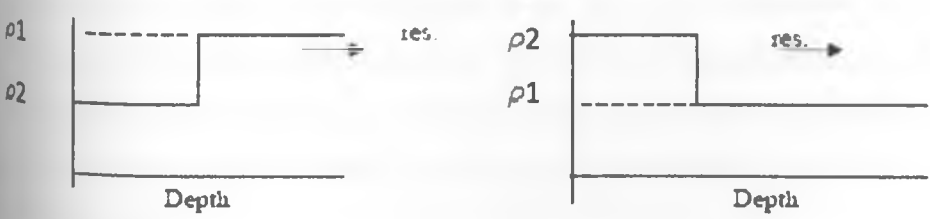
Figure 3.7: The figure showing a two layer section in schlumberger's configuration.

Three layers sections has four possibilities

(a) Type H: $\rho 1 > \rho 2 < \rho 3$

(b) Type K: $\rho 1 < \rho 2 > \rho 3$

(c) Type A: $\rho 1 < \rho 2 < \rho 3$

(d) Type Q: $\rho 1 > \rho 2 > \rho 3$
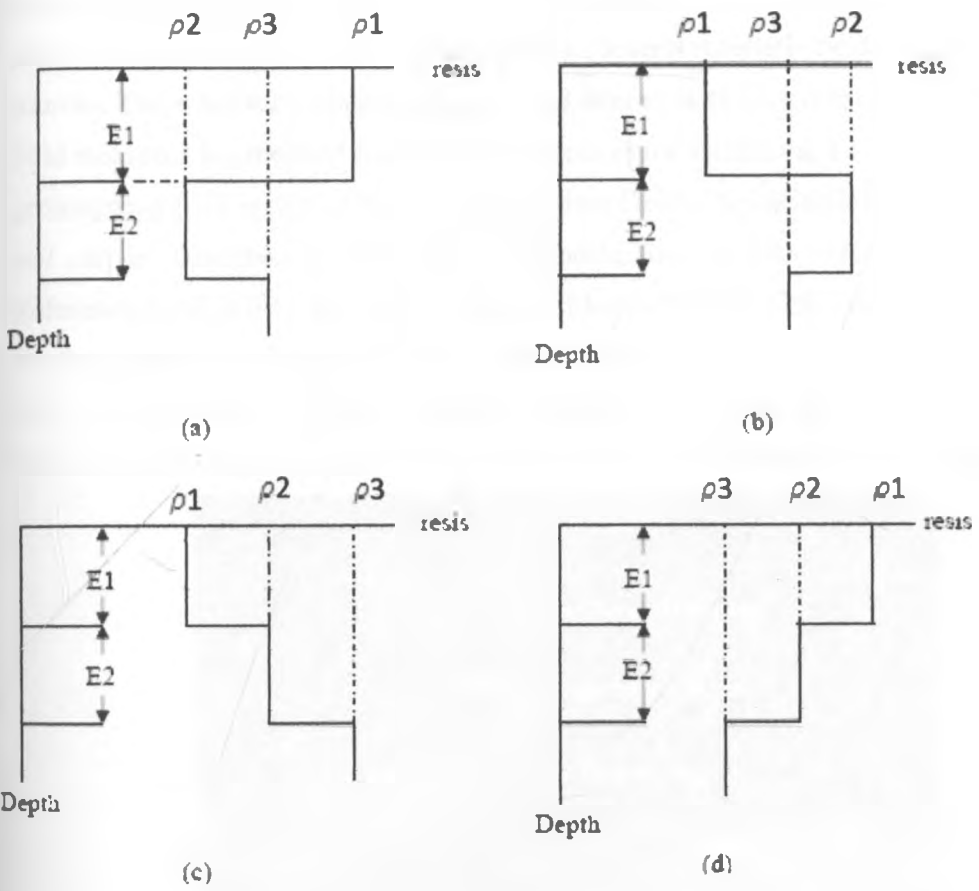
Figure 3.8: Three layer sections in Schlumberger's configuration.

For four layers sections, there are eight possibilities. The section may be identified by combination of three layer designation as AA will correspond to $\rho 1 < \rho 2 < \rho 3 < \rho 4$. Similarly HK will correspond to $\rho 1 > \rho 2 < \rho 3 > \rho 4$. In the present studies the type sections encountered are H and K type. In Most cases, the electrode separation is 100 meters only. It cannot penetrate greater depth. In the present investigation the H and the K type could be interpreted as:

H Type Top soil water saturated clay / sand

K Type Top soil water saturated clay

31

3.3 Basic principles of magnetic survey

The Earth acts like a great spherical magnet, in that it is surrounded by a magnetic field. The Earth's magnetic field resembles, in general, the field generated by a dipole magnet (a straight magnet with a north and South Pole) located at the center of the Earth. The axis of the dipole is offset from the axis of the Earth's rotation by approximately 11 degrees. At any point, the Earth's magnetic field is characterized by a direction and intensity which can be measured. So the geomagnetic field is a vector field. The geomagnetic field (see fig. 3.9) measured at any point on the Earth's surface is a combination of several magnetic fields generated by various sources. These fields are superimposed on and interact with each other. More than 90% of the field measured is generated internal to the planet in the Earth's outer core. This portion of the geomagnetic field is often referred to as the Main Field. The Main Field varies slowly in time and can be described by Mathematical Models such as then International Geomagnetic Reference Field (IGRF) and World Magnetic Model (WMM). Often the parameters measured are the magnetic declination, D, the horizontal intensity, H, and the vertical intensity, Z (see fig. 3.11). From these elements, all other parameters of the magnetic field can be calculated. The instrument used commonly in magnetic survey is the proton precession magnetometer.
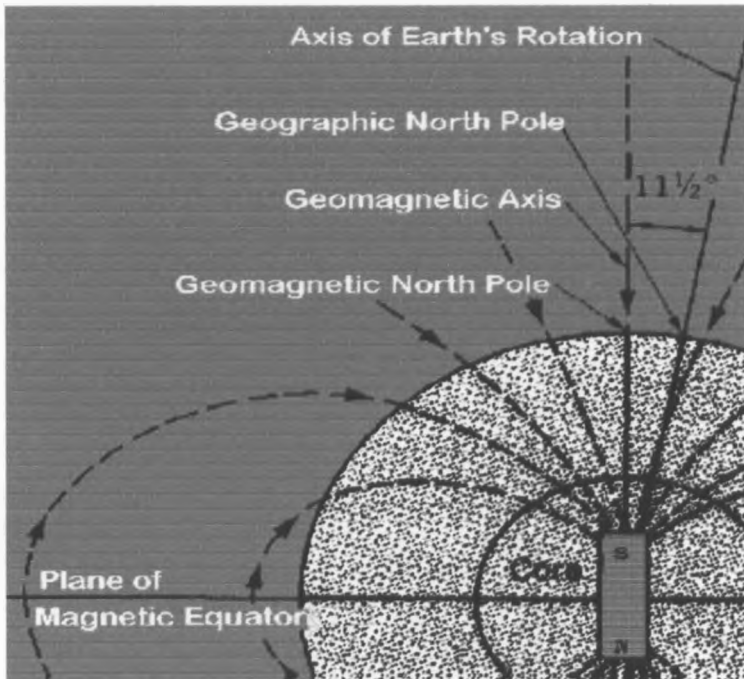
Figure 3.9: The figure showing the Earth's magnetic field. (After Waters, 1956)
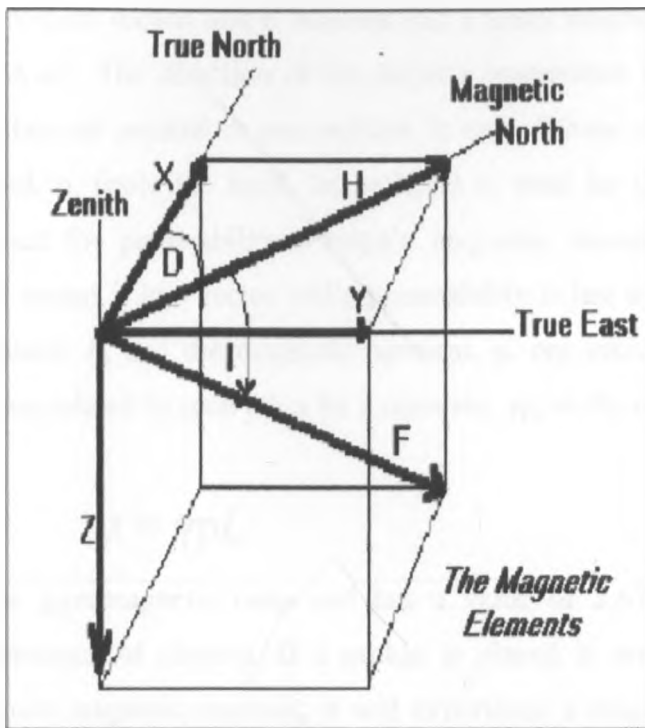
Figure 3.10: The figure showing major elements of earth's magnetic field.(After Haggard, 1970)

Total Intensity F, Declination D, Inclination I, Horizontal intensity H, North component X of the horizontal intensity, East component Y of the horizontal intensity, Vertical intensity Z

$$H = F \cos I$$
$$X = H \cos D = F \cos I \cos D$$
$$Y = H \sin D = F \cos I \sin D$$
$$Z = F \sin I$$

In Connecticut:

F ~ 56000 nT (gamma)
H ~ 19000 nT (gamma)
Z ~ 51000 nT (gamma)
D ~ 14 degree w. of true north
I ~ 70 degree

3.4 Physics of proton precession

The proton has both angular momentum and a magnetic moment. Having angular momentum means that one can think of it as having some 'spin' like a little top. The angular momentum is truly very small – just $5.27 \times 10\text{-}35$ kg-m^2/s.

The magnetic moment means that it behaves like a small magnet. It has a magnetic moment of $1.41 \times 10\text{-}26$ A-m^2. The direction of the angular momentum and the magnetic moment is identical since they are parallel to one another. In one of those minor misfortunes in physics, the same symbol, μ, (note the bold, italics here) is used for the magnetic moment of the proton as is used for permeability. Proton's magnetic moment has both magnitude and direction which means it is a vector while permeability is just a scalar constant. Because the angular momentum, L, and the magnetic moment, μ, are vectors which point in the same direction, they are related to each other by a constant, γp, in the equation:

$$\mu = \gamma p L \qquad (3.12)$$

γp is called the gyromagnetic ratio and has a value of 2.67512×108. γp is one of the fundamental constants of physics. If a proton is placed in an external magnetic field, B, because of its own magnetic moment, it will experience a magnetic torque. Because it also has angular momentum, this magnetic torque will cause it to precess – this is called 'Larmor precession' and the rate of precession depends on the magnitude of the external magnetic field. It turns out that the rate of Larmor precession is independent of the proton's orientation with respect to the external field and depends only on the magnitude of the external field. The rate of precession, ω, in radians per second, is given by the Larmor Equation:

$$\vec{\omega} = \gamma_p \vec{\beta} \qquad (3.13)$$

Where $\vec{\omega}$ is the angular frequency of precession,

γ is gyromagnetic constant − much higher for electrons than protons.

$\vec{\beta}$ is the magnetic induction

The proton precession magnetometer is based on the spin of protons in a magnetic field according to the Larmor equation, (equation 3.13). Typically, a sensor bottle containing a fluid with a large number of protons (such as kerosene) is subjected to a large direct current in a coil wound around the bottle (see fig.3.11). The current creates a corresponding induced field in a direction perpendicular to the earth's magnetic field. The current is then shut off and the protons precess with a frequency that is proportional to the magnetic induction. Accuracy of 0.1 nT (nano-Tesla, or gamma, relative accuracy – 0.1 / 55000), constrained by the polarization time, bottle of liquid (water, or other fluid with a large number of hydrogen nuclei) surrounded by a suitable coil is required.
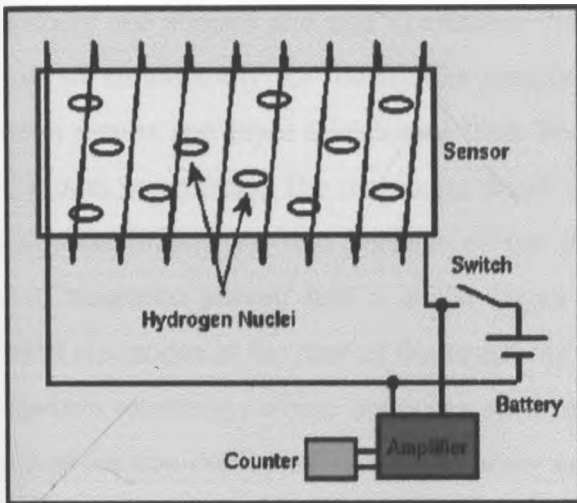
Figure 3.11: The figure showing the arrangement of proton magnetometer. Note the bottle of liquid (water, or other fluid with a large number of hydrogen nuclei) surrounded by a suitable coil. (After Serson, 1962)

CHAPTER FOUR

4.0 DATA ACQUISITION

4.1 Introduction

Detailed 2D Resistivity Imaging, 1D Vertical electric sounding and Magnetic surveys were carried out in the Kabatini area, from the 18th of December 2009 to the 3rd of January 2010. Selected locations, based on the pre-field work study were surveyed with the three methods. These methods are ERT, VES and Magnetic survey. ERT and VES were made first, followed by the magnetic survey in east – west profiles. The three methods were used in order to compliment one another and also to enhance the interpretation of the subsurface information in terms of conductivity for the aquifer mapping. The output of the 2D resistivity imaging inversion results and layer thicknesses from borehole information was used to generate the initial model parameters. The maximum depth investigation in the case of the 2D resistivity imaging was limited to 72m because of the maximum allowable electrode spacing (5m) whereas magnetic survey had a much larger depth investigation (> 100m).The use of grounded electrodes in the case of the resistivity methods can encounter problems in areas of high surface resistivity, where obtaining sufficient current flow can be difficult. Under such conditions the non-contacting magnetic survey can provide terrain resistivity data. The proton precession magnetometer survey method allows measurement to be made rapidly and therefore, larger areas could be surveyed in greater detail for comparable time. The equipments and materials used in data acquisition in this study included,

- Geological maps
- Topographical maps
- A GARMIN-make handheld GPS
- Tape measure
- Proton Magnetometer
- Previous related reports
- SYSCAL R2 Resistivity meter instrument (IRIS instrument of Orleans, France)
- SYSCAL R1 Switch-72 (IRIS instruments)
- MP2 SYNTREX proton magnetometer
- Laptop

4.2 Field surveys

Field work involved surveying of the Kabatini aquifer using Vertical Electrical Sounding, Electrical Resistivity Imaging (Tomography) and Proton Magnetic Survey. The three surveys were carried out on four profiles aligned in the east – west direction as shown in fig 4.1and 4.2.
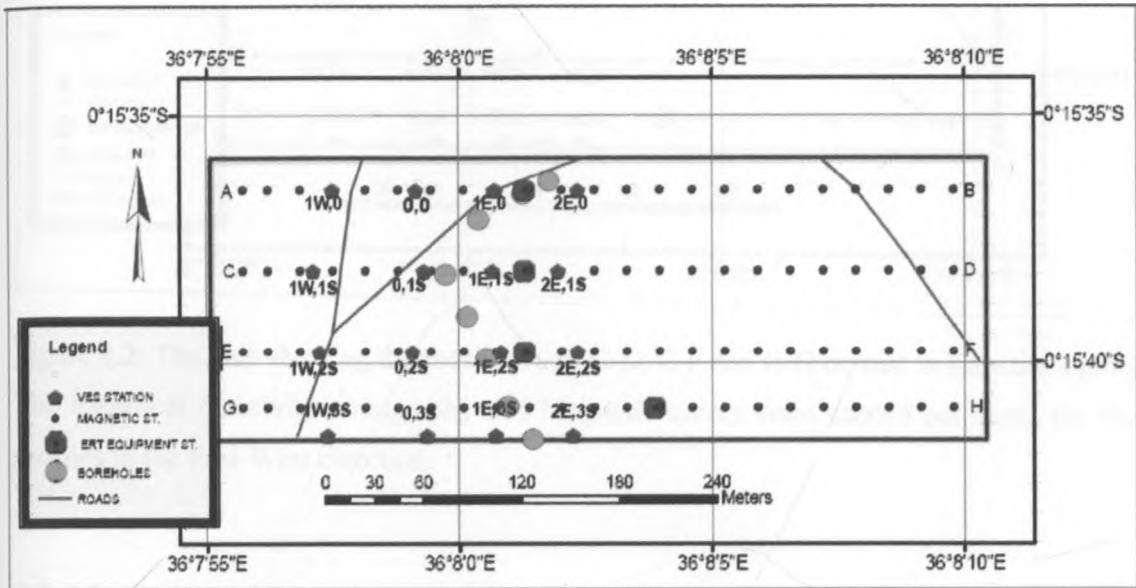
Figure 4.1: The Map showing profiles of Vertical electrical resistivity (VES) and Electrical resistivity tomography (ERT) in Kabatini aquifer
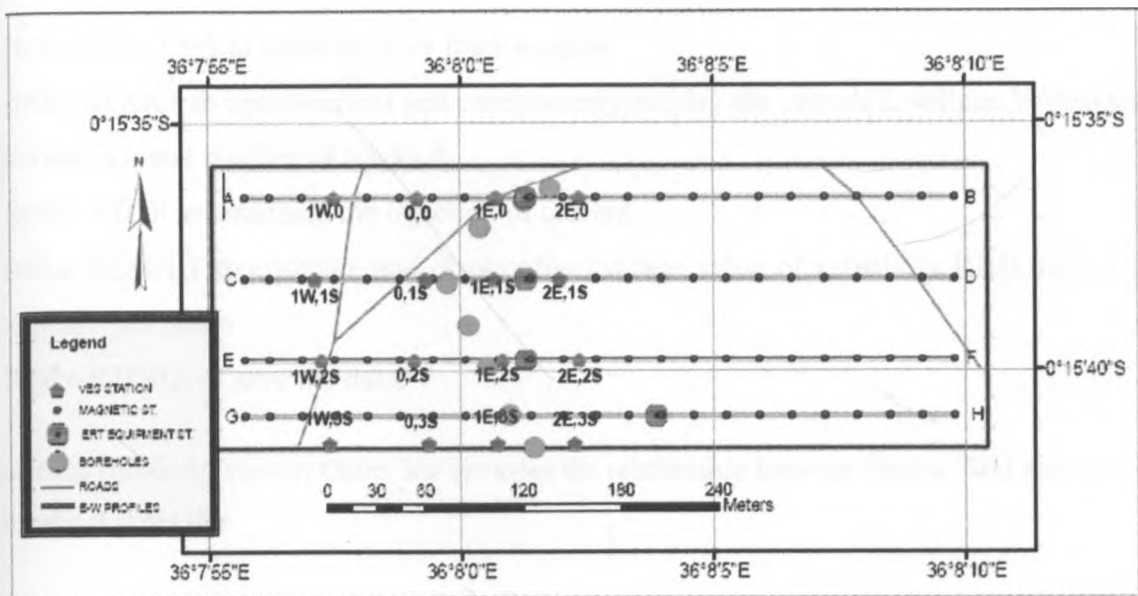
Figure 4.2: The map showing the profiles A-B, C-D, E-F and G-H carried in Kabatini aquifer. The Electrical resistivity tomography and Magnetic survey were carried out along the four profiles in the East-West direction.

4.2.1 Instrumentation

4.2.2 Vertical electrical sounding (VES) instrumentation

SYSCAL R2 Resistivity meter instrument (IRIS instrument of Orleans, France) was used for collecting field data for vertical electrical sounding. This is a high powered fully automatic resistivity meter designed for DC electrical resistivity surveys. It is operated using two power supplies which includes internal supply for the electronic circuits and external supply for ground energizing. The internal power supply consists of six 1.5 volts sized dry cells located at the lower site of the equipment. External power supply in the present study was a 12 volts car battery whose voltage was stepped up using a 250W DC/DC converter.

SYSCAL R2 is driven by the operator through easy-to-use interactive menus. Only a few keys control the operation of the instrument at each new reading. The following steps are followed during the operation of the equipment to acquire data.

1. Strike SPACING to enter the wire lines lengths
2. Strike START to inject current and continuously display the current I, voltage V, standard deviation q and number of stacks #
3. Strike STOP to terminate the injection of current.
4. Strike RESULT to compute and display the average value of resistivity RHO and of its standard deviation
5. Strike STORE to save the data.

In electrical resistivity survey; Ohms law provides the relationship between electric field and current density and it states that

$$\overline{J} = \sigma \overline{E} \tag{4.0}$$

Where: σ = Conductivity (a constant)

For an isotropic medium, the conductivity will be a scalar quantity so that J and E will be in the same direction. For anisotropic medium, the conductivity is a tensor of second rank σ_{ij} so that

$$\overline{J} = \sigma_{ij} \overline{E} \tag{4.1}$$

The subscript i and j may be any of the X, Y, or Z spatial directions. The basis of all resistivity prospecting with direct current is given by:

$$\nabla \sigma_{ij} \nabla V = 0 \tag{4.2}$$

In the isotropic case Eq4.2 reduces to Laplace's equation

$$\nabla^2 V = 0 \tag{4.3}$$

For a horizontal earth model the solution to Eq._4.3 according to Stefanesco *et al.* (1930) becomes

$$V(r) = \frac{I\rho_1}{2\pi}\left[\frac{1}{r} + 2\int_0^\infty \theta_n(\lambda) J_0(\lambda r) dr\right] \tag{4.4}$$

Where, $J_0 = \overline{I}$ is the zero order Bessel function of the first kind and θ_n, is called the kernel function which is a function of the thickness and reflection coefficient for an assumed earth model.

By differentiating 4.4, the Schlumbeger apparent resistivity over an n- layered earth becomes

$$\rho_a(r) = \rho_1 \left[1 + 2r^2 \int \lambda \theta_n(\lambda) J_1(\lambda r) d\lambda \right] \qquad (4.5)$$

Where, J_1 is the first order Bessel function of the first kind.

The evaluation of this integral of Eq. 4.5 has been done in a number of ways. In this study we have adopted, Ghosh (1971) in which it is possible to determine a linear digital filter, which converts resistivity transform samples into apparent resistivity values for theoretical models.

4.2.2.1 Vertical electrical sounding field measurement

A total of 16 vertical electrical soundings were carried out using Schlumbeger electrode configuration. Four profiles A- B, C- D, E - F G- H were located in the East – West direction (see fig. 4.2a). Each profile was separated from the adjacent profile by an interval of 50 meters. Sounding stations along the profile were also 50m apart. The direction of the profiles was selected depending on how open the terrain was to allow for a wider AB/2 electrode spread. East to west direction was found to be appropriate since it perpendicular to the principal structures in the area.
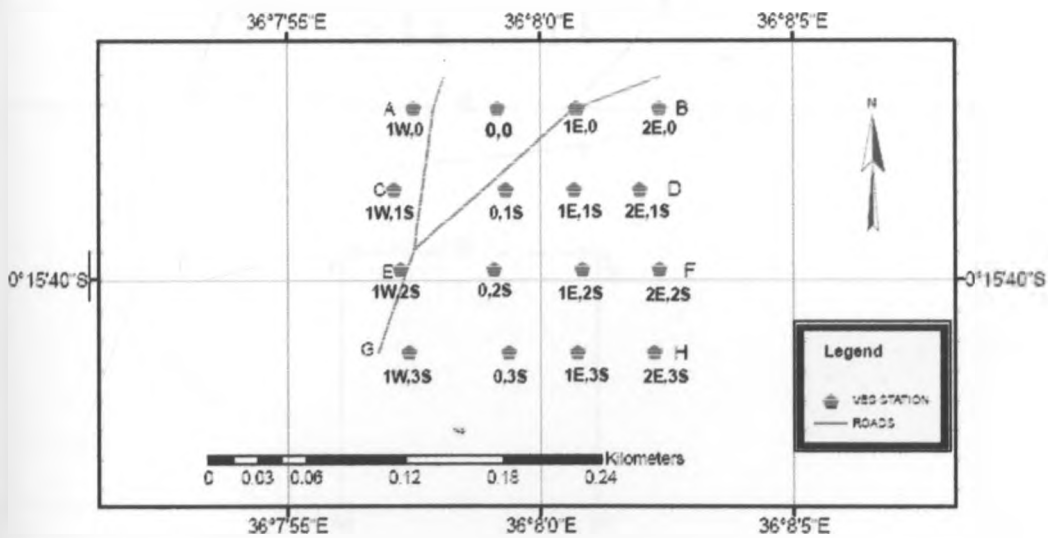
Figure 4.2a: The figure showing the Vertical electrical sounding field stations.

Geology, elevation and ground conditions were noted at and around each station down before spreading the cables and fixing the electrodes in the ground. The electrode position was fixed using a GPS on a straight line. The equipment was placed midway between the current and potential electrodes. The potential electrodes were connected to terminals M and N on the equipment. The current electrodes were also connected to terminals A and B of the equipment. The steel current and potential electrodes were then hammered into the ground. The machine was switched on to read the readings. The readings were recorded on prepared data sheets.

4.2.2.2 Schlumberger's Configuration

Schlumberger's configuration was adopted for VES data collection. In this method, all the four electrodes are placed collinear, but the potential electrodes are kept very close to the central point of the arrays, as compared to the current electrodes, (Whitely, 1973). Current (I) is sent to the ground through the outer electrodes, A and B and potential difference (V) is measured across the inner electrodes M and N (see fig 4.3). If 2L is current separation, 2l is potential electrode separation, the apparent resistivity (ς) for schlumberger's configuration is

$$\varsigma a = \frac{\pi}{2}\left[\frac{L^2}{1} - \frac{l^2}{1}\right] V/I \tag{4.6}$$
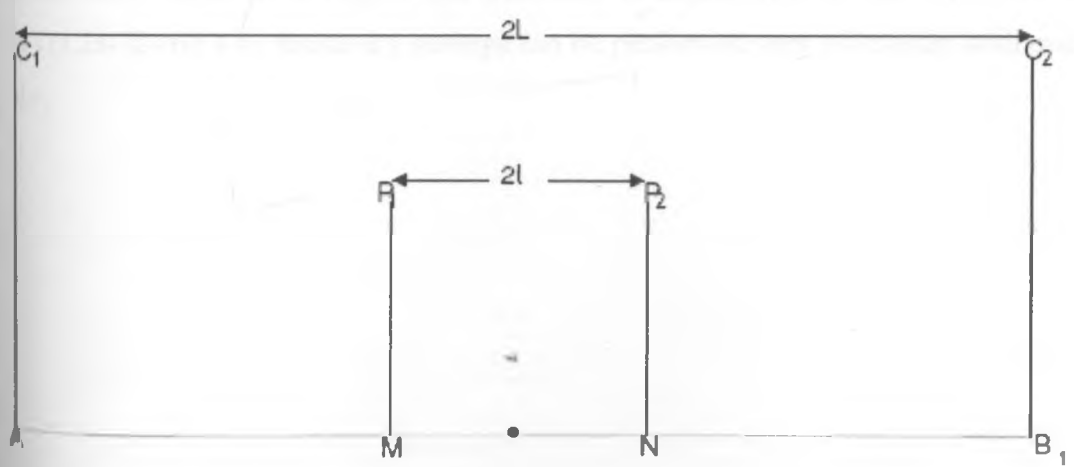
Figure 4.3: The Schlumberger array configuration used in acquiring data in Kabatini aquifer.

4.2.3 Electrical resistivity tomography instrumentation

The 2D Resistivity data were recorded using the ERT (Electrical Resistivity Tomography). The complete system consists of the ERT instrument console, the Swift interface box (the electronic switching unit),ERT to 12V battery communication cable, ERT to AB,MN cable, ERT - electrode cables connectors and stainless steel electrode stakes. The ERT can be used in four basic modes, namely the Manual, Automatic, User and PC modes. More information on these can be obtained from the Instruction Manual (RES2DINV, 2000).

SYSCAL R1 SWITCH PLUS-72 is a new all-in-one multinode resistivity imaging system. It features an internal switching board for 72 electrodes and an internal 200W power source. The output current is automatically adjusted (automatic ranging) to optimize the input voltage values and ensure the best measurement quality. The system is designed to automatically perform pre-defined sets of resistivity measurements with roll-along capability. Four strings of cable with 18 electrode take-out each are connected together on the back of the resistivity meter. Made of heavy duty seismic cable (see fig 4.5), these strings are composed of standard 5 m electrode spacing. Compact, easy-to-use and field proof, the SYSCAL R1 Switch-72 measures both resistivity and chargeability (IP). It is ideal for environmental and civil engineering applications such as pollution monitoring and mapping, salinity control, depth-to-rock determination and weathered bedrock mapping. It can also be used for shallow groundwater exploration (depth and thickness of aquifers).With the SYSCAL R1 PLUS SWITCH-72 (fig 4.4) resistivity surveys can be performed very efficiently with one operator only.
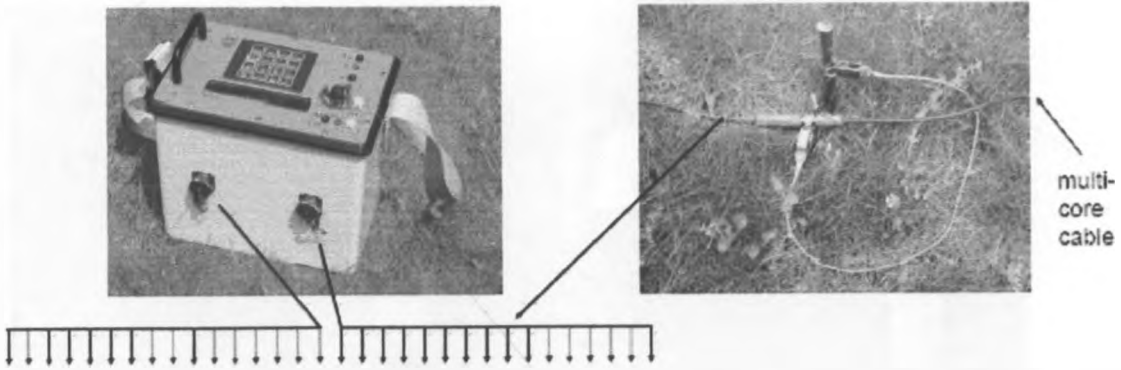
Figure 4.4: The figure shows Electrical resistivity tomography (ERT) equipment and the style on how the cable is attached to the electrode fixed in the ground.
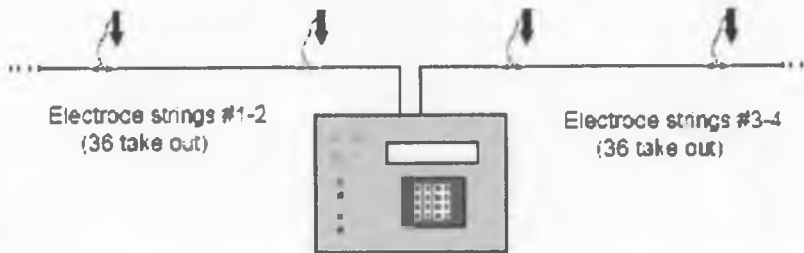
Figure 4.5 Field lay out for the ERT equipment in relation to the cables and electrodes

4.2.3.1 Electrical resistivity tomography data acquisition

A multi-electrode resistivity imaging system, SYSCAL R1 PLU Switch-72 of IRIS-make was used for the present study. A GARMIN-make handheld GPS was used to position location of all the electrodes. A total of four resistivity tomography profiles (Figure 4.2) were designed in the East to West direction. The separation of one electrode to another in the same profile was 5 mt. Resistivity data were collected using Wenner–Schlumberger array configuration with inter-electrode spacing of 5 m, during the survey.
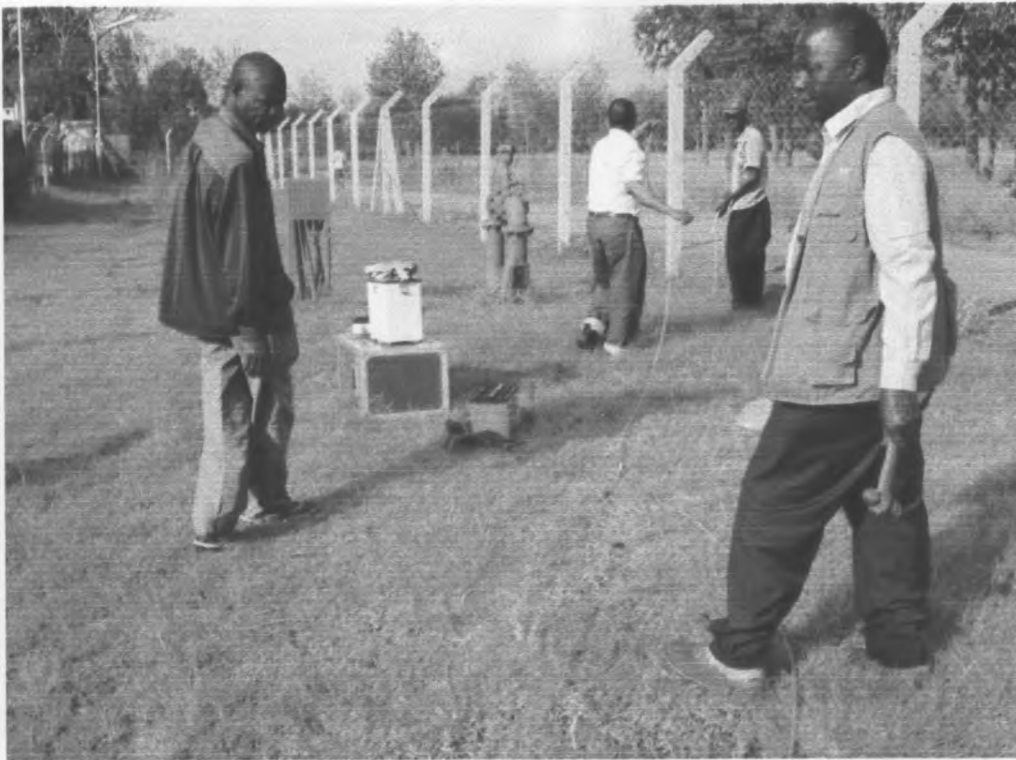
Figure 4.6: The author setting up ERT equipment to collect 2D resistivity image.

Topographic corrections and 2D inversion model measurements were made using the inversion algorithm proposed by Loke and Barker, (1996). For uniformity in the interpretation of different true resistivity sections along various profiles, a common colour code has been evolved and adopted for presentation of the results. The adopted colour code answers the key parameters of the aquifer characteristics, like the presence of low resistive clay/clayey sand horizons, demarcation of locked groundwater pockets, demarcation of the underground river boundary and identification of boulders and debris. The main factors that determined daily progress included the battery's power supply, the weather condition (rain and thunderstorms) and terrain accessibility (obstructions). After a successful collection of data from a particular spread, the measured apparent resistivity data was downloaded to a Laptop. Negative data are automatically removed during this process. The cable and electrodes were moved to the next-profile. Majority of the survey time was used in the packing, carrying and laying out the cable.

Figure 4.7: The author fixing the cable for Electrical resistivity tomography (ERT) along profile A – B in Kabatini aquifer.

In the field, command files were created to record "Werner-Schlumberger" data at a 5m electrode separation within the user mode option. The three command files were designed to measure different parts of the profile line. The first spread begins with cable1 and 2 followed by cable 3 and 4 with electrodes 1-36 and 37-72 respectively (fig.4.6 and 4.7). Measurement commences at electrodes 1, 2, 3, and 4 using its corresponding command file. The spacing is then doubled with active electrodes becoming 1, 3, 5, and 7. At each measurement, spacing is increased by one unit until the maximum spacing is reached after which the sequence is repeated starting with electrodes 2, 3, 4, and 5. Measurements were carried out with the designed corresponding command file in which overlapping measurements are avoided. Giving the maximum allowable electrode spacing of 5m by the equipment, and an array of 72 electrodes, some constraints were consequently placed on the length of profiles and the depth of investigation. Werner-Schlumberger spread with an array of 72 electrodes, and the maximum inter-electrode spacing of 5m, gives the maximum possible measurement separation of 365m. Half of the maximum possible measurement separation is the guide for the depth of investigation (182.5m). The Horizontal distance for one spread is 360m. The true depth after inversion of the data can be approximated to one-sixth (1/6) of the horizontal distance of one spread, 60m. In the field, the data collection always starts with placing the

stainless steel electrode stakes into the ground at intervals of 5m along selected lines. The swift cables are then laid out on the ground and a clip is used to fix the cable to the electrode, making sure that there is an electrical contact between them. The cables of electrodes 36 and 37 are then connected to the SYSCAL R1 PLUS SWITCH 72. The SYSCAL RI PLUS SWITHC 72 and the DC battery are also connected. The details of the traverse from which data is to be collected are entered into the SYSCAL RI PLUS SWITCH 72 and made ready for data collection (fig.4.8). A contact resistance test is run to check for poorly connected electrodes or abnormally high contact resistance reading. The actual measurement was carried out after the contact resistance test output gave good results, otherwise, the causative electrode(s) were checked and properly connected or watered some more. It took between 1.00 to 1.30 hours to complete one spread, so during the data collection period a new survey section was prepared for the next spread. The start and end locations of survey lines were mapped with a Global Positioning System (GPS). The Resistivity Imaging lines were carried out more or less along the Proton precession Magnetic survey profiles.

Fig 4.8: The author entering data in SYSICAL R1 PLUS SWITCH 72 in Kabatini aquifer.

The ERT algorithm used is based on an Occam's type inversion that yields a minimum roughness solution consistent with the data and their errors. The 2-D algorithm, based on a

finite element forward solver, is described by LaBrecque, et al. (1996b). LaBrecque, et al., (1999) describe a method for streamlining the forward solver using an iterative finite difference formulation and a method to reduce the computational load associated with the Occam's approach. Convergence for both algorithms is achieved when the root mean square error, normalized by the weights, is equal to the number of data.

4.2.4 Magnetometric Survey Instrumentation

The MP2 SCINTREX proton precession magnetometer from Scintrex Company of Canada provides a reliable, low cost solution for a variety of magnetic search and mapping applications. Single key stroke operation means the MP2 SCINTREX proton precession magnetometer can be operated by non-technical field personnel. It uses the well proven proton precession technology, allowing accurate measurements to be made with virtually no dependence upon variables such as sensor orientation, temperature, or location. The unit provides a repeatable absolute total field magnetic reading. The equipment has a Sensor which can be attached to the Staff when field measurements are taken.MP2 SCINTREX proton precession magnetometer is a portable and operated using eight dry cells of 1.5 V.

4.2.4.1 Magnetic survey data acquisition

Total intensity magnetic field measurements were carried out along ERT profiles with MP2 SCINTREX proton precession magnetometer made by Scintrex Company of Canada with one 1 nT sensitivity (see fig.4.9). The same magnetometer was used for base station recordings, to apply the diurnal variation correction as well as taking field measurements. Magnetic surveys are based on the premise that a target is limited in space and has a different physical property (e.g. magnetic susceptibility), from the surrounding formation. Unlike gravity surveying, however, the variation in magnetic susceptibility for various rock types is orders of magnitude greater than the variation in density for the same rock types. Thus, even knowing the types of rocks in a specific area does not provide sufficient information to constrain susceptibilities. Like density contrast, variations in susceptibility tradeoff strongly with other model parameters. Therefore, if susceptibility, or other model parameters, cannot be constrained from different observations, it is difficult to make quantitative estimates of the geologic structure based on magnetic observations alone.

In a particular survey, one may need additional constraints that allow him to use the magnetic observations in a quantitative fashion. This information is derived from other separate data sets, for example, formation layering from borehole logging. Once one has constrained the range of plausible geological models from other observations, he can design a magnetic survey to estimate the spatial extent of the structure and its susceptibility by in-lab forward modeling. In planning the magnetic survey, I had to predict the noise from sources not of interest in the survey, estimated the standard deviation of the random (operator and instrument) noise, calculate the shape of the signal (the theoretical anomaly produced by the assumed source), then decide whether the signal generated by the target of interest is above the noise level that allow me to conduct a meaningful interpretation. If the answer is affirmative, then I had to determine the survey parameters that will produce the best compromise between cost and data quality. The Magnetic survey orientation in Kabatini area was in the East – West Profile. Survey was carried out on four profiles at an interval of 20 m along each profile (see fig 4.2). The first there profiles on the northern part of the project area had a space interval of 50 meters from each other. MP2 SINTREX proton precession magnetometer was used to carry out the survey as shown in fig.4.9. Readings taken included position coordinates altitude, time and magnetic variations in nT/m

Fig 4.9: The author taking magnetic data in the field using MP2 SCINTREX proton precession magnetometer

Precautions taken during Magnetic survey include;

- Ensured that there were no metallic objects in my pockets.
- Made sure that the arrow on the sensor was pointing towards North. The sensors mounted vertically like a cylindrical drum.
- Chose a base station in an open area, with hopefully not close to any surface and buried metal objects (no beeps when collecting the data at the base station).
- Made sure that I go back to the base station to collect 3 data points after one hour, to the least every 2-3 hours.
- Made sure that I tune the magnetometer to its largest signal strength (enter 53-56) to find the largest signal strength (3.0-9.9).
- Made sure that I hit [read] and [store] to store the readings.
- Also ensured the voltage of the batteries is always above 8.4v; otherwise the batteries were changed (9 Size D cells of them).

The use of Magnetic technique for groundwater exploration, though not as wide spread as other electrical geophysical techniques (DC resistivity and Resistivity imaging) has increased considerably in recent years. Examples of its applicability to groundwater exploration include among others; characterizing local ground water system in arid alluvial environment (Taylor, et al., 1992) detection of salt or brackish water interfaces in fresh water aquifers and determination of hydro stratigraphy (Fitterman and Stewart, 1986).

CHAPTER FIVE

5.0 DATA PROCESSING, ANALYSIS AND INTERPRETATION

5.1 Introduction

The data collected from the field was processed individually depending on the method used to collect this data in the field. Vertical resistivity sounding data was processed using AGI EarthImager software. AGI EarthImager 1D is a Windows 32-bit platform based computer program that interprets one-dimensional (1D) electrical resistivity sounding data and produces a layered resistivity model that reveals subsurface geology. Resistivity values at depths 50m, 57m, 100m, 125m, and 150m were produced using SUFFER 8. Electrical resistivity tomography data was processed using RES2DINV software. The program subdivides the subsurface into rectangular blocks. It then determines the resistivity of these blocks and produces a pseudo section that coincides with the measurements. Magnetic data was interpolated and corrected to the pole to remove diurnal variations. This data was then processed using EULER software. Magnetic anomaly map was produced using SUFFER 32 software.

5.2 Electrical resistivity tomography (ERT) data processing and analysis

RES2DINV software package was employed in the processing of the resistivity imaging data. RES2DINV is a computer program designed by Loke, (1997) to invert the "apparent resistivity" data obtained from electrical imaging surveys into a two-dimensional (2D) "true resistivity" model of the subsurface in an automatic and robust manner with minimal input from the user. The program determines a resistivity model which approximates the measured data within the limits of data errors and which is in agreement with all a priori information.

The program first subdivides the subsurface into a number of rectangular blocks, the arrangement of which is loosely tied to the distribution of the measured data points in the pseudo-section but it can also be manipulated. It then determines the resistivity of the rectangular blocks that will produce an apparent resistivity pseudo-section that agrees with the actual measurements. It is worth stating that for the same data set, there would be a range of equivalent models whose calculated apparent resistivity values would agree with the measured values to the same degree. The program minimizes the difference between the measured and the calculated apparent resistivity values, but the inversion method also attempts to reduce other quantities that will produce certain undesired characteristics in the resulting model (Loke, 2000, Loke and Barker, 1996)

The RES2DINV program uses a forward modeling subroutine (smoothness-constrained method) to calculate apparent resistivity values and a non-linear least-squares optimization technique (deGroot-Hedlin and Constable, 1990) for the inversion routine. As indicated earlier, the optimization method tries to reduce the difference between the calculated and the measured apparent resistivity values by adjusting the resistivity of the model blocks (RES2DINV, 2000). The difference between the measured and calculated apparent resistivity values is given by the root mean- squared (RMS) error.

The raw data were downloaded to a computer where bad data, particularly negative values were deleted in the process by the program. These raw data files are converted into the appropriate format (DAT) readable by the inversion software RES2DINV.EXE (see fig 5.1). The individual (DAT) input files for all the resistivity imaging survey lines were generated and made ready for inversion into 2D "true resistivity" image in the program. The routine practice is to open a file of a particular traverse results, and view the apparent resistivity data values in a form of profiles for each data level and to eliminate or remove any inherent bad datum points. The reason for this step was to manually remove bad data points (i.e. obviously too large or too small compared to the neighboring data points). Though, careful procedures were adopted in the field, during the data collection, nevertheless, bad data could come from sources such as, the failure of the relays at one of the electrodes, poor electrode-ground contact due to dry soil, or shorting across the cables due to the very wet ground conditions, if such data points occur, then they must be removed, else they can influence the final output model. After editing the input data, inversion of the data set was then carried with least squares inversion routine. The final output file displayed after inversion was the measured and the calculated apparent resistivity pseudo-sections and the true resistivity model section.

```
┌─────────────────────────────────────────────────────────────┐
│        IMPORT RAW DATA FILES INTO THE COMPUTER              │
└─────────────────────────────────────────────────────────────┘
                            ↓
┌─────────────────────────────────────────────────────────────┐
│        CONVERTING THE RAW FILES INTO DAT. FILES             │
└─────────────────────────────────────────────────────────────┘
                            ↓
┌─────────────────────────────────────────────────────────────┐
│      OPENING THE "DAT" FILES IN RES2DINV PROGRAM            │
└─────────────────────────────────────────────────────────────┘
                            ↓
┌─────────────────────────────────────────────────────────────┐
│  VIEWING OF DATA IN PROFILE FORMAT SHOWING THE DIFFERENT DATA│
│                         LEVELS                              │
└─────────────────────────────────────────────────────────────┘
                            ↓
┌─────────────────────────────────────────────────────────────┐
│      REMOVING THE UNWANTED DATA POINTS MANUALLY             │
└─────────────────────────────────────────────────────────────┘
                            ↓
┌─────────────────────────────────────────────────────────────┐
│ RUNNING THE RES2DINV. PROGRAM TO PRODUCE THE TRUE 2D RESISTIVITY│
│              IMAGE OF THE SUBSURFACE                        │
└─────────────────────────────────────────────────────────────┘
```
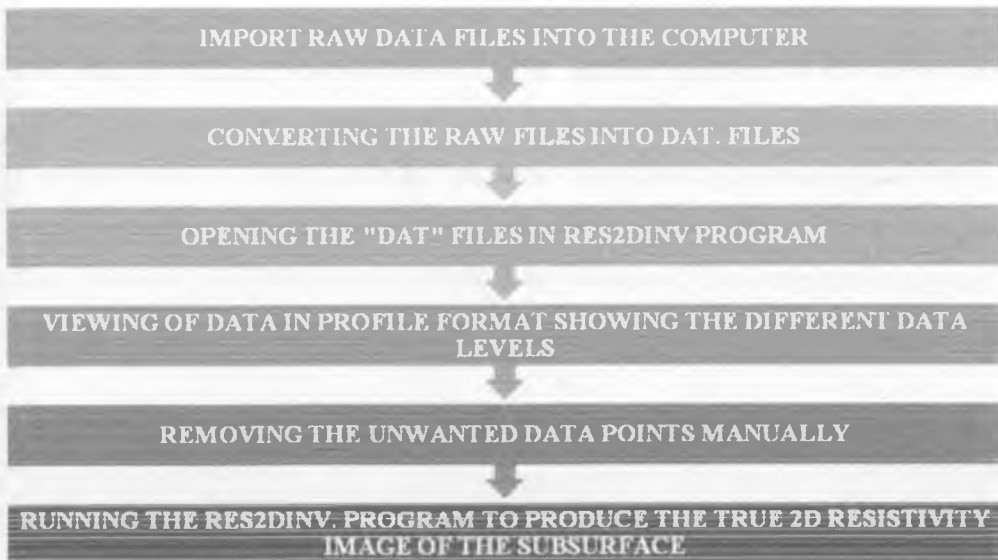
Figure 5.1, The stages involved in processing ERT the data.

5.3 Vertical sounding data processing

AGI EarthImager 1D is a Windows 32-bit platform based computer program that interprets one-dimensional (1D) electrical resistivity sounding data and produces a layered resistivity model that reveals subsurface geology. EarthImager 1D software was used to processes vertical electrical sounding (VES) data collected with Schlumberger. The processing of the data using this software involved the steps shown in fig 5.2

```
┌─────────────────────────────────────────────────────────────┐
│          Reading a data file from the computer.            │
└─────────────────────────────────────────────────────────────┘
                            ↓
┌─────────────────────────────────────────────────────────────┐
│  Changing inversion settings or reading a settings file (*.ini)│
└─────────────────────────────────────────────────────────────┘
                            ↓
┌─────────────────────────────────────────────────────────────┐
│                    Starting inversion                       │
└─────────────────────────────────────────────────────────────┘
                            ↓
┌─────────────────────────────────────────────────────────────┐
│ Improving the starting model based on the inversion results by Combine-│
│        Layers or manually modifies the model               │
└─────────────────────────────────────────────────────────────┘
                            ↓
┌─────────────────────────────────────────────────────────────┐
│                 Running inversion again                     │
└─────────────────────────────────────────────────────────────┘
                            ↓
┌─────────────────────────────────────────────────────────────┐
│                  View inversion results.                    │
└─────────────────────────────────────────────────────────────┘
                            ↓
┌─────────────────────────────────────────────────────────────┐
│      Save and print the raw data and inversion results     │
└─────────────────────────────────────────────────────────────┘
```
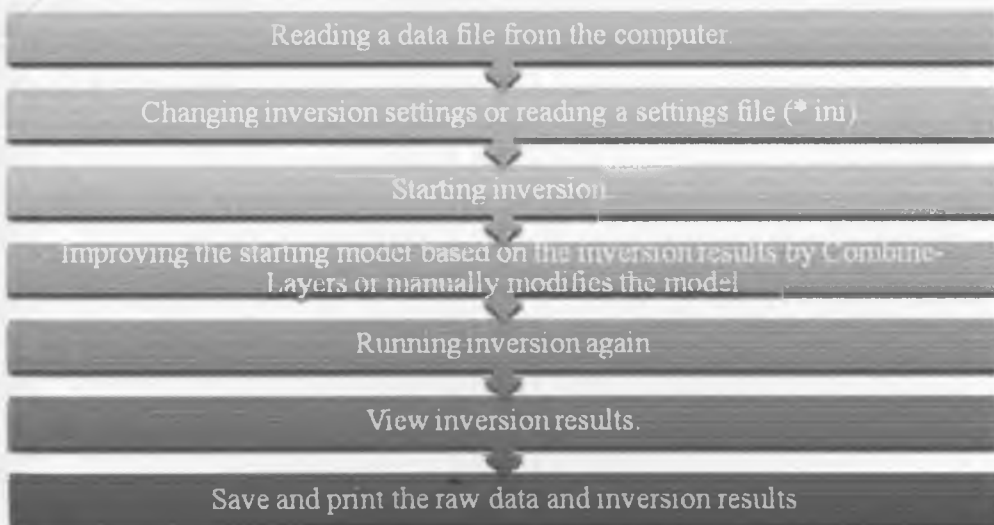
Figure 5.2: The stages involved in processing of Vertical electrical sounding data

5.4 Magnetic survey data processing

The obtained values were corrected for the normal gradient of the earth's magnetic field (IGRF); the corrected magnetic values were contoured using suffer 32 software and Euler. The final result is a total intensity magnetic map showing the anomalies noted in the study area. The steps in data processing involved interpolation of the field data with the base station data. This data was then corrected for diurnal variation. The corrected data was plotted into a map showing the anomalies using SUFFER 32. These steps are summarized in fig.5.3
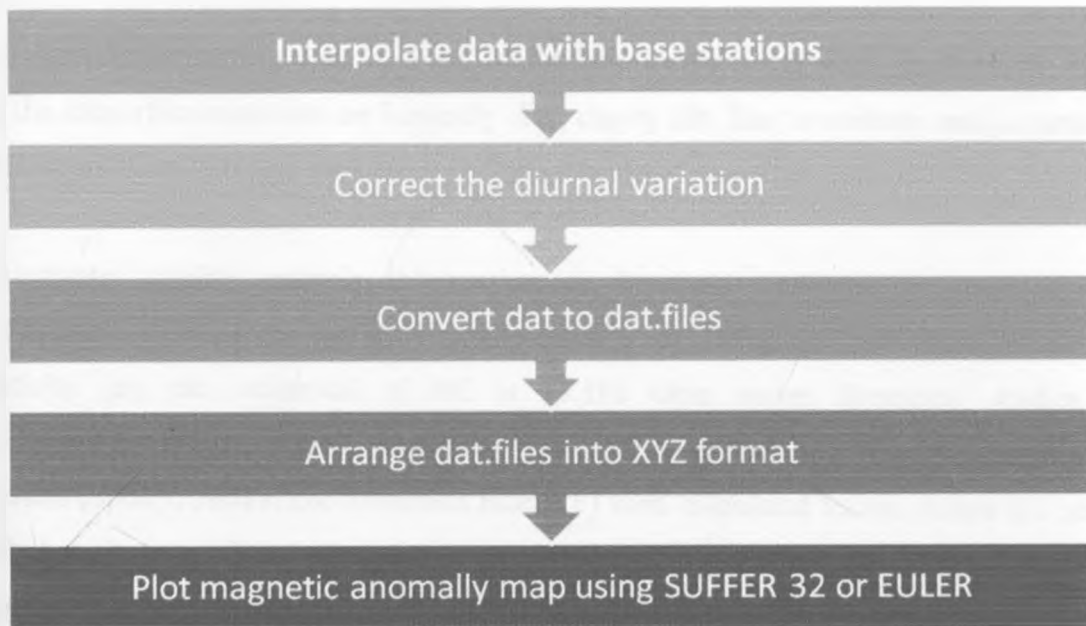
Figure 5.3: Stages involved in processing Magnetic data obtained in Kabatini aquifer.

5.5 Results and geological interpretation

Resistivity is a fundamental electrical property of rocks, which is closely related to rock lithology of which the main controlling factors are bulk rock porosity, pore structure, amount and salinity of water, temperature and the presence of clays. To convert the resistivity picture into a geological one requires some knowledge of the typical resistivity values for the different types of subsurface materials and geology of the surveyed area. Though most of the geological data from existing boreholes were unavailable, the information obtained from the available lithological log done by Prof. Mathu near location 0,E along profile A-B showed that the subsurface materials are basically clay, clayey silt, fine to medium sand, coarse sand, pebbles, boulders, tuff and lava.

Groundwater quality analysis information on boreholes indicate the mean electrical conductivity (EC) of the waters is approximately to 550µS/cm and therefore its mean resistivity (ρ), the reciprocal of EC is 18.181 Ohm meter. Empirical studies have demonstrated that a correlation exists between F and the particle size (fig.5.4) of sedimentary materials (Sporry, 2001) .The formation factor (F) were calculated for the station 0,E near the boreholes along profile A-B where vertical resistivity sounding surveys was carried out using the following formula.

$$F = \frac{\rho_f}{\rho_w}$$

where ρ_f is the resistivity of formation ,and ρ_w is the resistivity of pore water. This relation is a derivation from Archie's Law (Keller and Frischknecht, 1966). The general relationship between F and grain-sizes established in NW-Europe (Sporry, 2001) has been adopted as a rough guide, because it fitted well with borehole log and the calculated F values (fig 5.5 and Table 5.1).

F	Grain size
1	Clays
1.5 -2	Sandy clays
2 -2.5	Silty and clay Sands
3	Fine sands
4 – 5	Medium coarse sands
6 - 7	Coarse sands
> 8	Very coarse sands and pebbles

Figure 5.4: Relationship between F values and grain sizes from various studies in NW Europe

Lithological interpretation of station 0,E according to Archie's Law						Lithological interpretation according to borehole log done by Prof. Mathu's on profile A –B near station 0,E
DEPTH	EC	ρw	ρf	F	GRAIN SIZE	
0.787	550	18.181	40.194	2.210769	Silty and clayey sand	Brownish white loose soils
1.251	550	18.181	46.554	2.560585	Silty and clayey sand	Brownish white loose soils and gravel cemented by clay and ash
1.771	550	18.181	120.162	6.609207	Coarse sand	Gravel cemented by clay and ash
3.154	550	18.181	237.341	13.05434	Very coarse sand and pebbles	Brownish white loose soils and gravel cemented by clay and ash
4.931	550	18.181	156.829	8.625983	Very coarse sand and pebbles	Graded coarse sands and gravel cemented by argillaceous material
7.033	550	18.181	61.613	3.388867	Fine sand	Loose medium brown graded fine sands
12.911	550	18.181	40.818	2.245091	Clayey sand	Pale brownish (buff) tuff with a thin layer of sediments from 10 – 12 m depth
19.64	550	18.181	67.371	3.705572	Fine sand	Loose sediments of clay (20%), sand (30%) and gravel (30%) with trachyte and phonolite clasts Loose sediments of clay (20%), sand (30%) and gravel (30%) with trachyte and phonolite clasts Medium dark grey tuff and ash with few hard rock fragments and white patches of feldspar and ash
34.875	550	18.181	165.304	9.092129	Very Coarse sand and pebbles	Dark yellowish tuff with few medium to dark grey patches
59.832	550	18.181	142.246	7.823882	Very Coarse sand and pebbles	Weathered erosional horizon followed immediately by dark almost black basalt rock composed of a layer dominated by mafic minerals and subordinate quartz, Medium to slightly dark grey volcanic ash with lapith fragments (approx. 1 – 2 cm in size), Light grey pumiceous horizon with few rounded loose gravels, Medium grey rhyolite with obsidic fragments, Light tunic white tuff, Loose to cemented rounded clasts omposed of pumice pebbles, sands and occasionally cemented by brownish mud, Dark grey to black, tough moderately weathered rock with glassy sandstone phenocrysts, Brownish weathered rounded clasts of dark grey to black phonolite Medium grey highly felsic trachyte (tough rock)
106.905	550	18.181	67.764	3.727188	Fine sand	Greyish white tuff
165≥	550	18.181	21.759	1.196799	Clays	Greyish white tuff, not strongly indurated, and mixed with redish mud

Figure 5.5: F values of BH 8 in Kabatini aquifer which is located on the profile A – B (see fig.4.2)

Table 5.1: Borehole log (Courtesy of Prof. E. M. Mathu) compared with the vertical electrical sounding (VES) log from results shown in Figure 5.5 of station 1E,0. Borehole log information matches approximately well with the VES log.

Borehole log			VES log		
	Depth (m)	Rock Type	Depth (m)	Resistivity (ohm-m)	Resistivity (ohm-m)
A1	0 - 4	Brownish white loose soils and gravel cemented by clay and ash	0-4.93	Low to high	40.194 - 156.829
A3	8 – 16	Pale brownish (buff) tuff with a thin layer of sediments from 10 – 12 m depth	7.03-12.91	Low	40.818
A4	16 – 20	Loose sediments of clay (20%), sand (30%) and gravel (30%) with trachyte and phonolite clasts	12.911-19.64	moderate	67.371
A5	20 – 26	Buff white tuff (at the top) and medium to dark grey ash at the bottom	19.64-34.87	Moderate	165.304
A6	26 – 32	Medium dark grey tuff and ash with few hard rock fragments and white patches of feldspar and ash	34.87-59.832	Moderate	142.246
A7	32 – 34	Weathered erosional horizon followed immediately by dark almost black basalt rock composed of a layer dominated by mafic minerals and subordinate quartz			
A8	34 – 62	Medium to slightly dark grey volcanic ash with lapith fragments (approx. 1 – 2 cm in size)	59.832 - 106	Low	67.764
A9	62 – 66	Light grey pumiceous horizon with few rounded loose gravels			
A10	66 – 76	Medium grey rhyolite with obsidic fragments			
A11	76 – 78	Light tunic white tuff			
A12	78 – 80	Loose to cemented rounded clasts omposed of pumice pebbles, sands and occasionally cemented by brownish mud			
A13	80 – 92	Dark grey to black, tough moderately weathered rock with glassy sandstone phenocrysts			
A14	92 – 100	Brownish weathered rounded clasts of dark grey to black phonolite			
	100 – 106	Medium grey highly felsic			
A16	106 – 128	Trachyte ,Greyish white tuff, not strongly indurated, and mixed with redish mud	>106	Very Low resistivity Buried river horizon)	21.759

The aim of geological interpretation of resistivity sounding data is to determine the thickness and resistivity of different horizons from a study of the Vertical Electrical Sounding (VES) field curves and to use these results to obtain a complete geological picture of the area under investigation. The Vertical Electrical Sounding data obtained in this work was analyzed by using the Zohdy's method (1989) and computer based inversion using EarthImager software, which allows the performance of automatic interpretation of the Schlumberger sounding curves to obtain the equivalent n-layer model from the apparent resistivity curve of each sounding. This procedure was used for all the sounding points obtained in the study area, in order to obtain the equivalent apparent resistivity models of each sounding, their depths as well as thicknesses. Different curve types were identified in the area showing different geo-electric layers. These layers are of different shapes and characteristics which is typified by the formation. The numerous layers that were generated by the computer were grouped into relevant geologic depth intervals called geo-electric sections and the resulting layer parameters were then given geologic interpretation. The type of curves, the resistivity of the sediments and the lithological logs from nearby boreholes were used in conjunction with the knowledge of the local geology of the study as guides in the interpretation and analysis of the geologic section in terms of shallow structures and buried river channels. The knowledge of the local geology of Kabatini was used in constructing the earth model. The lithology indicates broadly that within the depth penetrated; the succession is clay, clay silt, and fine to medium sand, coarse sand, pebbles, boulders, tuffs and lava.

5.5.1 Interpretation of Vertical electrical sounding results

1. **Analysis of VES stations on profile A – B**

Profile A –B is located on the northern part (latitude 9971210) of the study area and consists of stations (1 W, 0), (0, 0), (1 E, 0) and (2E, 0)

a. **Station 1W,0**
Layers 1-3 have moderate resistivity values between 56.369 and 87.823 ohm meter. There is an ascending trend in the resistivity values from the surface to layer 5. The resistivity values then decline abruptly from 145.373 on layer five to 76.099 and 45.05 of layers 6 and 7 respectively. Layer 8 and 9 shows an increase in the resistivity values which declines again on layers 10, 11 and 12. The curve indicates two conductive layers, of which one is confined between layers 5 and 8. The other conductive layer begins from layer 10 to the layer 12(see

fig.5.6 and table 5.2). The thickness of layer 12 cannot be determined because it occurs at the bottom. The curve shows a combination of K – H – K

Figure 5.6: Resistivity values of layered earth model for station 1W,0 along profile A -B

Table 5.2: Table shows the layer thickness and resistivity for station 1W,0

Layer sequence from surface	Number of layers	Depth (meters)	Thickness (meters)	Resistivity (ohmmeter)
1	0-1	0.168	0.168	56.369
2	1-2	0.462	0.294	69.441
3	2-3	1.118	0.656	87.823
4	3-4	2.102	0.984	115.697
5	4-5	3.848	1.746	145.373
6	5-6	5.883	2.035	76.099
7	6-7	9.933	4.05	45.057
8	7-8	14.965	5.032	116.438
9	8-9	28.121	13.156	183.47
10	9-10	38.321	10.2	47.609
11	10-11	75.734	37.413	49.37
12	11-12	> 75.734	> 89.266	38.186

b. Station 0,0

The first layer of station (0,0) consist of very low resistivity material which could be clay saturated with water. Resistivity values for layers 2,3,4 and 5 are 20.1,44.3,215.1 and 657.5 ohm meter respectively. There is an ascenting trend of the curve for this layers. The values of layers 6,7,8, and 9 show descenting trend of the resitivity values indicating the shallow strucutres containing low resistivity at a depth of 15m. The inversion curves of K-H-K is observed in this station (fig. 5.7).
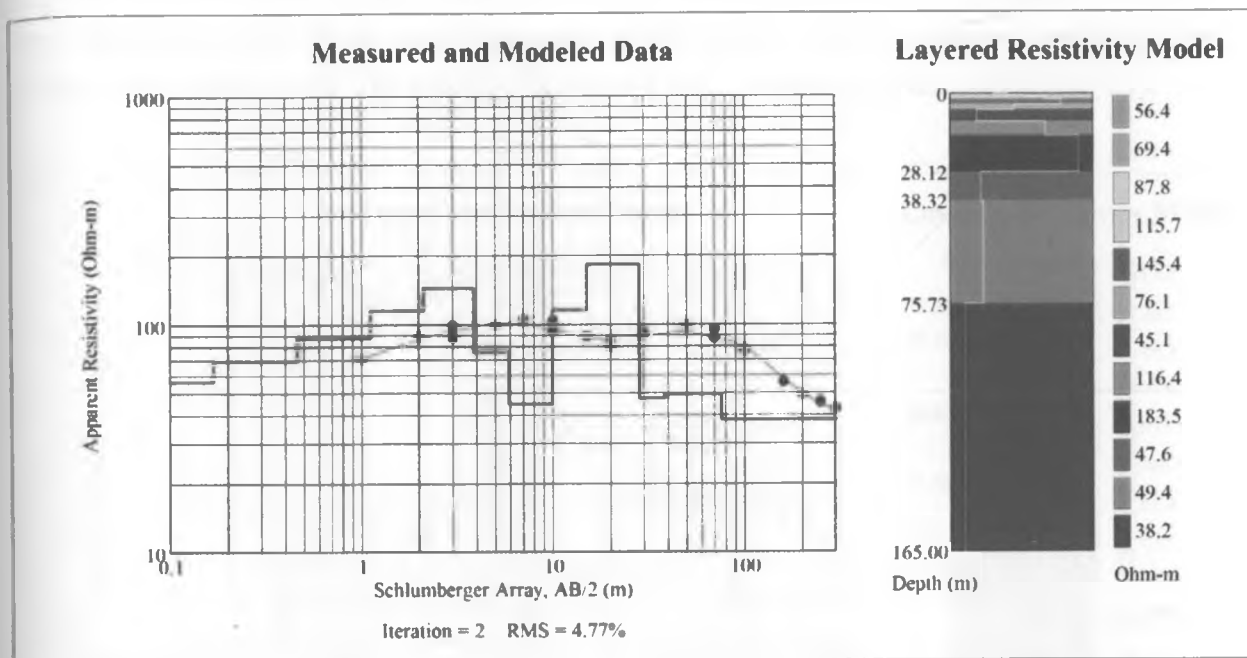

Figure 5.7: Resistivity values of layered earth model from station 0, 0 along profile A -B

Table 5.3: Table shows the layer thickness and resistivity for station 0,0

Layer sequence from surface	Number of layers	Depth (meters)	Thickness (meters)	Resistivity (ohmmeter)
1	0-1	0.11	0.11	12.051
2	1-2	0.374	0.264	20.118
3	2-3	0.646	0.272	44.303
4	3-4	0.868	0.222	215.083
5	4-5	2.465	1.597	657.49
6	5-6	4.3	1.835	306.877
7	6-7	5.736	1.436	65.377
8	7-8	17.33	11.594	42.538
9	8-9	29.304	11.974	89.849
10	9-10	56.09	26.786	179.792
11	10-11	81.084	24.994	78.814
12	11-12	> 81.084	>83.916	30.881

60

Layers 1, 2 and 3 have moderate resistivity values that indicate the presence of conductive materials (fig 5.7 and table 5.3). Resistivity values increases abruptly in layer 4, 5 and 6 indicating the presence of nonconductive material probably the boulder of Phonolite material. The resistivity values of layer 7 and 8 are low indicating the existence of conductive material in these two layers. Layers (more than 11.5 meters) showing the indication of shallow confined aquifer. The ninth and tenth layer indicates high to very resistivity respectively showing the presence of non conductive material in layer 10. The values of resistivity declines in layer 11 from 78 ohm meter to 30 ohm meter showing the presence of conductive body that goes deeper into the earth.

c. **Station 1E,0**

The resistivities of the first two thin layers from the surface are low. The values of resistivity rise abruptly in the second and third layers to 120 and 237.341 ohm meter respectively and begin to decline on the fifth layer and sixth layer as a result of highly conductive material (Table 5.4). This sixth layer is underlain by high resistivity material in the seventh and eighth layers. Drastic decline in resistivity values is observed in the eleventh and twelfth layer at the bottom. The curve of this station consists of K-H-K type (see fig 5.8).
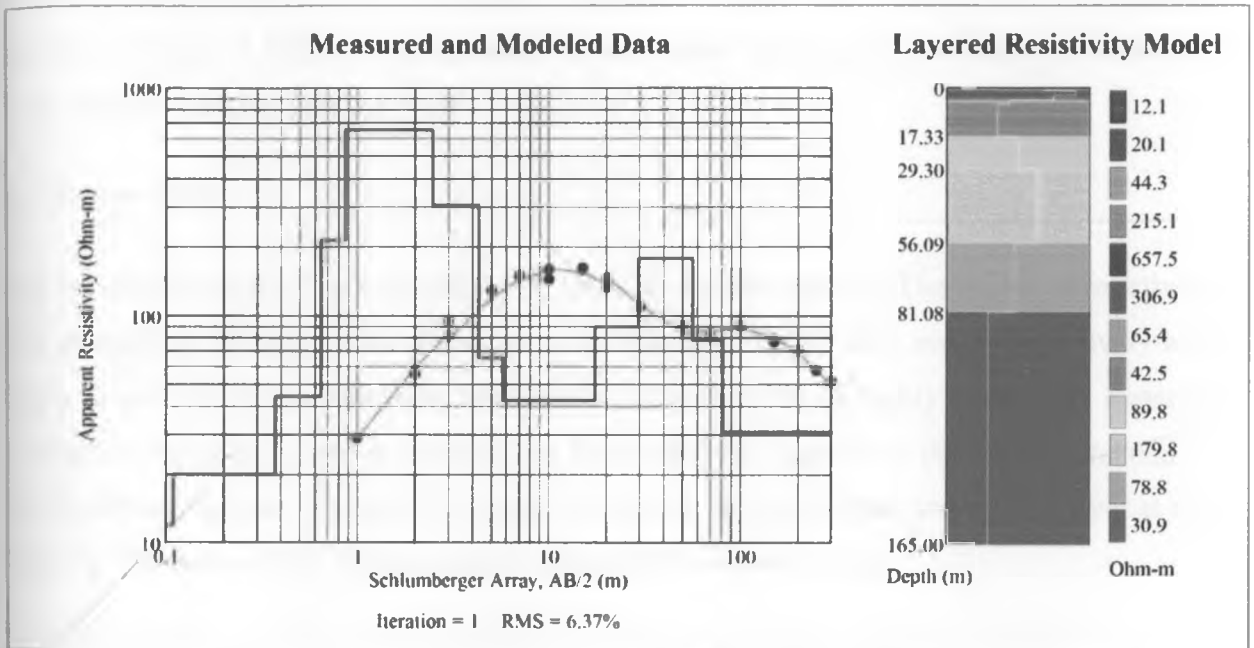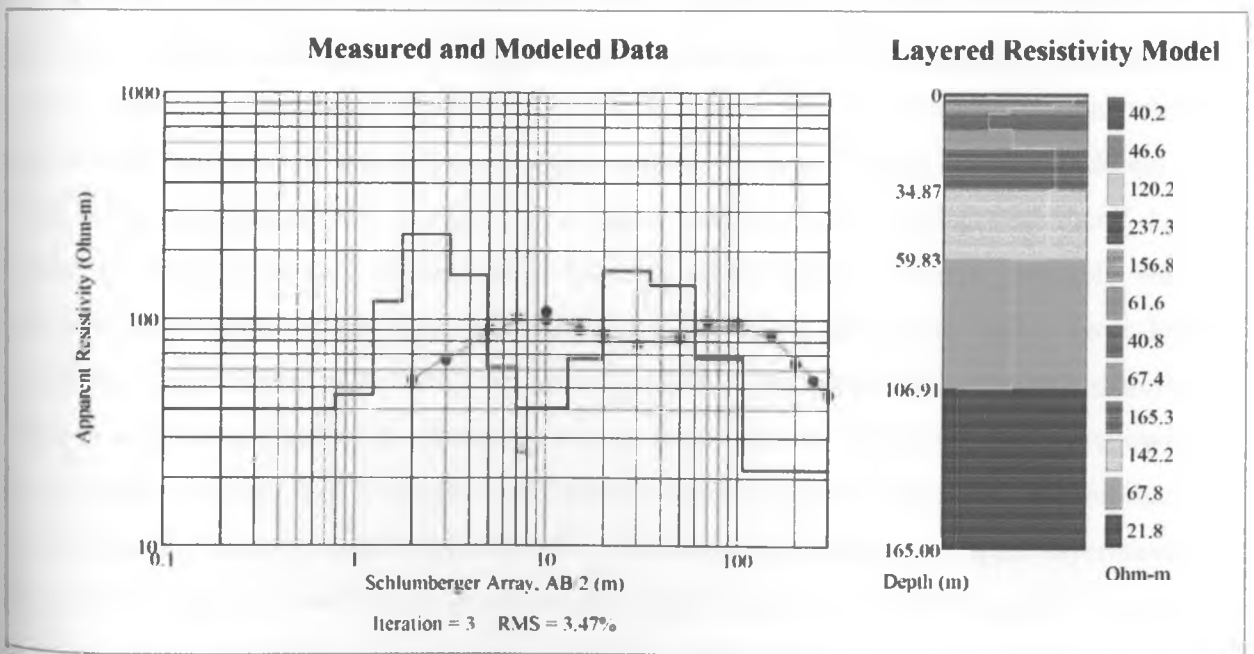

Figure 5.8, the shows the resistivity values of layered earth model from station 1E,0 along profile A –B on fig 4.2a

Table 5.4: Table shows the layer thickness and resistivity for station 1E,0

Layer sequence from surface	Number of layers	Depth (meters)	Thickness (meters)	Resistivity (ohmmeter)
1	0-1	0.787	0.787	40.194
2	1-2	1.251	0.464	46.554
3	2-3	1.771	0.52	120.162
4	3-4	3.154	1.383	237.341
5	4-5	4.931	1.777	156.829
6	5-6	7.033	2.102	61.613
7	6-7	12.911	5.878	40.818
8	7-8	19.64	6.729	67.371
9	8-9	34.875	15.235	165.304
10	9-10	59.832	24.957	142.246
11	10-11	106.905	47.073	67.764
12	11-12	>106.905	>58.095	21.759

d. Station 2E,0

This station occurs to the east of the of station 1E,0 on profile A-B. The first five layers from the surface are thin layers whose resistivity values vary from very low to moderately low. Resistivity value of layer one is 57.72 ohm meter indicating that this is a clay silty formation which is relatively dry. Layers 2, 3 and 4 (Table 5.5) have very low resistivity values which indicate the existence of a highly conductive material. Layer 6 which has the thickness of 3.598 m has moderate resistivity value that is higher than the underlying layer number 7. Low resistivity value of layer 7 shows that it has a good conductive material probably water saturated body forming the first upper aquifer. The eighth and ninth layers have high resistivity values indicating that these layers are probably Phonolite or have basaltic material. There is a declining trend of the resistivity values from layer 10 to the bottom layer showing the occurrence of very highly conductive material probably a second type of an aquifer that is semi confined. The curve displayed shows K –H curve pattern whereby an upper layer having high resistivity values overlies a lower layer with lower resistivity values (fig 5.9). This layer overlies a layer of higher resistivity values which is underlain by a layer with low resistivity values.

Measured and Modeled Data   **Layered Resistivity Model**

Figure 5.9, the figure shows the resistivity values of layered earth model from station 2E, 0 along profile A –B on fig 4.2a.

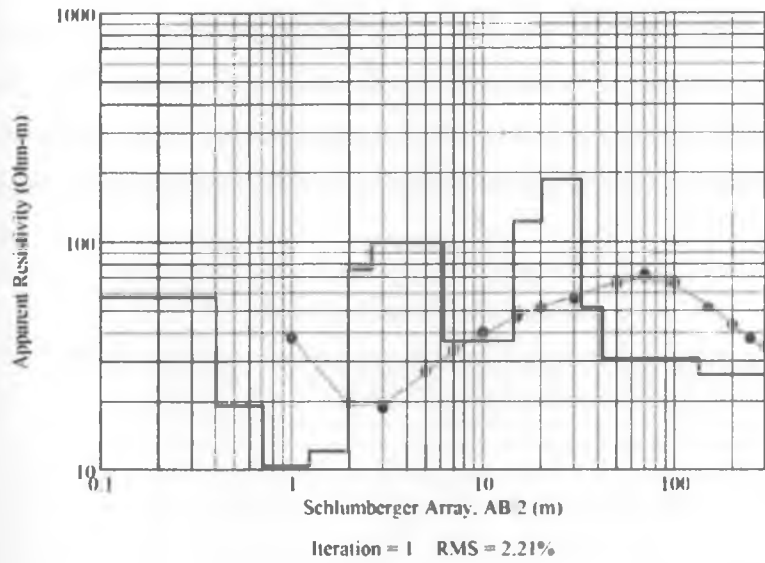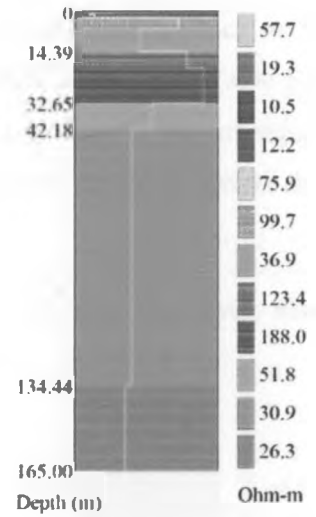Table 5.5: Table shows the layer thickness and resistivity for station 2E,0

Layer sequence from surface	Number of layers	Depth (meters)	Thickness (meters)	Resistivity (ohmmeter)
1	0-1	0.403	0.403	57.725
2	1-2	0.708	0.305	19.272
3	2-3	1.237	0.529	10.471
4	3-4	1.981	0.744	12.179
5	4-5	2.625	0.644	75.874
6	5-6	6.223	3.598	99.702
7	6-7	14.394	8.171	36.884
8	7-8	20.201	5.807	123.392
9	8-9	32.65	12.449	187.973
10	9-10	42.177	9.527	51.828
11	10-11	134.443	92.266	30.914
12	11-12	>134.443	>30.557	26.258

2. Analysis of Profile C-D

This profile occurs to the south of profile A – B along latitude 991160. The profile runs in the east to west direction and contains VES stations (1W,1 S),(0,1S),(1E,1S) and (2E,1S) whose coordinates are listed in table 4.1a

a. Station 1W,1S

The curve obtained in this station displays K-H-K pattern (fig 5.10). This indicates that the top most layers has lower resistivity values which increases up to the sixth layer and then declines on the seventh layer indicating the existence of high conductive material in a shallow structure (Table 5.6). The resistivity values increases again in the ninth layer to 152.864, but declines in the subsequent layers indicating another deeper structure containing conductive material up to the depth greater than 165 m.
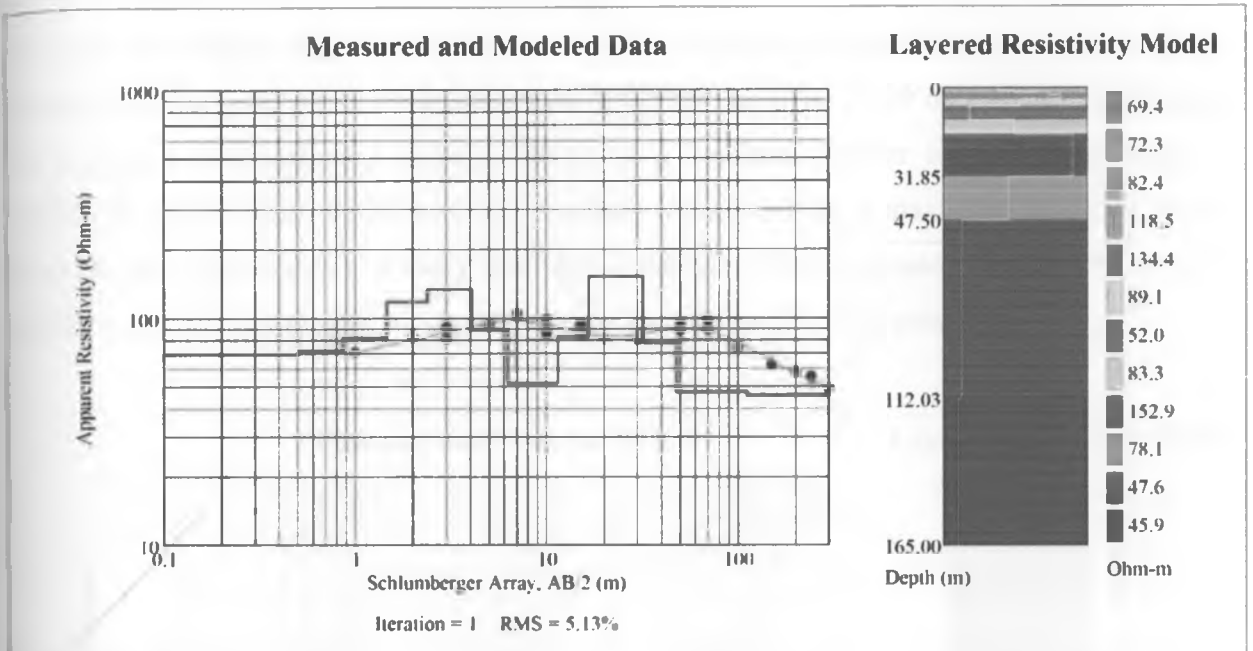

Figure 5.10, the figure shows the resistivity values of layered earth model from station 1W, 1S along profile C-D on fig 4.2a.

Table 5.6: Table shows the layer thickness and resistivity for station 1W,1S

Layer sequence from surface	Number of layers	Depth (meters)	Thickness (meters)	Resistivity (ohm meter)
1	0-1	0.506	0.506	69.435
2	1-2	0.861	0.355	72.268
3	2-3	1.461	0.6	82.398
4	3-4	2.39	0.929	118.52
5	4-5	4.078	1.688	134.42
6	5-6	6.255	2.177	89.128
7	6-7	11.451	5.196	51.971
8	7-8	16.568	5.117	83.258
9	8-9	31.846	15.278	152.864
10	9-10	47.499	15.653	78.083
11	10-11	112.028	64.529	47.588
12	11-12	>112.028	>52.972	45.91

b. Station 0,1S

The type of the curve observed in this station is a combination of Q-H-A (fig 5.11) indicating very high resistivity values on the bottom layer. The first layer on the top has high resistivity value of 140.88 ohm meter (Table 5.7). The resistivity values drops abruptly to 14.542 ohm meter in the second layer. The resistivity values increases slowly on the third, fourth and fifth layer and then begins dropping again on the sixth, seventh and eighth layer. The eighth layer whose thickness is 25.15 m thick has a low resistivity value of 20.05 ohm meter signifying the existence of conductive material which is a confined aquifer in shallow structure. Resistivity values begin to increase on the ninth layer reaching a maximum of 708.9 ohm meter on the tenth layer. The tenth layer has a thickness that is greater than 210 m which indicates that this layer could be part of an intrusion within the study area.
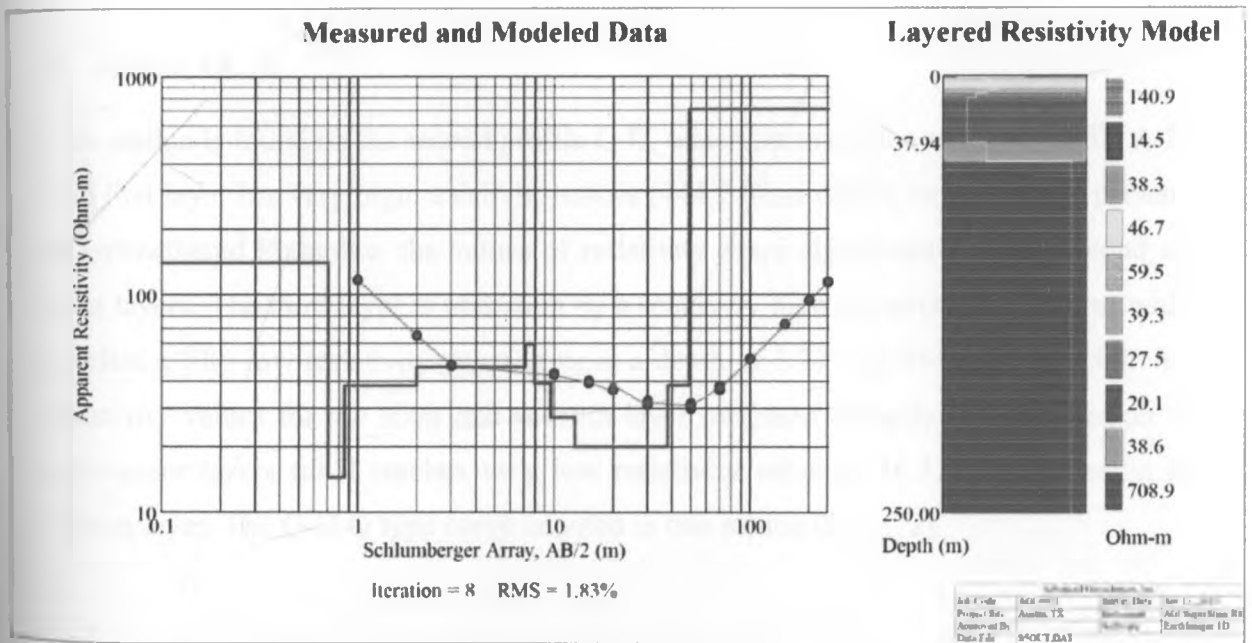

Figure 5.11, the figure shows the resistivity values of layered earth model from station 0,1S along profile C-D on fig 4.2a

Table 5.7: Table shows the layer thickness and resistivity for station 0,1S

Layer sequence from surface	Number of layers	Depth (meters)	Thickness (meters)	Resistivity (ohmmeter)
1	0-1	0.702	0.702	140.888
2	1-2	0.851	0.149	14.542
3	2-3	1.983	1.132	38.349
4	3-4	7.111	5.128	46.652
5	4-5	7.947	0.836	59.547
6	5-6	9.619	1.672	39.314
7	6-7	12.792	3.173	27.532
8	7-8	37.942	25.15	20.052
9	8-9	48.828	10.886	38.627
10	9-10	>48.828	> 201.172	708.861

c. Station 1E,1S

This station is found on the second profile C-D, which occurs to the south of profile A-B. The first layer has very high resistivity values (444.7 Ohm meter) indicating the presence of unweathered Phonolite, the values of resistivity drops significantly in the second and third layers. The third layer is underlain by a relatively high resistivity value layer which overlies a fifth low resistivity value layer at a depth of 3.77 to 6.844 m (Table 5.8). The resistivity values for the sixth and seventh layer increases abruptly but declines on the subsequent layers till it reaches very low resistivity value of 16.33 ohm meter on the bottom layer. The Q-H-Q type curve is noted in this station (fig 5.12).

Measured and Modeled Data   **Layered Resistivity Model**
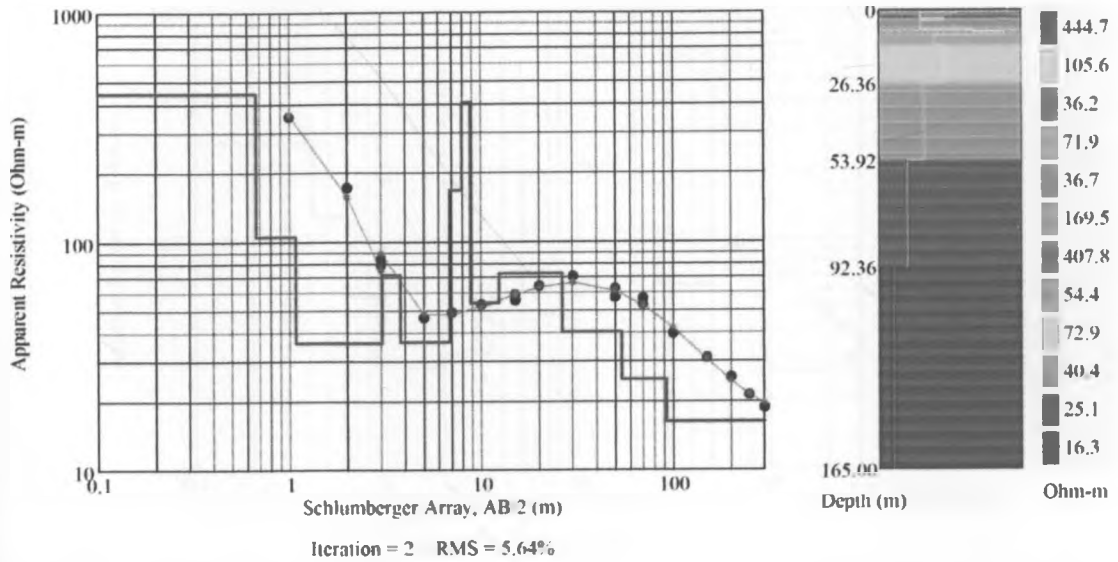
Iteration = 2   RMS = 5.64%

Figure 5.12, the shows the resistivity values of layered earth model from station 1E, 1S along profile C-D on fig 4.2a.

Table 5.8: Table shows the layer thickness and resistivity for station 1E,1S

Layer sequence from surface	Number of layers	Depth (meters)	Thickness (meters)	Resistivity (ohmmeter)
1	0-1	0 - 0.667	0.667	444.71
2	1-2	0.667 - 1.076	0.409	105.618
3	2-3	1.076 - 3.038	1.962	36.182
4	3-4	3.038 - 3.77	0.732	71.874
5	4-5	3.77 - 6.844	3.074	36.661
6	5-6	6.844 - 7.939	1.095	169.475
7	6-7	7.939 - 8.781	0.842	407.774
8	7-8	8.781-12.357	3.576	54.372
9	8-9	12.357 - 26.364	14.007	72.891
10	9-10	26.364- 53.924	27.56	40.38
11	10-11	53.924 - 92.365	38.441	25.076
12	11-12	> 92.365	> 72.635	16.33

d. Station 2E,1S

The first four layers show a decline in resistivity values (Table 5.9). Resistivity values begin to rise on the fifth layer up to the eighth layer. The values for the underlying layers show a decline up to the bottom layer which has 26.85 ohm meters. The curve shows an H - K. trend (fig 5.13)

Measured and Modeled Data — **Layered Resistivity Model**
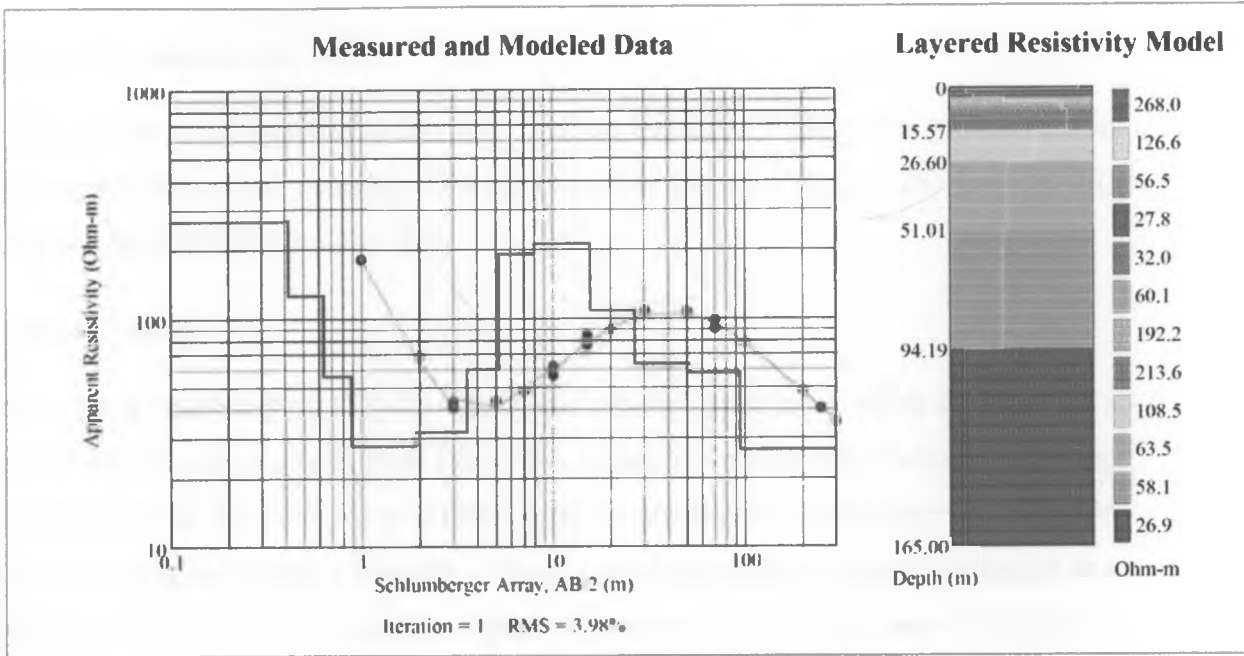
Iteration = 1   RMS = 3.98%

Figure 5.13, the shows the resistivity values of layered earth model from station 2E,1S along profile C-D on fig 4.2a.

Table 5.9: Table shows the layer thickness and resistivity for station 2E,1S

Layer sequence from surface	Number of layers	Depth (meters)	Thickness (meters)	Resistivity (ohmmeter)
1	0-1	0.417	0.417	268.038
2	1-2	0.632	0.215	126.637
3	2-3	0.881	0.249	56.459
4	3-4	1.911	1.03	27.813
5	4-5	3.516	1.605	31.989
6	5-6	5.176	1.66	60.103
7	6-7	7.952	2.776	192.174
8	7-8	15.565	7.613	213.598
9	8-9	26.605	11.04	108.47
10	9-10	51.007	24.402	63.481
11	10-11	94.191	43.184	58.1
12	11-12	> 94.191	>70.809	26.85

3. Analysis of Profile E – F

This profile occurs to the south of profile C – D along latitude 9971110. The profile runs in the east to west direction and contains VES stations (1W, 2S), (0, 2S), (1E, 2S) and (2E, 2S) whose coordinates are shown in table 4.2a.

a. Station 1W, 2S

This station has a resistivity of 131.433 ohm meter on the upper layer which increases to a maximum of 433.42 ohm meter in third layer. The resistivity values then decline steadily up to 63.73 ohm meter on the ninth layer (Table 5.10). The ninth layer has a thickness of 23.346 m thick with moderate resistivity because of having relatively high conductive material at a depth of 45.49 m from the surface. The resistivity values of the tenth layer increases to 118.937 ohm meter, but the drops gradually on the eleventh layer. Bottom layer has got very low resistivity as compared with the resistivity of the layers above it. The curve obtained in this station is a K –Q curve (fig. 5.14)
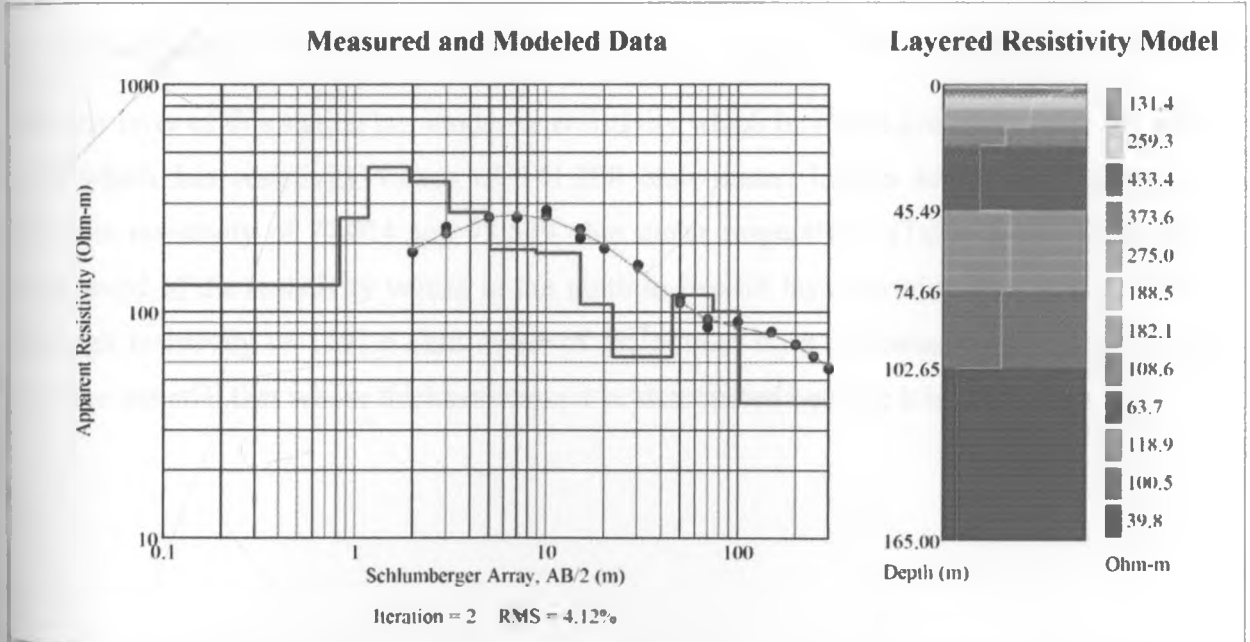

Figure 5.14, the shows the resistivity values of layered earth model from station 1W, 2S along profile E –F on fig 4.2a.

Table 5.10: Table shows the layer thickness and resistivity for station 1W,2 S

Layer sequence from surface	Number of layers	Depth (meters)	Thickness (meters)	Resistivity (ohmmeter)
1	0-1	0.832	0.832	131.433
2	1-2	1.172	0.34	259.29
3	2-3	1.934	0.762	433.42
4	3-4	3.11	1.176	373.622
5	4-5	5.05	1.94	275.005
6	5-6	8.827	3.777	188.497
7	6-7	15.026	6.199	182.08
8	7-8	22.144	7.118	108.646
9	8-9	45.49	23.346	63.73
10	9-10	74.662	29.172	118.937
11	10-11	102.651	27.989	100.521
12	11-12	>102.651	>62.349	39.775

b. Station 0,2S

The first layer of this station has moderate resistivity which increases gradually up to the fifth layer which has resistivity values of 141.208 ohm meter. Layers seven and eight have moderate resistivity of 72.024 and 73.539 ohm meter respectively (Table 5.11). There is a rising trend of the resistivity values in the ninth to twelfth layer forming K – A (fig. 5.15). The high resistivity of 1197.9 ohm meter of the bottom layer indicates the existence of an intrusive material that whose thickness cannot be determined because it is the bottom layer.

Measured and Modeled Data

Layered Resistivity Model
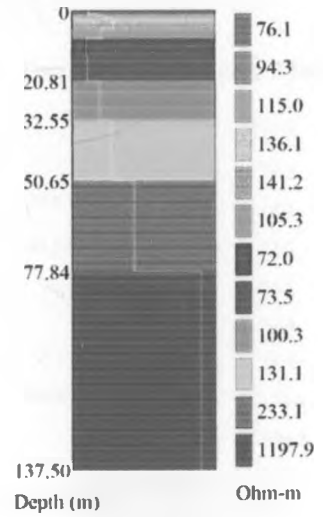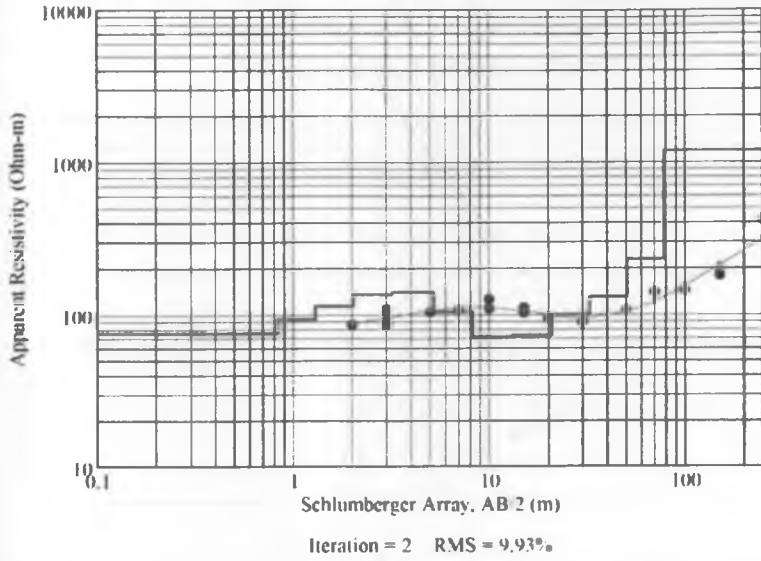
Iteration = 2   RMS = 9.93%

Figure 5.15, the shows the resistivity values of layered earth model from station 0,2S along profile E-F on fig 4.2a.

Table 5.11: Table shows the layer thickness and resistivity for station 0,2S

Layer sequence from surface	Number of layers	Depth (meters)	Thickness (meters)	Resistivity (ohmmeter)
1	0-1	0.835	0.835	76.126
2	1-2	1.301	0.466	94.278
3	2-3	2.026	0.725	115.022
4	3-4	3.19	1.164	136.146
5	4-5	5.19	2	141.208
6	5-6	8.196	3.006	105.301
7	6-7	13.103	4.907	72.024
8	7-8	20.813	7.71	73.539
9	8-9	32.554	11.741	100.28
10	9-10	50.651	18.097	131.08
11	10-11	77.84	27.189	233.072
12	11-12	>77.84	>59.66	1197.865

c. Station 1E,2S

The first layer in this station has a very low resistivity value which increases in the second layer (Table 5.12). The resistivity of the third layer indicates clay material overlying the fifth layer that has moderate resistivity of 84.426 ohm meter. The low resistivity values of the sixth and seventh layer

increase to the peak of 169.027 ohm meter in the ninth layer after which the trend declines to 23.546 ohm meter on the twelfth layer. The type of the curve formed in this station is K curve (fig 5.16)
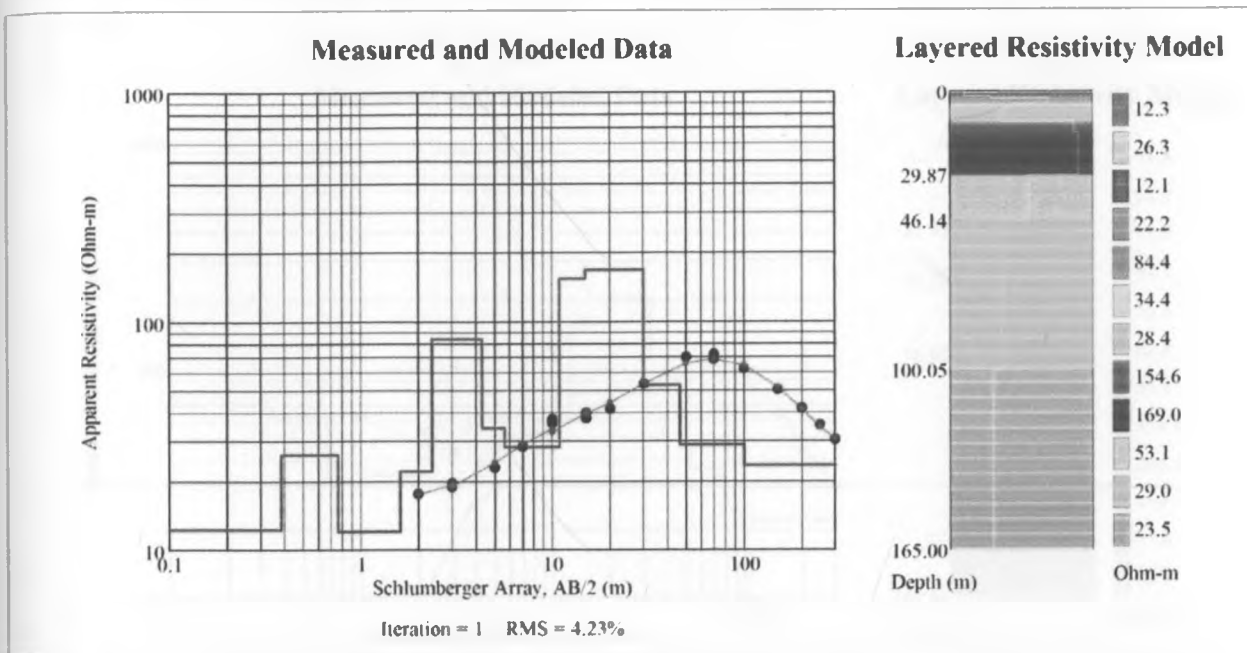

Figure 5.16: The figure shows the resistivity values of layered earth model from station 1E, 2S, along profile E –F (fig 4.2a)

Table 5.12: Table shows the layer thickness and resistivity for station 1E,2 S

Layer sequence from surface	Number of layers	Depth (meters)	Thickness (meters)	Resistivity (ohmmeter)
1	0-1	0.384	0.384	12.324
2	1-2	0.759	0.375	26.306
3	2-3	1.606	0.847	12.08
4	3-4	2.362	0.756	22.248
5	4-5	4.311	1.949	84.426
6	5-6	5.638	1.327	34.364
7	6-7	10.856	5.218	28.444
8	7-8	14.827	3.971	154.591
9	8-9	29.865	15.038	169.027
10	9-10	46.138	16.273	53.095
11	10-11	100.045	53.907	28.966
12	11-12	>100.045	>64.955	23.546

d. Station 2E,2S

The first layer shows moderate resistivity value of 71.483 ohm meter which declines up to 34.657 ohm meter in the fourth layer (Table 5.13). The trend of the resistivity values rises from the fifth

layer to the ninth layer. Resistivity values drops gradually from the tenth layer up to 22.119 ohm meter in the twelfth layer. The type of the curve obtained in the station is the H-K curve (fig 5.17).
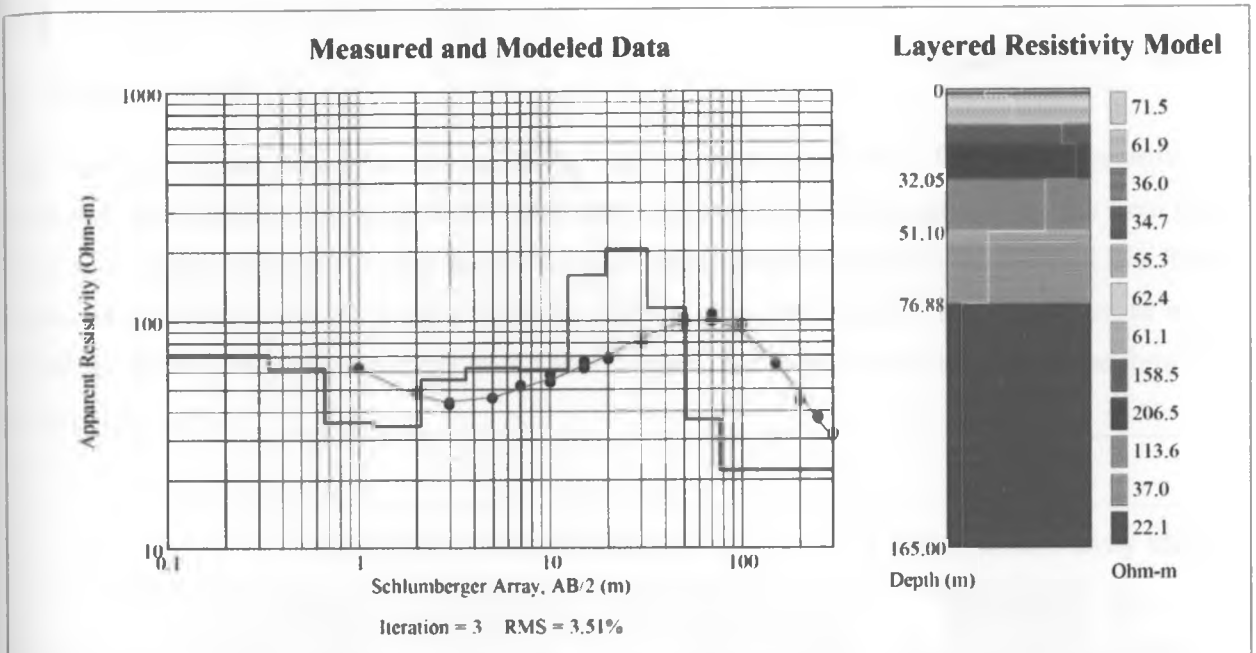

Figure 5.17, the figure shows the resistivity values of layered earth model from station 2E, 2 S along profile E-F on fig 4.2a

Table 5.13: Table shows the layer thickness and resistivity for station 2E, 2 S

Layer sequence from surface	Number of layers	Depth (meters)	Thickness (meters)	Resistivity (ohmmeter)
1	0-1	0.338	0.338	71.483
2	1-2	0.66	0.322	61.915
3	2-3	1.184	0.524	35.98
4	3-4	2.11	0.926	34.657
5	4-5	3.645	1.535	55.286
6	5-6	6.879	3.234	62.362
7	6-7	12.365	5.486	61.082
8	7-8	19.458	7.093	158.519
9	8-9	32.047	12.589	206.477
10	9-10	51.098	19.051	113.586
11	10-11	76.881	25.783	36.987
12	11-12	>76.881	>88.119	22.119

4. Analysis of Profile G – H

This profile occurs to the south of profile E - F along latitude 9971058. The profile runs in the east to west direction and contains VES stations (1W,3S),(0,3S),(1E,3S) and (2E,3S) whose coordinates are shown in Table 4.2a.

a. Station 1W,3S

The first layer of this station has low resistivity value of 41.42 ohm meter. The trend of resistivity increases up to 369.573 ohm meter in the fifth layer. The resistivity values then decreases from the sixth layer which has 234.194 ohm meter to 55.874 ohm meter in eighth layer (Table 5.14). The values of resistivity increases again slightly to 118.101 ohm meter after which it declines to low resistivity values of 32.293 ohm meter in the bottom layer. The curve of this station is in the form of K curve (fig 5.18).
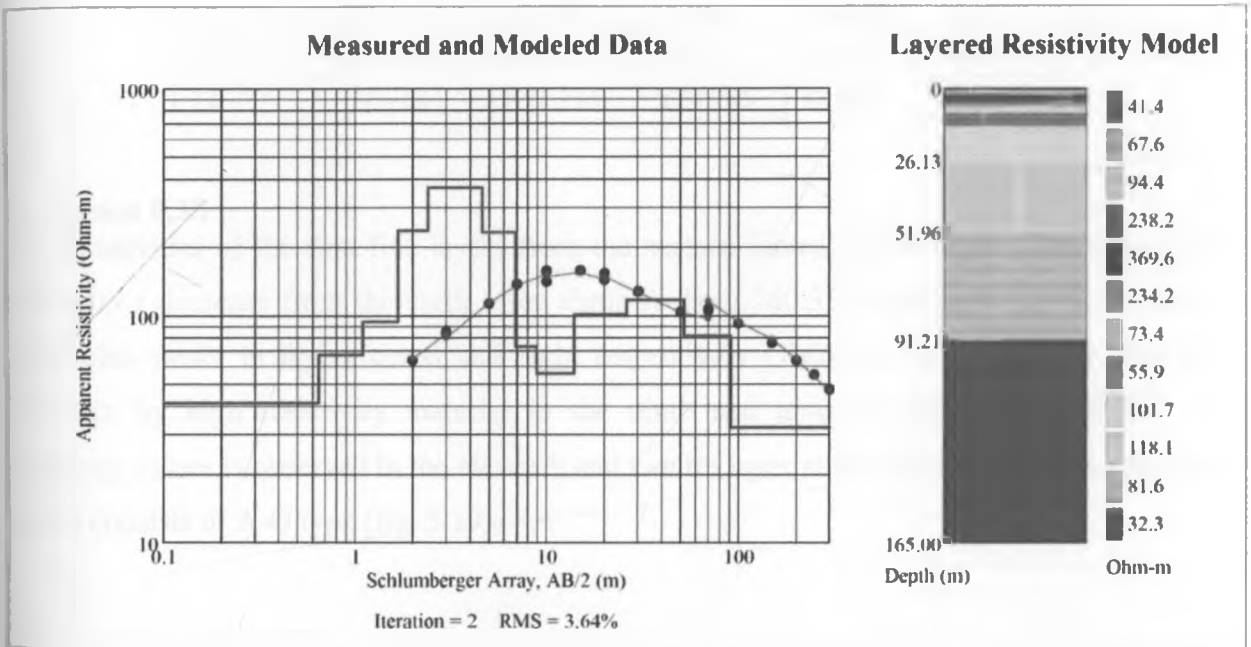

Figure 5.18, the shows the resistivity values of layered earth model from station 1W, 3S along profile G-H on fig 4.2a
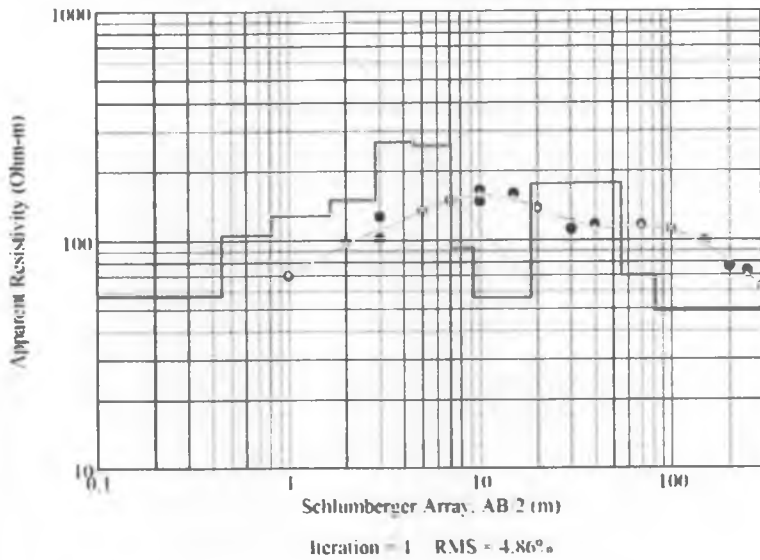
Table 5.14: Table shows the layer thickness and resistivity for station 1W,3 S

Layer sequence from surface	Number of layers	Depth (meters)	Thickness (meters)	Resistivity (ohmmeter)
1	0-1	0.647	0.647	41.42
2	1-2	1.095	0.448	67.56
3	2-3	1.673	0.578	94.399
4	3-4	2.396	0.723	238.203
5	4-5	4.618	2.222	369.573
6	5-6	6.901	2.283	234.194
7	6-7	8.882	1.981	73.36
8	7-8	13.906	5.024	55.874
9	8-9	26.126	12.22	101.737
10	9-10	51.962	25.836	118.101
11	10-11	91.215	39.253	81.617
12	11-12	>91.215	>73.785	32.293

b. Station 0,3S

The resistivities of the first five layers from the surface increase with depth. The values of resistivity r decrease from the sixth layer abruptly from 260.351 ohm meter to 92.497 and 56.11 ohm meter in layers seven and eight respectively (Table 5.15). The eighth layer is underlain by high resistivity material in the ninth and tenth layers. Drastic decline in resistivity values is observed in the eleventh and twelfth layer at the bottom. The curve of this station consists of A-Q type (fig. 5.19).

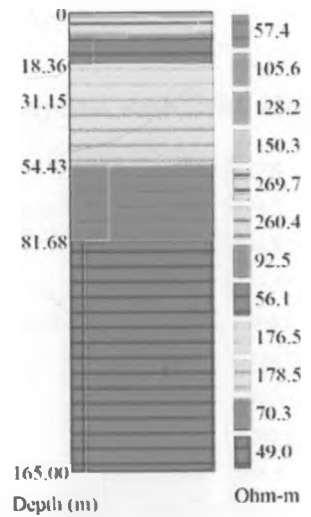**Measured and Modeled Data**   **Layered Resistivity Model**

Figure 5.19, the shows the resistivity values of layered earth model from station 0,3S along profile G-F on fig 4.2a

Table 5.15: Table shows the layer thickness and resistivity for station 0,3 S

Layer sequence from surface	Number of layers	Depth(meters)	Thickness (meters)	Resistivity (ohm meter)
1	0-1	0.444	0.444	57.45
2	1-2	0.813	0.369	105.589
3	2-3	1.648	0.835	128.166
4	3-4	2.851	1.203	150.294
5	4-5	4.495	1.644	269.716
6	5-6	7.047	2.552	260.351
7	6-7	9.191	2.144	92.497
8	7-8	18.364	9.173	56.11
9	8-9	31.151	12.787	176.518
10	9-10	54.431	23.28	178.47
11	10-11	81.676	27.245	70.323
12	11-12	>81.676	>83.324	48.994

c. **Station 1E, 3S**

The first layer in this station has low resistivity value which increases in the second, third, fourth, fifth and sixth layer (Table 5.16). The resistivity of the seventh layer is lower than the overlying and underlying layers. The low resistivity values of the seventh layer increase to the peak of 200.766 ohm

meter in the ninth layer after which the trend declines to 37.1151 ohm meter on the twelfth layer. The type of the curve formed in this station is K curve (5.20).
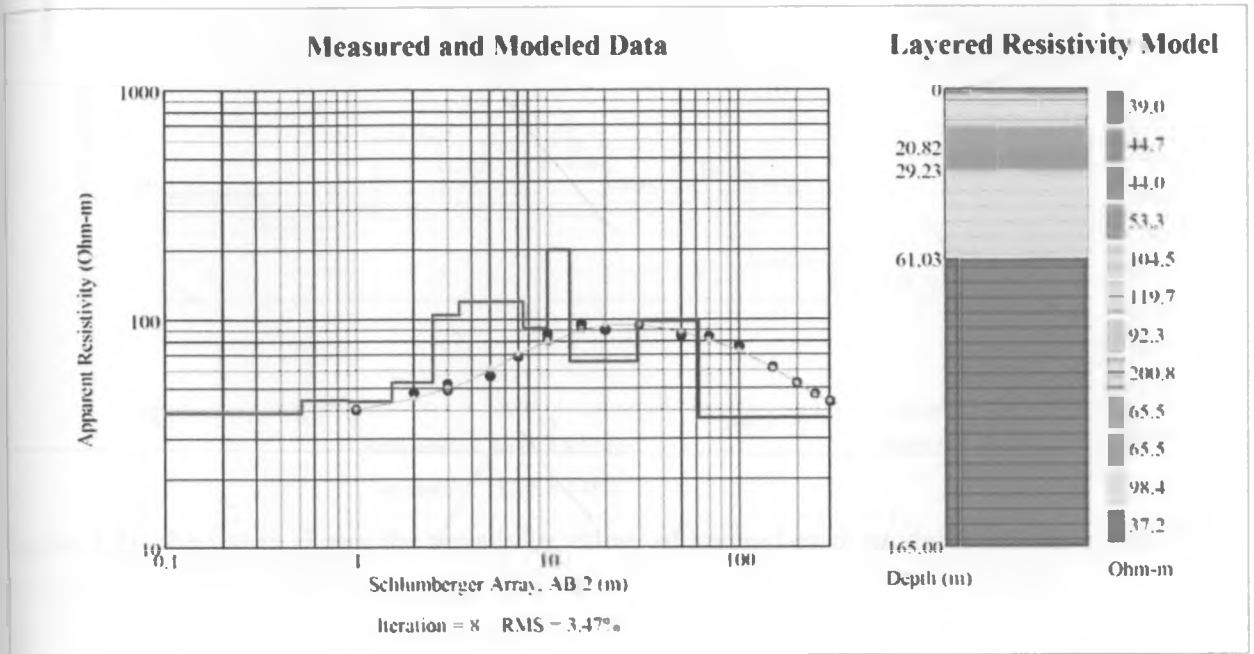

Figure 5.20, the shows the resistivity values of layered earth model from station 1E, 3 S along profile G-H on fig 4.2a
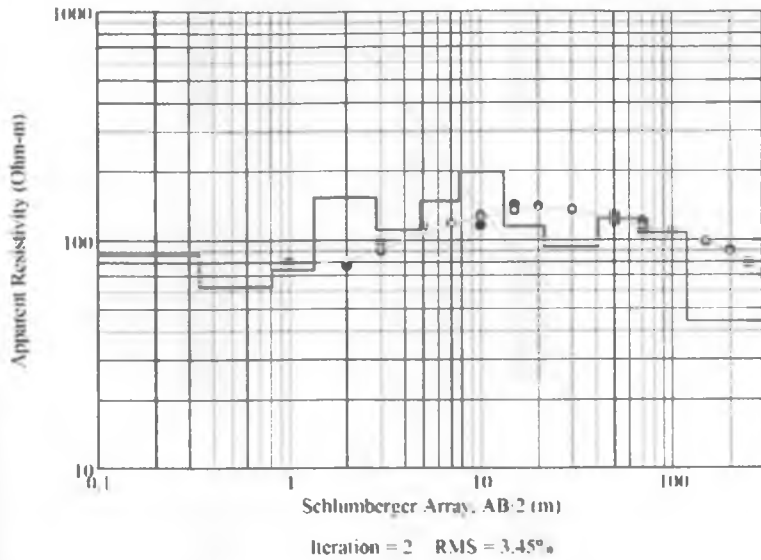
Table 5.16: Table shows the layer thickness and resistivity for station 1E, 3 S

Number of layers	Layer sequence	Depth(meters)	Thickness (meters)	Resistivity (ohm meter)
1	0-1	0.516	0.516	38.993
2	1-2	0.909	0.393	44.655
3	2-3	1.526	0.617	44.003
4	3-4	2.494	0.968	53.319
5	4-5	3.447	0.953	104.533
6	5-6	7.418	3.971	119.745
7	6-7	9.958	2.54	92.282
8	7-8	13.014	3.056	200.766
9	8-9	20.815	7.801	65.503
10	9-10	29.227	8.412	65.479
11	10-11	61.028	31.801	98.37
12	11-12	>61.028	>103.972	37.151

d. Station 2E,3S

The curve of this station indicate a general ascending trend corresponding to a gradual increase in the resistivity with depth up to 13 meters after which the resistivity falls gradually 44 ohm meter in the bottom layer (Table 5.17). The curve displayed at this station is K type curve (fig 5.21)
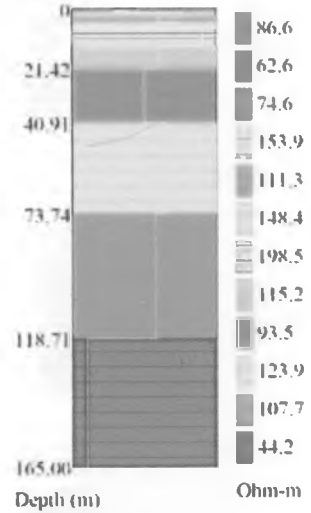
Figure 5.21, the figure shows the resistivity values of layered earth model from station 2E, 3S along profile G-H on fig 4.2a

Table 5.17: Table shows the layer thickness and resistivity for station 2E, 3S

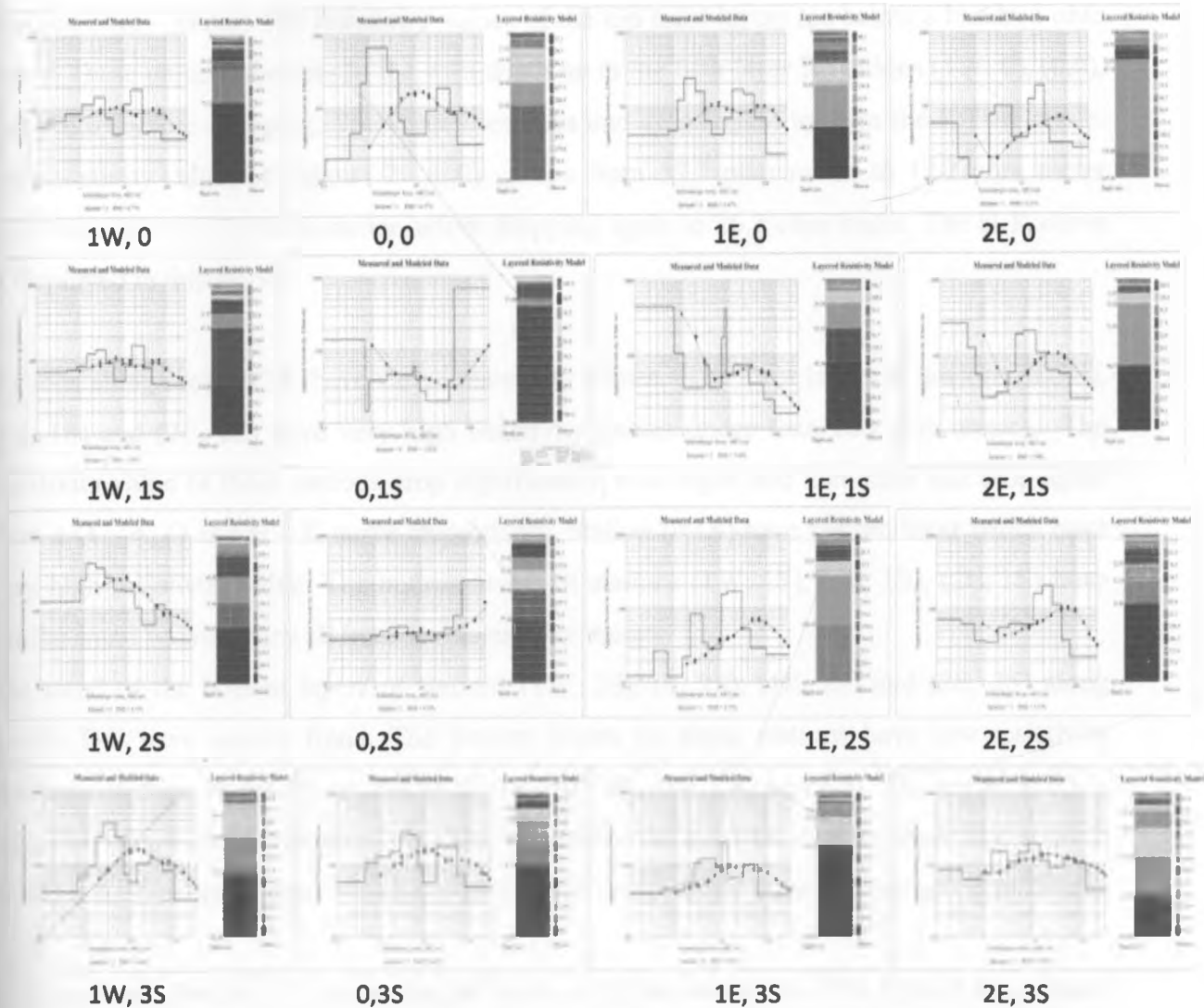| Number of layers	Layer sequence	Depth(meters)	Thickness (meters)	Resistivity (ohm meter)
1	0-1	0.337	0.337	86.643
2	1-2	0.805	0.468	62.571
3	2-3	1.339	0.534	74.643
4	3-4	2.834	1.495	153.908
5	4-5	4.811	1.977	111.317
6	5-6	7.645	2.834	148.388
7	6-7	13.204	5.559	198.546
8	7-8	21.42	8.216	115.164
9	8-9	40.91	19.49	93.452
10	9-10	73.744	32.834	123.949
11	10-11	118.706	44.962	107.717
12	11-12	>118.706	>46.294	44.216

Fig 5.21a: 1D resistivity earth models for interpretation of the four profiles in Kabatini aquifer; Profile A-B {(1W, 0), (0, 0), (1E, 0), (2E, 0)}, Profile C-D {(1W, 1S), (0,1S), (1E, 1S), (2E, 1S)}, Profile E-F {(1W, 2S), (0,2S), (1E, 2S), (2E, 2S)}, Profile G – H {(1W, 3S), (0,3S), (1E, 3S), (2E, 3S)}, on fig 4.2a

5.5.2 Comparison and similarity of the resistivity values of the four VES profiles

Profiles A – B and G – H (fig. 5.21a) have low resistivity values in the bottom layers indicating the presence of highly conductive material which could be water. Profile A – B occurs on the northern side of the study area, while profile G – H occurs on the southern part of the study area. Profiles C- D and E – F have bottom layers of high resistivity values at stations 0,1S and 0,2S respectively.

The bottom layers of stations (1W, 0), (0, 0), (1E, 0), (2E, 0) on profile A –B have low resistivity values. Resistivity values of all the four stations along profile A – B are below a

hundred ohm – meter. The resistivity values of the top most layers are below a hundred ohm meter. These values increases in the with depth up to the fifth layer in stations (1W, 0), (0,0), and (1E,0) before dropping. The value then rises and drops again to form the K-H-K curve. The resistivity values of station (2   E,0)   drops from 57.7 ohm meter to 12.2 ohm meter and then rises to 188.0 ohm meter before dropping again to 26.3 ohm meter. The H-K curve is displayed in this station.

Stations along profile C-D have varied resistivity values. Top most layers of stations (0, 1S), (1E, 1S) and (2E, 1S) have very high resistivity values (more than 100 ohm meter). The resistivity value of these stations drop significantly with depth and then rises and drop again form a Q – A, Q and H – K curve respectively. Station (0,1S) have bottom layer which have very high resistivity value. The bottom layers of stations (1W, 1S), (1E, 1S), (2E, 1S) have similar trend because they all have low resistivity values.

The trend of the bottom layers of stations (1W, 2S), (0, 2S), (1E, 2S) and (2E, 2S) along profile E-F have similar trend. The bottom layers for these stations have low resistivity readings. Bottom layers of stations (1W, 2S), (0, 2S), (1E, 2S) and (2E, 2S) are 39.8, 23.5, and 22.1 ohm – meter respectively. The resistivity value of the bottom layer for stations (0,2S) is 1197.9 ohm- meter which is very high as compared to other stations along profile E-F.

Stations along Profile G-H show similar trend on the bottom layers. The bottom layers have low resistivity values indicating the presence of highly conductive material. The trend shows that the top most layers have also low resistivity. These low resistivity values increases with depth and later drops in the bottom layers along this profile.

5.6.0   Iso – resistivity Maps

Horizontal and vertical Iso-resistivity maps were constructed in order to understand the variation of resistivity in two dimensions. Iso-resistivity maps are also used to show the geometry and location of the river channel in the study area.

5.6.1   2D Vertical Iso – resistivity maps

Apparent resistivity contouring was carried out along the four profiles to show variation of resistivity values with depth along the profiles.

5.6.1.1 Vertical section Iso – resistivity map of profile A –B

Iso- resistivity maps of profile A-B which occurs on the northern part of the study area (fig. 4.2). Vertical section of this profile shows that resistivity of values greater than 100 ohm – meter occurs between 0 m – 80 m depth. Resistivities values occurring below 80 m have are less than a hundred which indicates the presence of high conductivity material like a mass of water (fig.5.22). Very low resistance material occurring on the eastern part of the profile indicates the presence of the river channel in this location. The low resistance values extend beyond the depth of 165m showing that the depth of the river channel and the aquifer of Kabatini exceeds 165m.
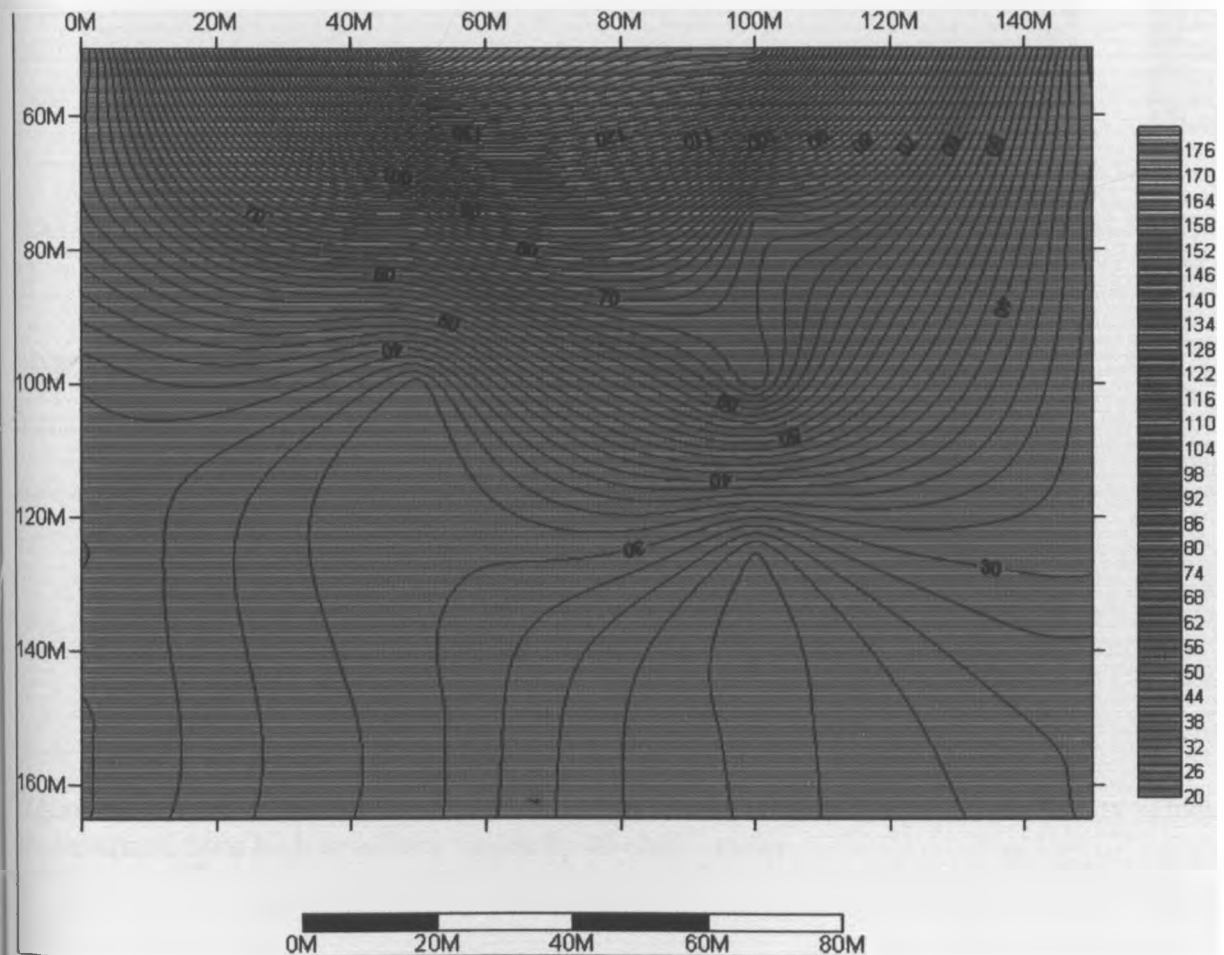

Figure 5.22: Vertical section for profile A – B (as shown on map 4.2a).

5.6.1.2 2D Vertical section of profile C-D

The eastern part of this pseudo-section has low resistivity values (fig. 5.23) indicating the location of the river channel. High resistance is observed from 50 m to a depth greater than 165 m between 40m to 60 m from C towards D on the western part of this profile. The depth of the aquifer along the profile is greater than 165m. The high resistance material observed along this profile could be the un-weathered Phonolite material.
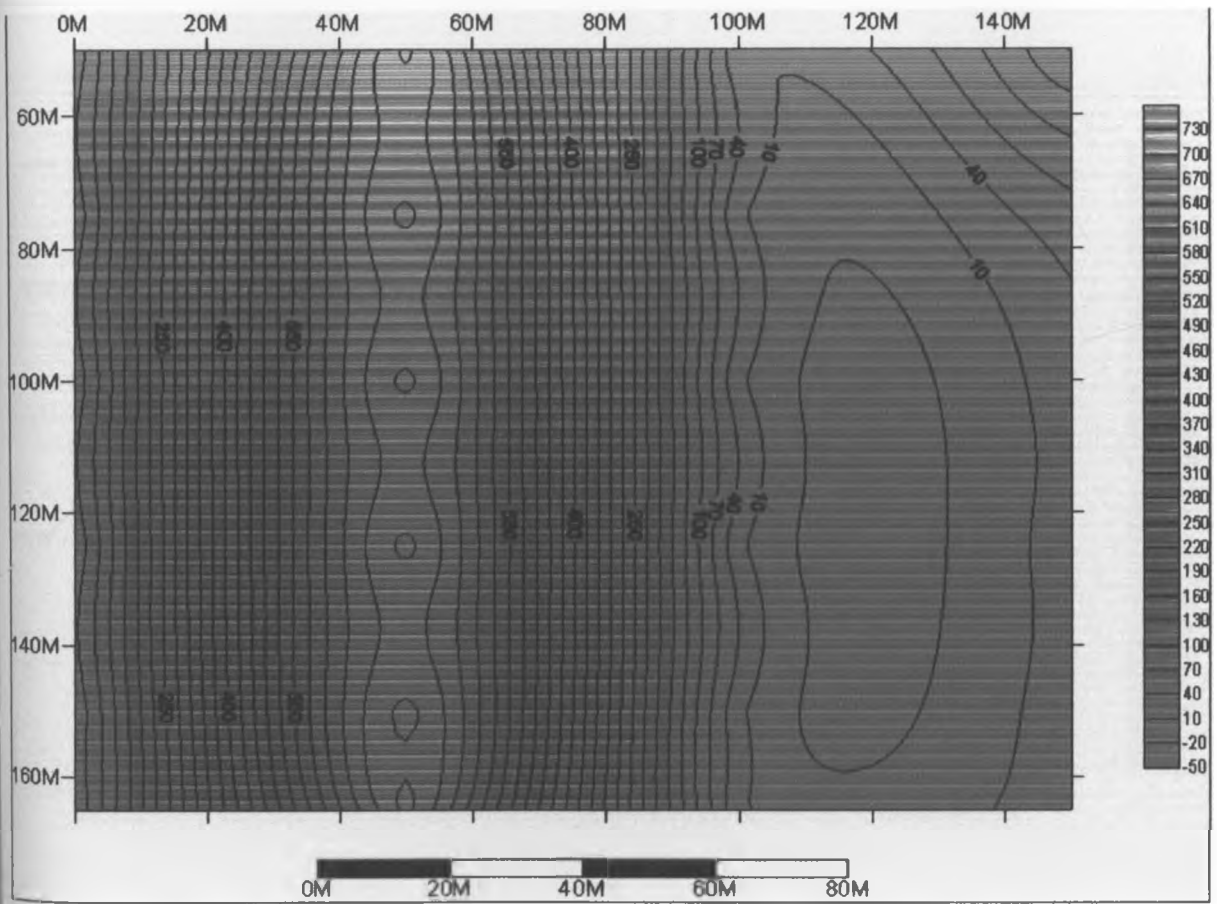

Figure 5.23: Vertical section for profile C – D (as shown on map 4.2a). Low resistivity values are separated from high resistivity values by 40 ohm – meter.

5.6.1.3 2D Vertical section of profile E-F

Vertical Iso – resistivity map of profile E-F shows higher conductivity material concentrating on the eastern part of VES profile while low conductive material occurring mostly on the western part of the area to the depth that is more than 165 m (fig 5.24). The low resistance material of the eastern part of the VES profile (fig.4.2a) indicates the presence of the river channel in the study area. The high resistance material on the eastern part of the profile E-F of the vertical electrical sounding pseudo-section (fig 5.24) indicates the existence of an intrusion in the study area.
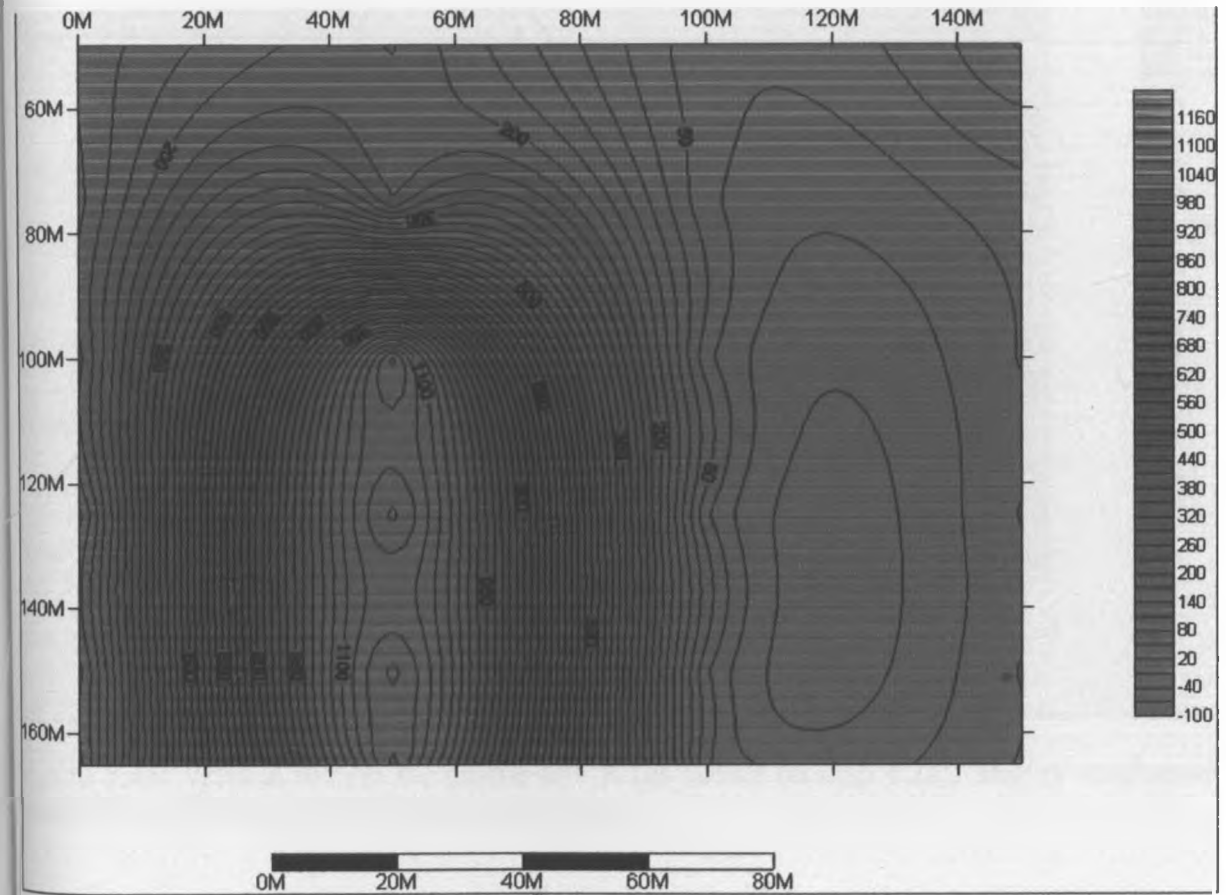

Figure 5.24: Vertical section for profile E – F (as shown on map 4.2a). Low resistivity values are separated from high resistivity values by 50 ohm – meter level contour.

5.6.1.4 2D Vertical section of profile G-H

Vertical Iso-resistivity of profile G-H (fig.4.2a) shows moderate resistance material non-uniformly distributed from the surface to the depth of a bout 100 m. (fig. 5.25). Low resistance material is also distributed non-uniformly along this profile. Very low resistance material is found to concentrate more on the eastern part of the profile G-H.
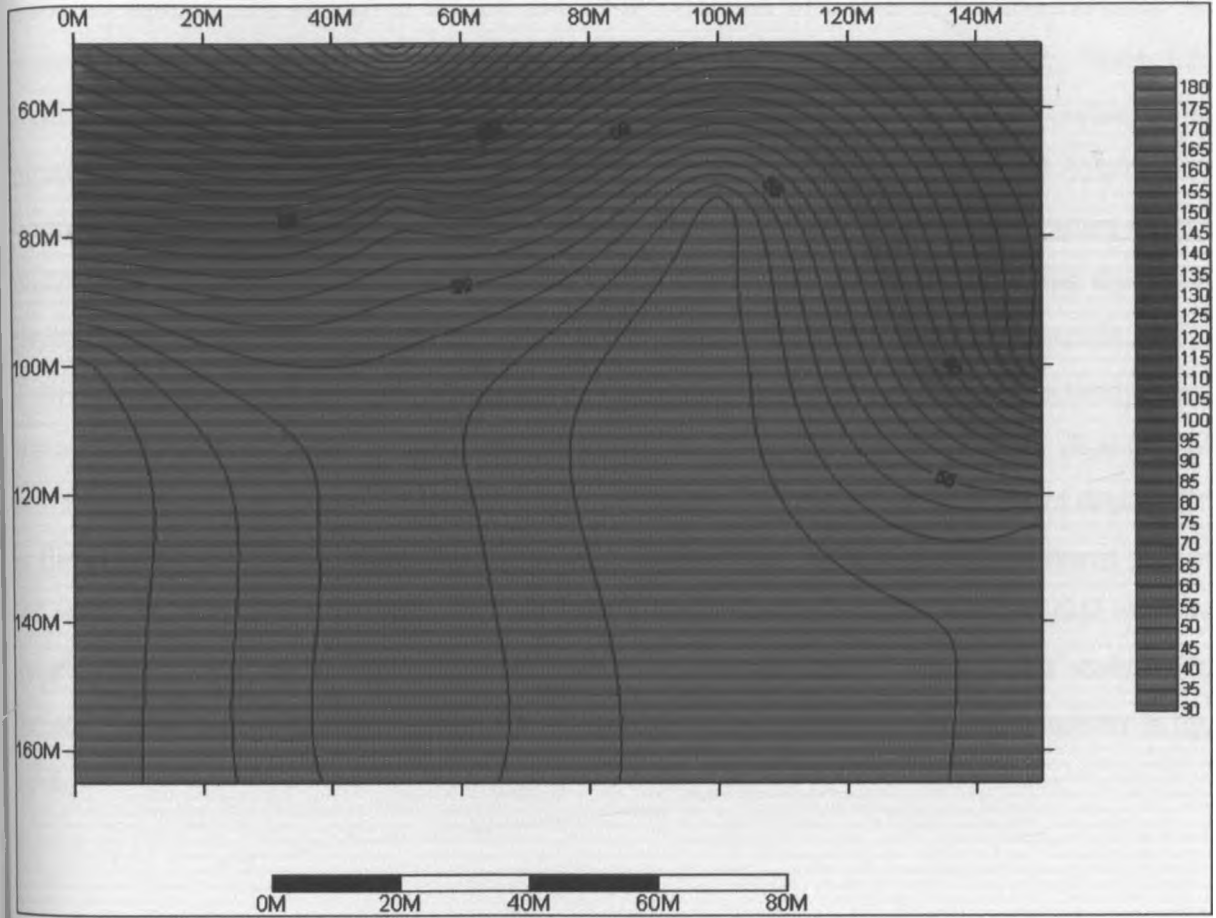

Figure 5.25: Vertical section for profile G – H (as shown on map 4.2a). Highly conductive material exists beyond 100m below the surface.

5.6.2 Horizontal Iso-resistivity Maps

Apparent resistivity contours through five depth levels were constructed. The depth levels through which this contours were constructed are 50 m depth level, 75 m depth level, 100 m depth level, 125 m depth level and 150 m depth levels. Iso –resistivity map for 50 m depth level indicates the trend of low resistivity values concentrating on the eastern part of the Kabatini aquifer. The pattern of the low resistivity contours with southerly trend indicates the presence of a conductive media in the direction of NNS – SSE (see fig 5.26). The linear like conductive media is a river flowing at a shallow depth of 50 meters below the surface. The figures for Iso – resistivity contours at the depth of 75 m, 100 m, 125 m and 150 m (see figures 5.27, 5.28, 5.29 and 5.30,) show the same pattern of low resistivity values on the Eastern part of the study area. The pattern whose trend is southerly indicates that there is a river flowing in the NNE – SSW direction. The trend is of Iso – resistivity contours is in N – S direction on the eastern part of the area at a depth of 125 m and 150 m respectively. This are contours showing deeper structure containing the buried river flowing in the direction of N – S. An overlay of the Iso – resistivity maps of 50 m depth, 75 m depth, 100 m depth, 125 m depth and 150 m depth produced the same pattern of low resistivity on the eastern part of the area (fig. 5.31). The high resistivity contours that concentrate on the western side indicate the presence of n intrusion the goes down beyond 165 meter depth. The intrusion observed in the study area and indicated by high resistivity values is modeled into three dimensions in fig. 5.32.
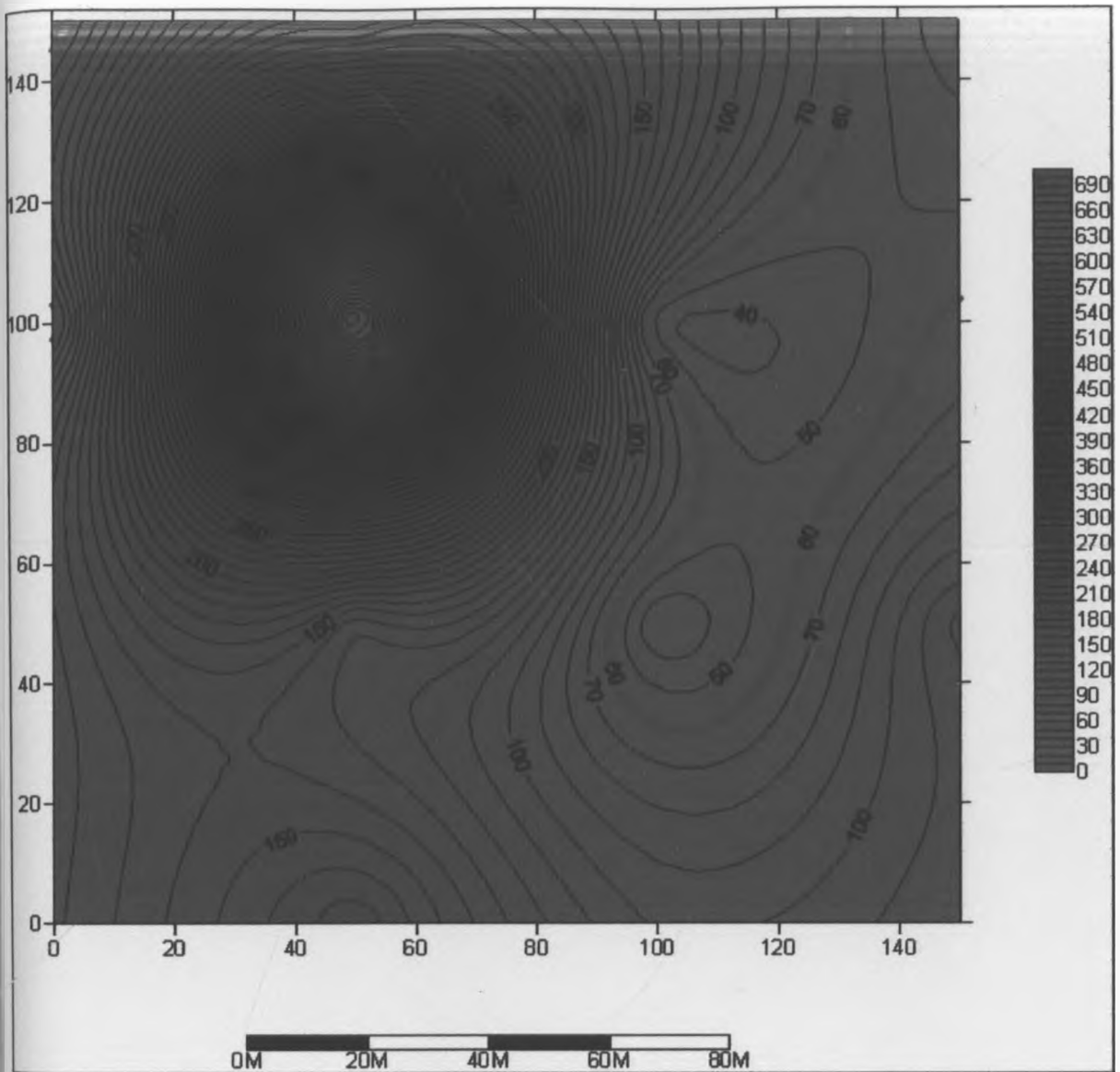
Fig 5.26: The Iso –Resistivity contour map of Vertical electrical resistivity sounding at a depth of 50 m. The river channel is geometrically oriented on the eastern part of the VES stations in north – south direction as indicated by 60 m contour (marked red).
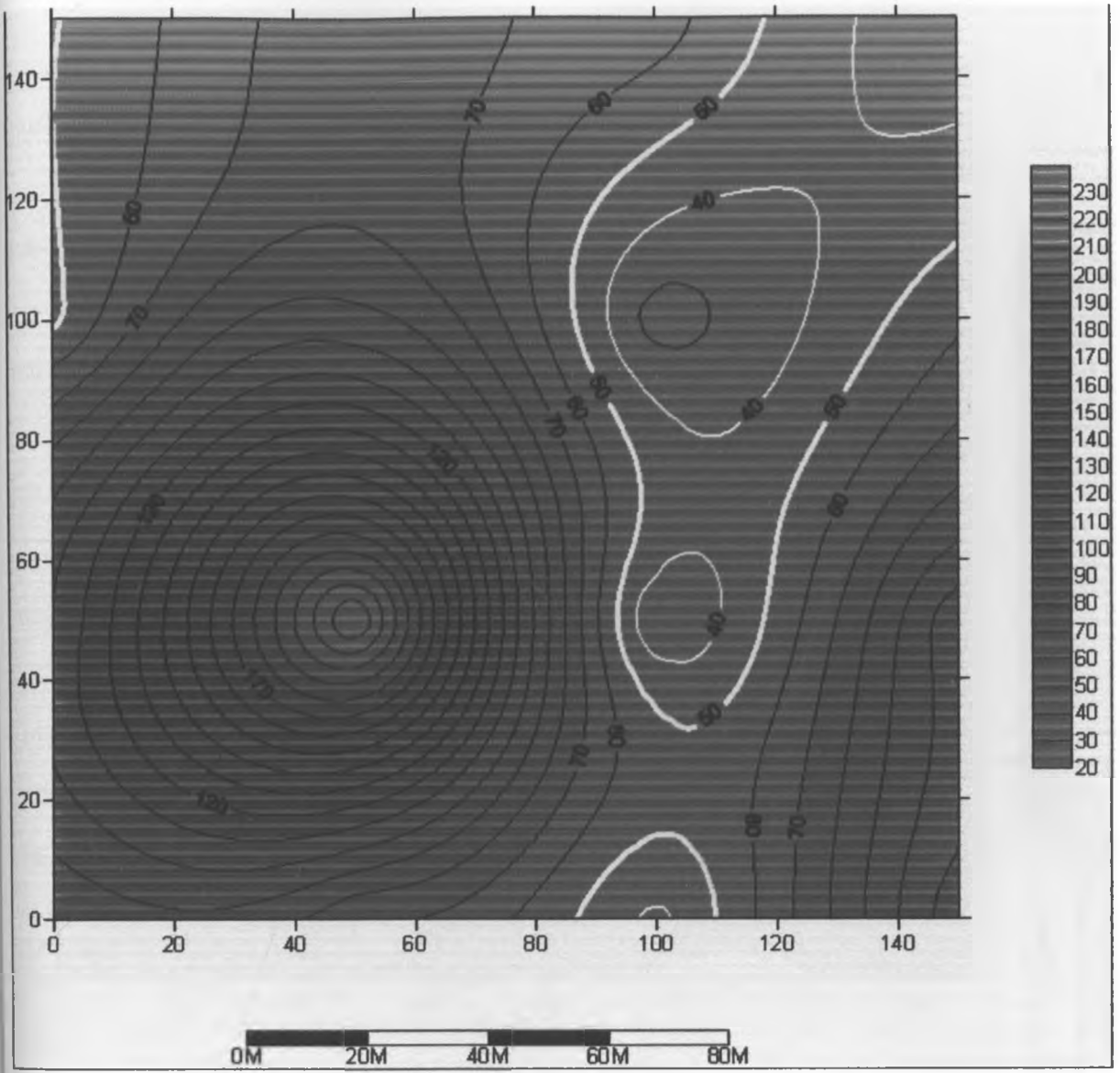
Fig 5.27: The Iso –Resistivity contour map at 75 meter depth for the Vertical electrical resistivity sounding.
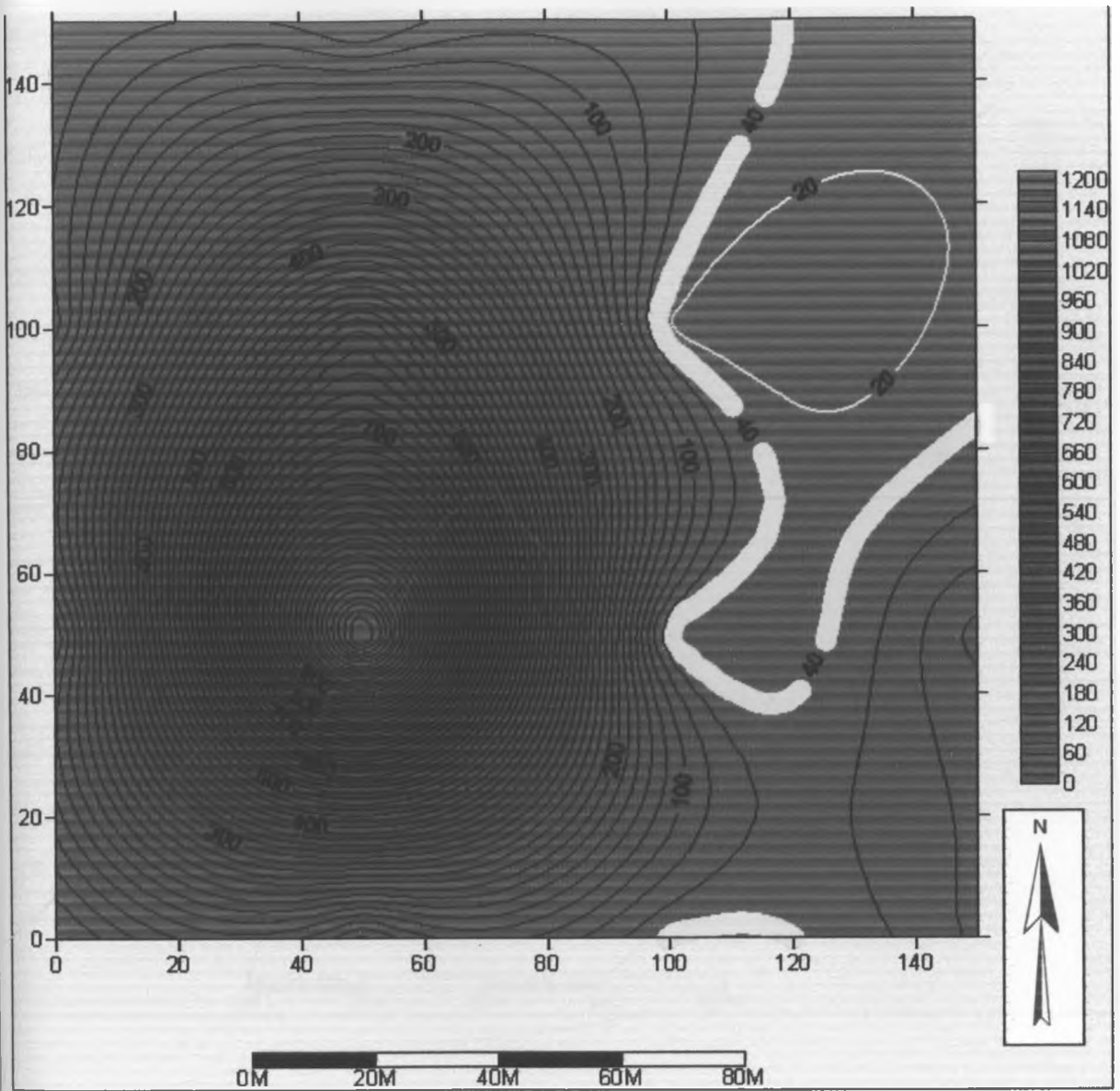
Fig 5.28: The Iso –Resistivity contour map at 100 meter depth for the Vertical electrical resistivity sounding. The river channel is geometrically oriented on the eastern part of the VES stations in north – south direction as indicated by 20 m and 40 m contour (marked yellow)
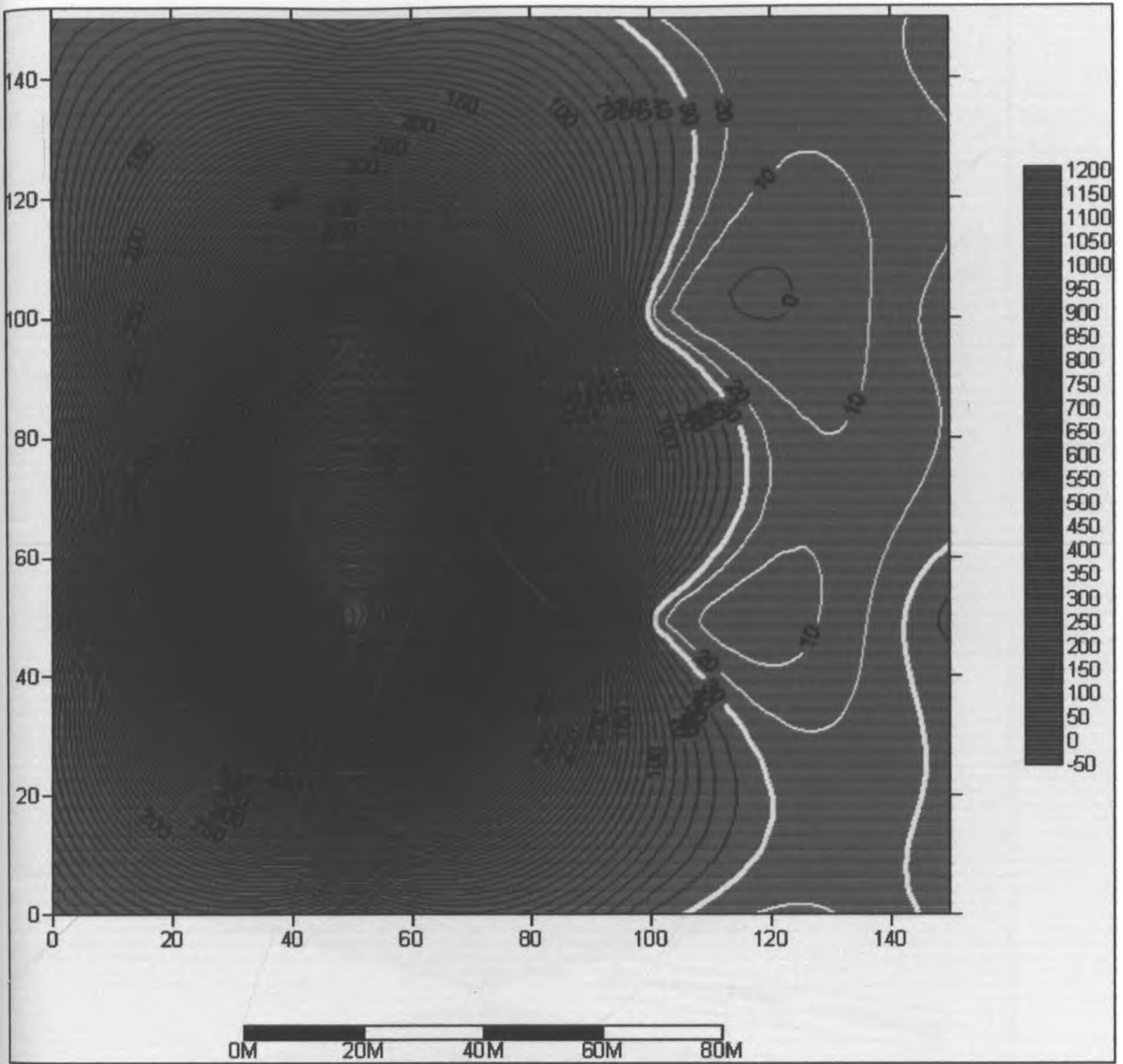
Fig 5.30: The Iso –Resistivity contour map at 150 meter depth for the Vertical electrical resistivity sounding. The river channel is geometrically oriented on the eastern part of the VES stations in north – south direction as indicated by 20 m and 30 m contour (marked yellow)
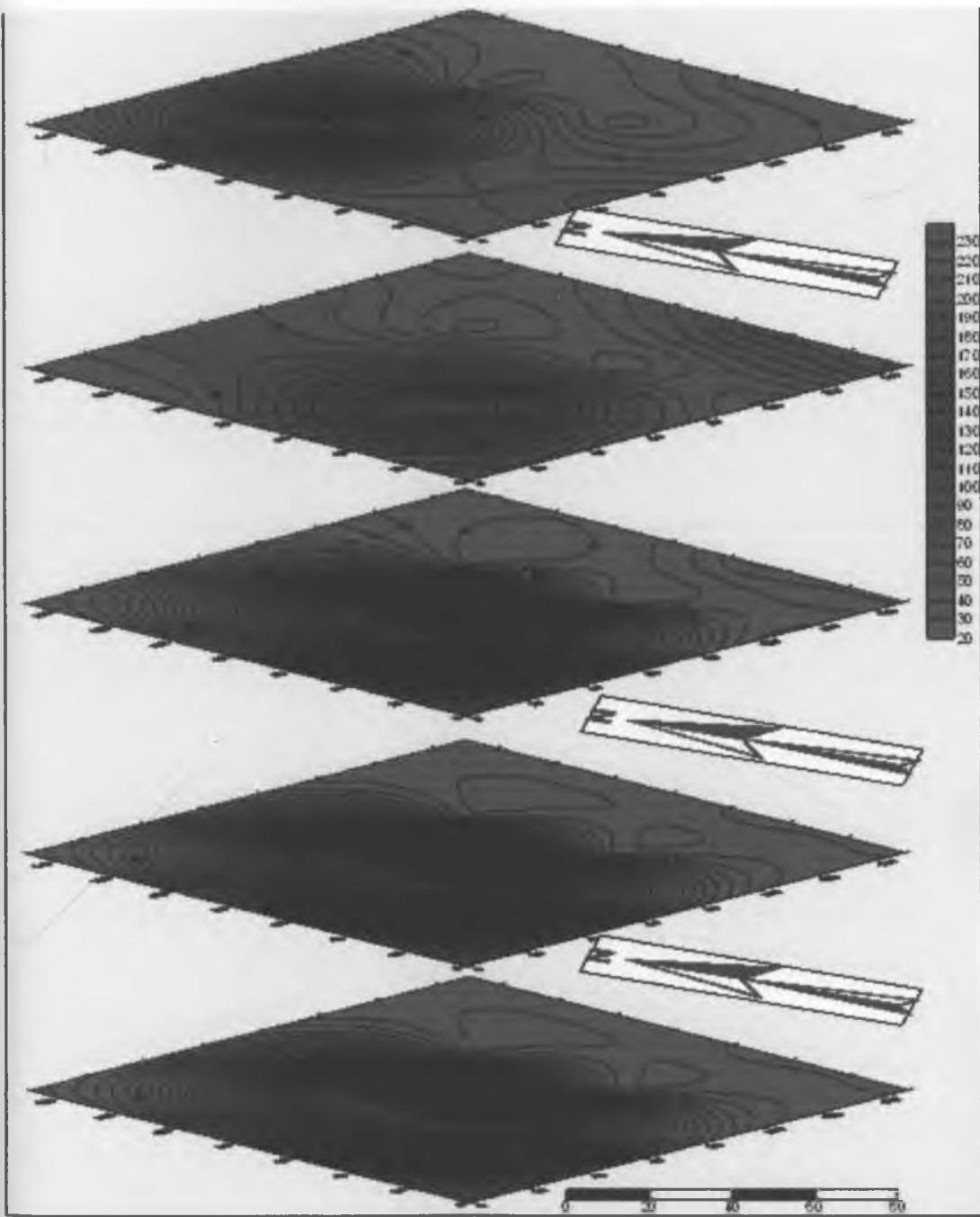
Fig 5.31: The overlay of Iso –Resistivity contour maps at 50 m75 m,100 m, 125 m, and 150 m, depth for the Vertical electrical resistivity sounding
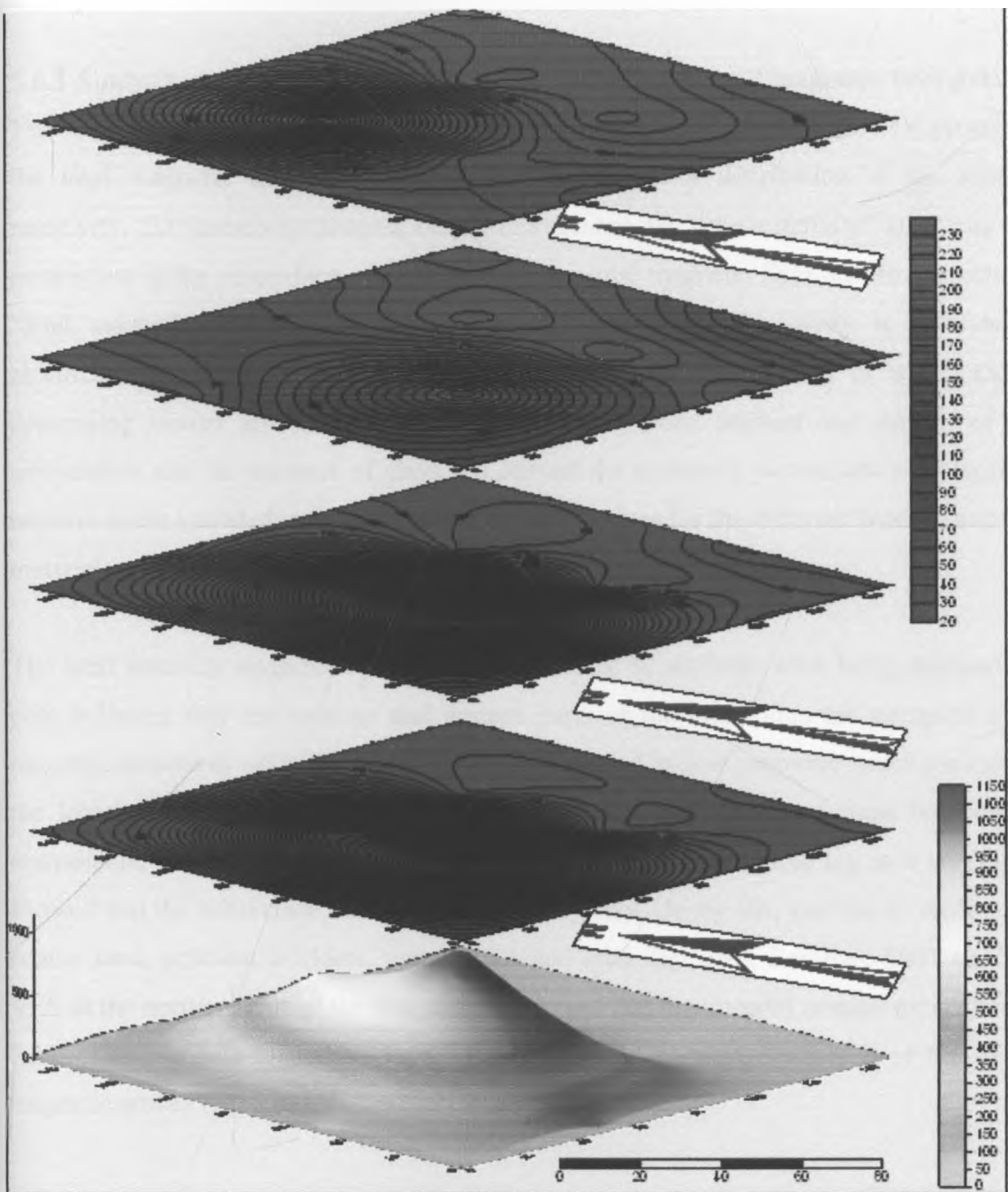
Fig 5.32: An overlay of Iso –resistivity maps and there 3D model indicating the trend of low resistivity values concentrating on the eastern part of the Kabatini aquifer with an intrusion on western side. The pattern of the low resistivity contours with southerly trend indicates the presence of a buried river channel.

5.6.3 Analysis and interpretation of electrical tomography and magnetic field data

The inversion results of the 2D Resistivity Imaging data with the RES2DINV program and the total magnetic data results gave similar patterns of distribution of the subsurface resistivity. 2D Resistivity imaging output represented the "true resistivity" and "true depth" parameters of the subsurface materials whiles the total magnetic field results represented the "total magnetic field" and "apparent depth" parameters. Resistivity is a fundamental electrical property of rocks that is closely related to rock lithology of which the main controlling factors are bulk rock porosity, pore structure, amount and salinity of water, temperature and the presence of clays. To convert the resistivity picture into a geological one requires some knowledge of the typical resistivity values for the different types of subsurface materials and geology of the surveyed area.

The total intensity magnetic map made using suffer 32 software after being reduced to the pole indicates that the western and eastern parts of the study area are occupied by high magnetic structures while the central part is represented by low magnetic structures indicating the location of the buried river. Though the geological data from most boreholes was unavailable, the lithological log information obtained from borehole log at 0,1E (Fig. 4.2) showed that the subsurface materials are basically clay, clayey silt, and fine to medium sand, coarse sand, pebbles, boulders, pyroclastics and lava (fig.5.36). Barongo, 2007 carried out VES in the northern part of the area and deciphered that the material contain pyrocalstics (fig 5.33a).The borehole logged by Prof. Mathu is in line with profile A – B of the ERT and magnetic survey (fig 5.33).
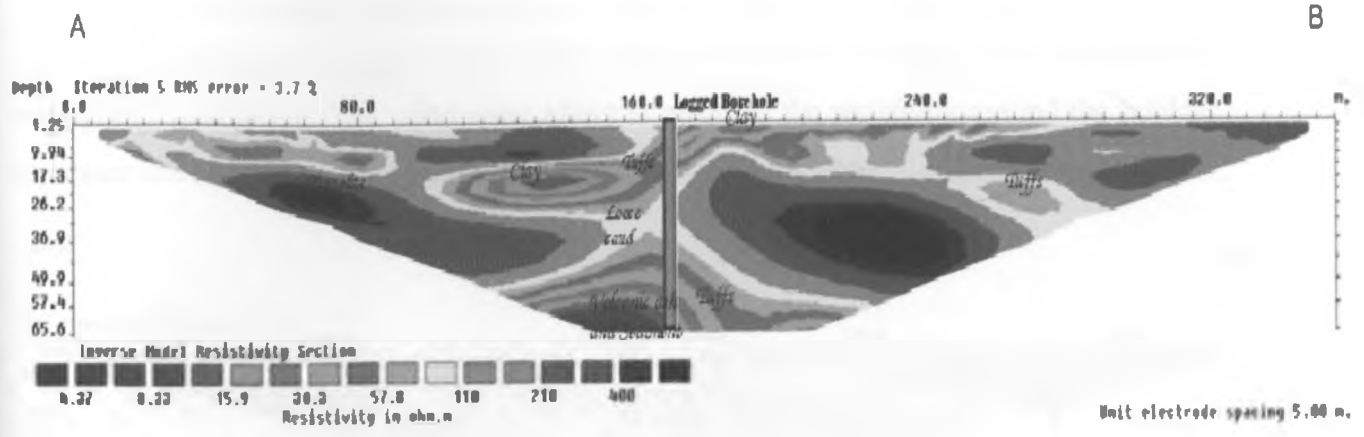
Fig 5.33: Pseudo section of profile A – B, showing the rivers channel at the tip of the bore hole and other shallow structures
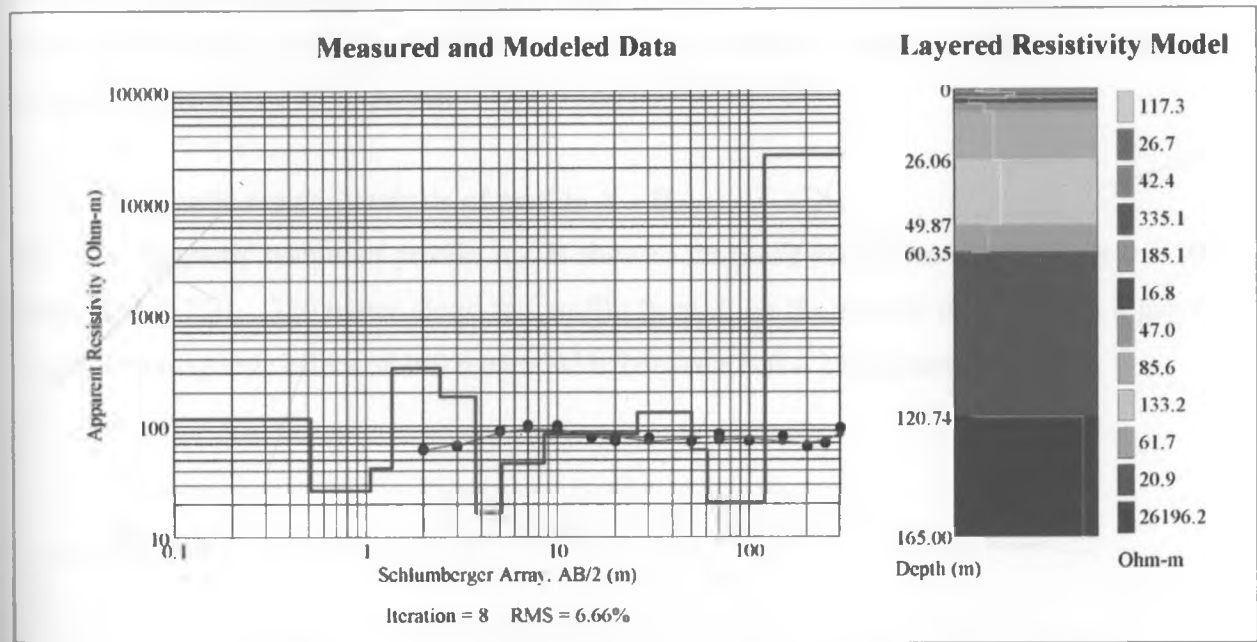

Fig 5.33a: VES model done on the northern part of the study area (after Barongo,2007)

1. **Profile A –B**

   a. **Electrical resistivity tomography results analysis**

Traverse A – B was conducted on the northern part of the project area in the East – West direction. Low resistivity material is noted between 125 meters and 175 meters along the traverse from A at a depth of 57 to 65 meters (fig 5.34). This low resistivity material indicates the existence of buried river channel. This is confirmed from the geological logs of done on the borehole along the profile (fig. 5.32). Low resistivity is also note at a shallow level of

94

about 17 meters indicating shallow structures saturated with water. High resistivity is noted at two locations along the profile. This could indicate boulders of Phonolite that are slowly undergoing weathering. The weathering effect is noted as the resistivity around the boulder decreases circularly from the center of the boulder to the outer zone.
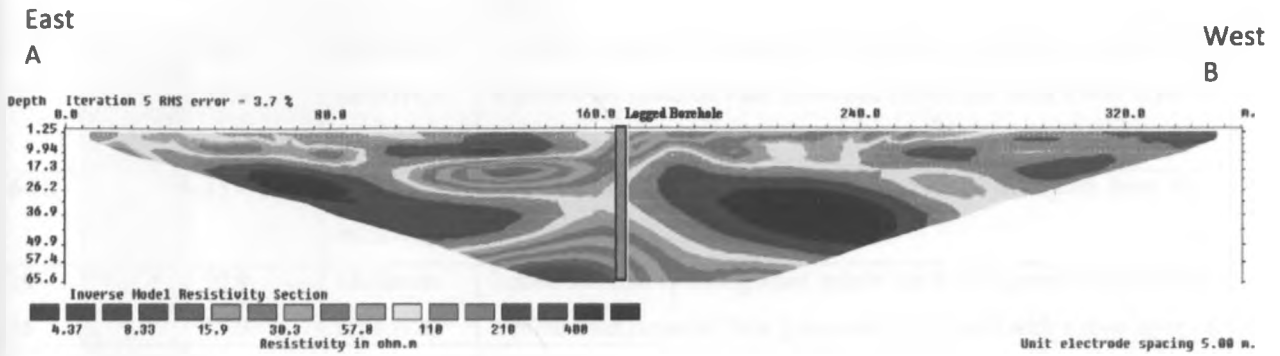

Figure 5.34 Electrical resistivity tomography pseudo – section along traverse A - B shown in map 4.2 (Kabatini well field). The images mark the approximate boundaries of the buried fault/fracture zone occupied by the Ngosur river channel

b. Magnetic results analysis of profile A – B

The total magnetic results of profile A – B showed magnetic anomalies appearing at 0 – 100 meter and at 250 – 350 meter along the profile from A on the eastern part. There's a gap of anomalous magnetic effect of 100 meters wide between 100 – 250 meters (fig 5.35).
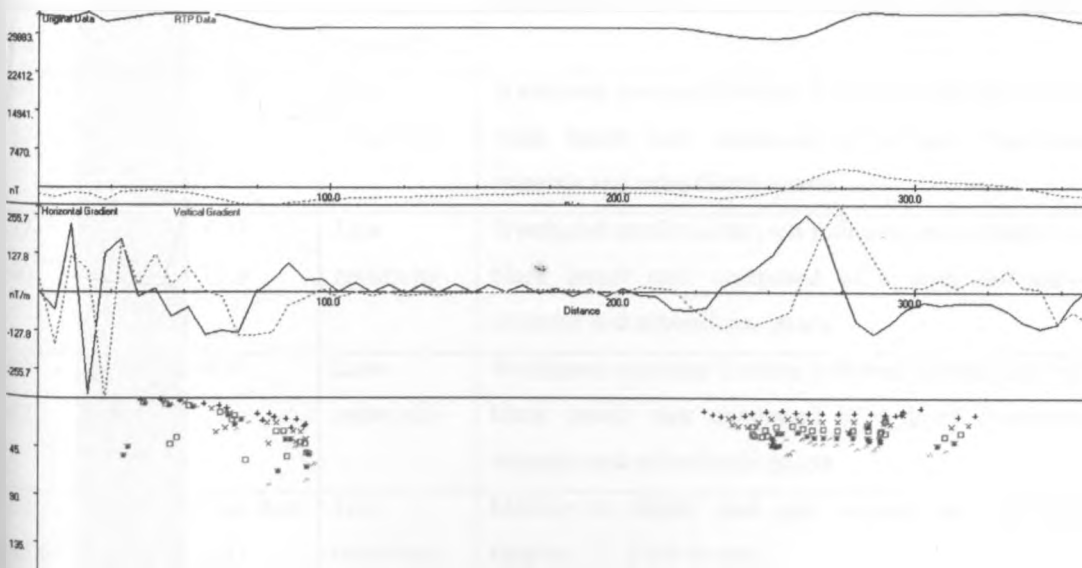

Figure 5.35: The magnetic a normally map showing the width of buried river (100 m) on profile A – B.

Dept h(m)	ERT colour code	ERT resistivity ranges	Relative resistivity	Borehole log (courtesy of Prof. Mathu) of a borehole on profile A – B
0-4		57 - 110	High resistivity	Brownish white loose soils and gravel cemented by clay and ash, Buff white tuff (at the top) and medium to dark grey ash at the bottom
4 -6		30.9 - 57.9	Moderate resistivity	Loose medium brown graded coarse sands and gravel cemented by argillaceous material Pale brownish (buff) tuff with a thin layer of sediments
6-10		15 - 30.9	Moderate resistivity	Pale brownish (buff) tuff with a thin layer of sediments from 10 – 12 m depth
10-16		30.9 - 57.9	Moderate resistivity	Loose medium brown graded coarse sands and gravel cemented by argillaceous material Pale brownish (buff) tuff with a thin layer of sediments
16-20		57	Moderate resistivy	Loose sediments of clay (20%), sand (30%) and gravel (30%) with trachyte and phonolite clasts Medium dark grey tuff and ash with few hard rock fragments and white patches of feldspar and ash
20 - 32		57 - 110	Moderate resistivity	Brownish white loose soils and gravel cemented by clay and ash, Buff white tuff (at the top) and medium to dark grey ash at the bottom
32 - 34		57	Moderate resistivity	Loose sediments of clay (20%), sand (30%) and gravel (30%) with trachyte and phonolite clasts Medium dark grey tuff and ash with few hard rock fragments and white patches of feldspar and ash
34 - 38		30.9 - 57.9	moderate resistivity	Dark yellowish tuff with few medium to dark grey patches
38 - 48		15.9	Moderate resistivity	Dark yellowish tuff with few medium to dark grey patches
50 - 57		15.9	Low resistivity	Weathered erosional horizon followed immediately by dark almost black basalt rock composed of a layer dominated by mafic minerals and subordinate quartz
57-60		4.37 - 15.9	Low resistivity	Weathered erosional horizon followed immediately by dark almost black basalt rock composed of a layer dominated by mafic minerals and subordinate quartz
60 - 62		4.37	Low resistivity	Weathered erosional horizon followed immediately by dark almost black basalt rock composed of a layer dominated by mafic minerals and subordinate quartz
62 - 65.6		Less than 4.37	Low resistivity	Medium to slightly dark grey volcanic ash with lapili fragments (approx. 1 – 2 cm in size)

Fig 5.36: The figure shows the comparison of ERT , VES and borehole log by Prof.Mathu

2. Profile C – D

a. Electrical resistivity tomography results

Traverse C – D indicates the presence of the layers having low resistivity at two levels (fig 5.38). The upper level of low resistivity runs from 70th meter from the C to 205th meter a long the traverse. The lower level of low resistivity is found at 60th meter depth indicating the presence of another channel of the river. High resistivity material that is almost horizontally placed overlies the lower level river channel. The lower level river channel is 70 meters wide along the traverse. It appears at 165th meter to 235th meter. Two regions of very high resistivity are noted on the eastern and western side of the traverse indicating the presence of Phonolite boulders that are undergoing weathering due to the water flowing in the river channel.
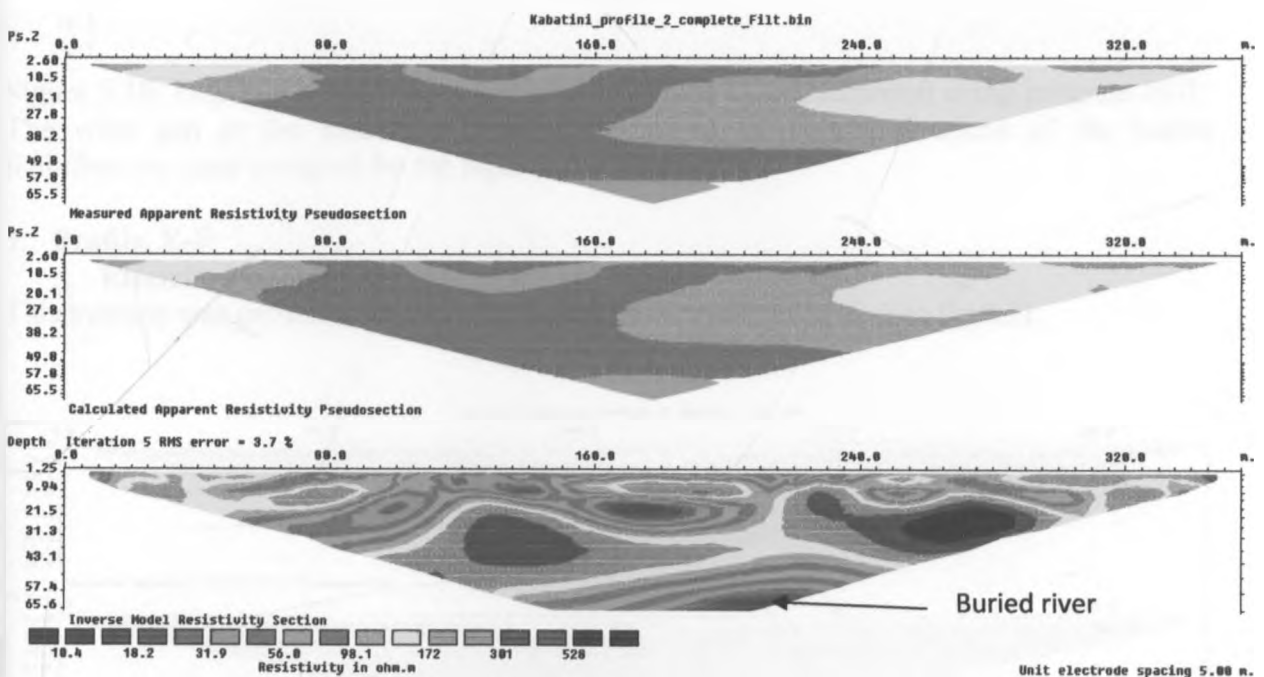

Fig.5.37: Electrical tomography images along profile C- D shown in fig. 4.2 (Kabatini well field). The images mark the approximate boundaries of the buried fault/fracture zone occupied by the Ngosur river channel

b. Total magnetic results

The results indicate the gap of anomalous effect from 125 – 175 meters from position A (western part) towards B (eastern part). Anomalous effect of magnetism is noticed at 100 meter and 200 meter along A –B (fig 5.38).
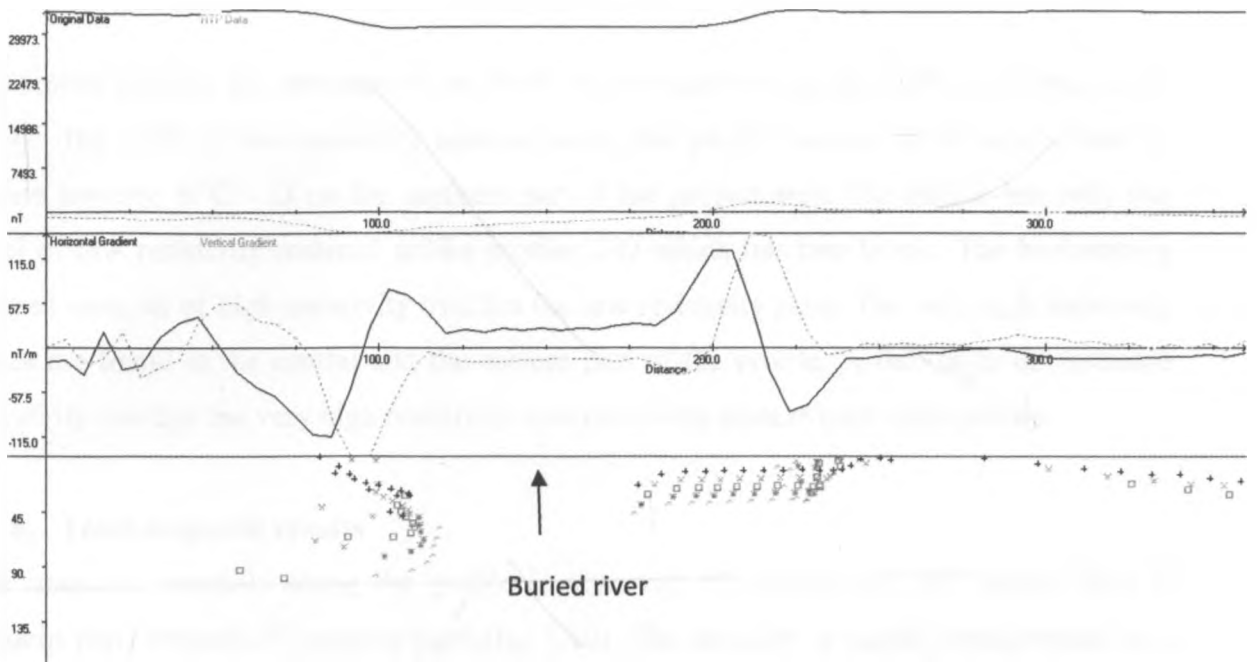
Figure 5.38: Depth-to-magnetic sources along traverse C-D interpreted using program EUL. The wide gap in the middle of the profile marks the east-west extent of the buried fault/fracture zone occupied by the Ngosur river channel.

3. Profile E-F
a. Electrical resistivity tomography results
This traverse was carried out on the southern part of traverse C – D (see fig 4.2).
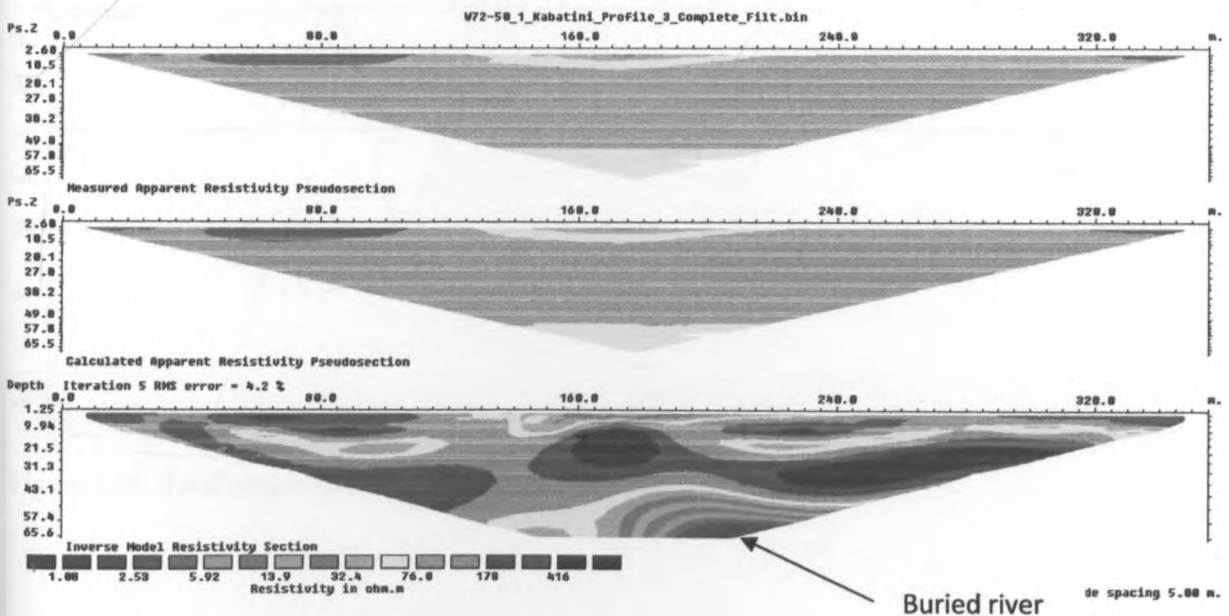

Figure 5.39: Electrical tomography images along traverse E-F shown in fig. 4.2 (Kabatini well field). The images mark the approximate boundaries of the buried fault/fracture zone occupied by the Ngosur river channel

The results indicate the presence of one level of low resistivity at the depth of 60 meters (fig 5.39). The width of low resistivity material along this profile reduces to 40 meters from 70 meters traverse of C – D on the northern part of the project area. The profile has only one level of low resistivity material unlike profile C-D which has two levels. The horizontally layered material of high resistivity overlies the low resistivity zone. The very high resistivity zones are found at the central and the eastern part of the profile. A thin layer of moderate resistivity overlies the very high resistivity material on the eastern part of the profile.

b. Total magnetic results

The magnetic anomaly along the profile is observed 50 meters and 240 meters from E (eastern part) towards F (western part),(fig 5.40). The anomaly is mostly concentrated at a shallow depth with two exceptional places at 90 meter and 140 meters from the eastern part of the profile. Magnetic anomaly is noted to be deeper than other places along the profile.
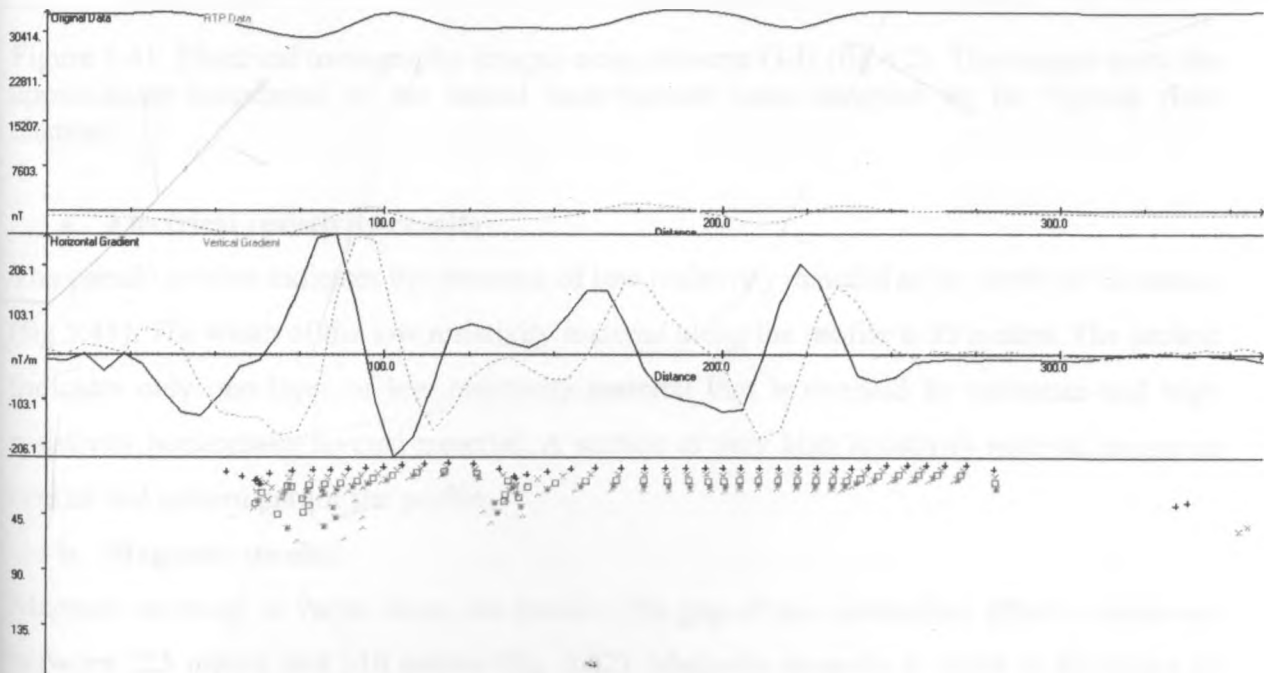

Figure 5.40, Total magnetic a normally along profile E – F

4. Profile G-H

This traverse was carried out on the southern part of traverse E-F in the project area (see fig 4.2).
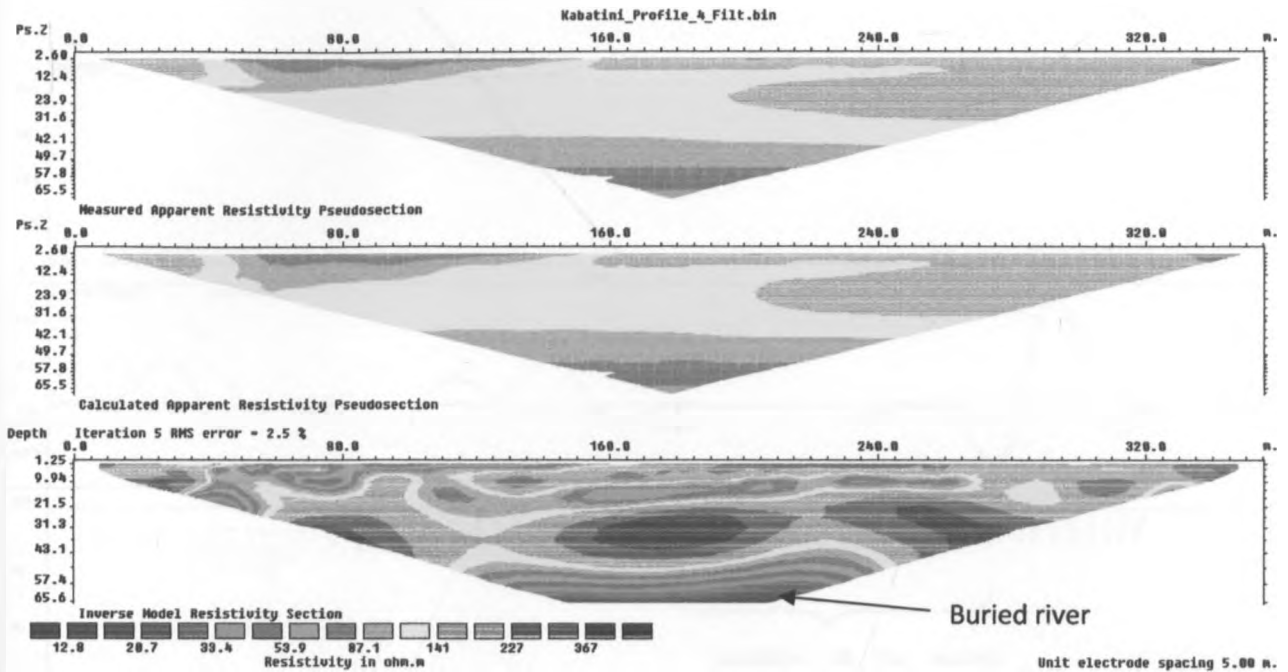

Figure 5.41: Electrical tomography images along traverse G-H (fig 4.2). The images mark the approximate boundaries of the buried fault/fracture zone occupied by the Ngosur river channel

a. Electrical resistivity results

The pseudo section indicates the presence of low resistivity material at the depth of 62 meters (fig 5.41). The width of the low resistivity material along the profile is 95 meters. The section indicates only one layer of low resistivity material that is overlaid by moderate and high resistivity horizontally layered material. A section of very high resistivity material occurs at central and eastern part of the profile.

b. Magnetic results

Magnetic anomaly is varies along the profile. The gap of non anomalous effect is observed between 225 meters and 310 meters (fig. 5.42). Magnetic anomaly is noted at 40 meters to 225 meter from point G on the eastern part of the profile. The anomaly breaks and a gap of anomalous effect that is noted from 225 meters to 310 meters and reappears after 310 meters to the end of the profile.

Location of the buried
river along profile G - H
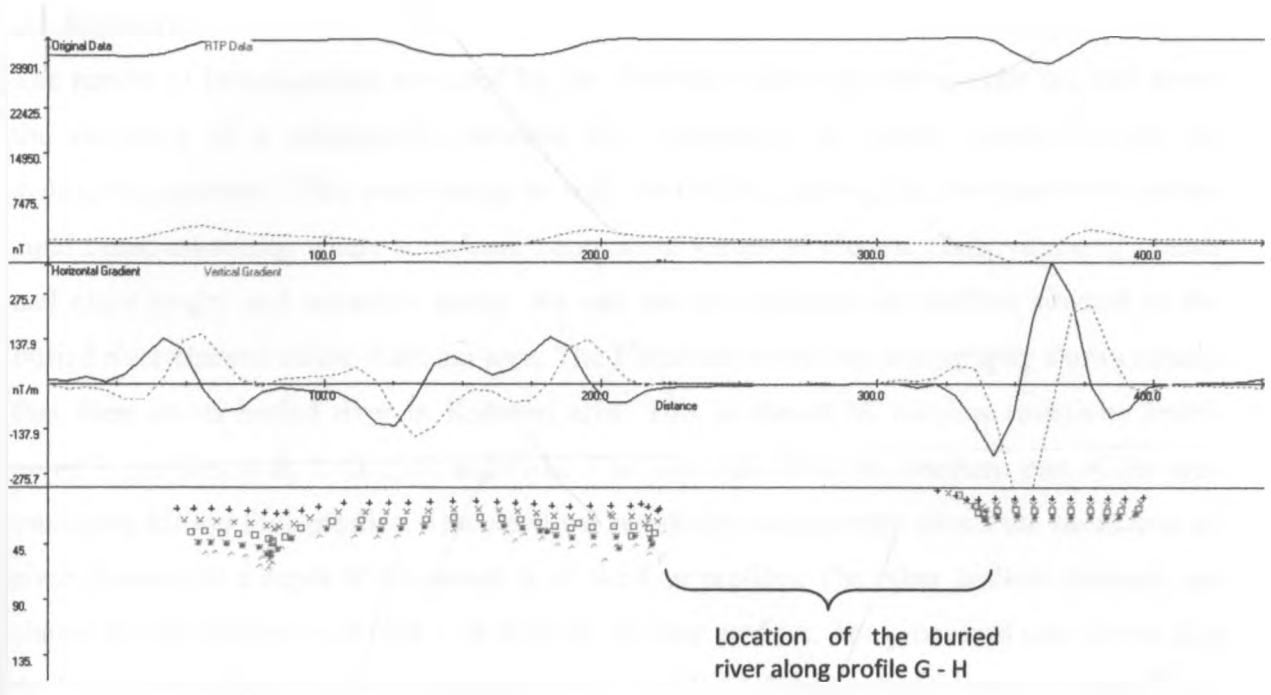
Figure 5.42: Depth-to-magnetic sources along traverse G-H interpreted using program EULER. The wide gap in the middle of the profile marks the east-west extent of the buried fault/fracture zone occupied by the Ngosur river channel.

5.6.4 Total magnetic anomaly distribution in the project area

The magnetic contours of 29000,29500, 30000,30500,31000 , 31500 and 32000 show anomalous regions. The high anomalous regions contours are 32500,33000,and 3350. Contour 31500 occupies awider area on the northern part of the area, narrows down to center and widens again at the southern part of the project area. The low low level contours indicate the location of the buried river (fig 6.3).

CHAPTER SIX

6.0 SUMMARY AND CONCLUSION

6.1 Summary

The results of investigations executed by the electrical resistivity tomography method prove the existence of a relationship between the distribution of electric resistivity and the geological structure. This relationship is well visible in a geological structure with simple conditions, especially where soils have contrasting values of electric resistivity, e. g., sands and clays or dry and saturated sands. We can see this situation on profiles situated in the buried river channel of the Kabatini area. The Electrical resistivity tomography shows clearly that there exists buried river in Kabatini area. This is shown by the low resistivity levels noted in profiles A-B, C-D, E-F, and G-H. The river runs from the northern part of the area traversing all the four profiles. The electrical resistivity tomography shows the existences of river channels at a depth of 60 meters in all the four profiles. The other shallow channels are shown by low resisvitly at 10m – 18 m in all the four profiles. The processed data shows that the buried river flows from the northern part of profile A-B to southern part of profile G –N, (see fig 6.1 and 6.2). The width of the river channel along profiles A – B, C-D, E-F, and G-H is 100m, 80m, 50m and 100m respectively according to the electrical resistivity tomography results
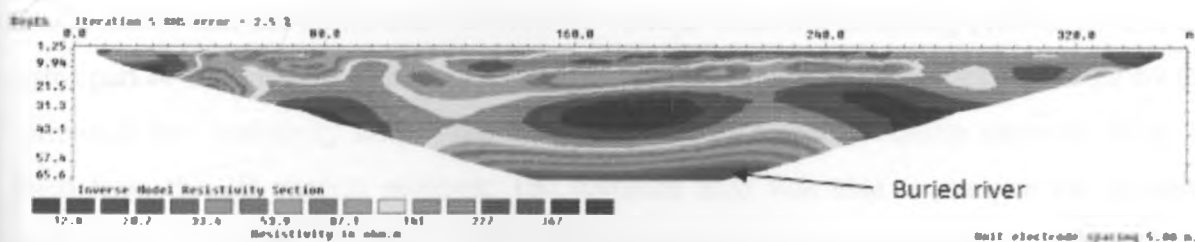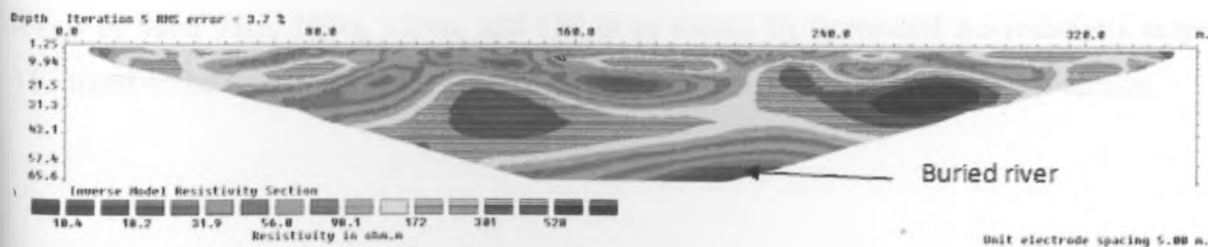

Fig 6.1(a)

Fig 6.1(b) Pseudo-sections showing buried river channel occurring at a depth of 60 m. The width of the river is about 100 m as indicated by fig 6.1a above for profile G - H.
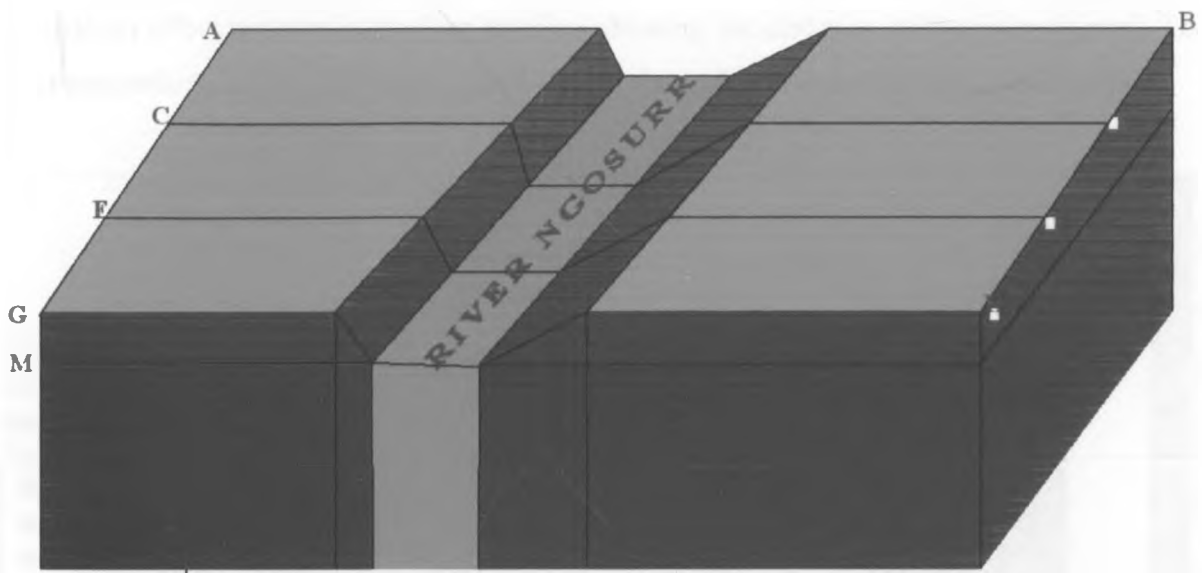
Figure 6.2: River Ngosur shown traversing the four profiles (AB, CD, EF, and GH) at a depth of 60 meters (G – M and H – N) from the surface

The vertical electrical sounding indicates that there is an underground river channel in Kabatini area. The channel is confined by a layer of resistivity values varying between low to high. The river channel flows in the north – south direction and when it reaches kabatini, some of its water disperses into the highly porous material to feed kabatini aquifer. VES results shows that the entire area covered by vertical electrical sounding (150 m by 150 m) forms part of the kabatini aquifer. The aquifer extends outside the study area as noted by the horizontal Iso- resistivity maps. The average depth of Kabatini aquifer exceeds 165m as noted from the 2D vertical sections. The software used was able to analyze the Kabatini aquifer up to the depth of 165 m. While it is noted that some water feeds the aquifer, the rest flows to the south defining a north – south geometrical trend. The trend is noted at depth levels of 50m, 75m, 100m, 125m, and 150 m as shown by horizontal Iso-resistivity maps. The trend of the river is controlled by the fault line running in the north – south direction.

The location of these channels is also recorded by the total magnetic effect survey. The anomalous effect appears in the four profiles, showing the direction of the river channel. The total magnetic map (fig.6.3) shows that the river channel is oriented in the N – S direction.
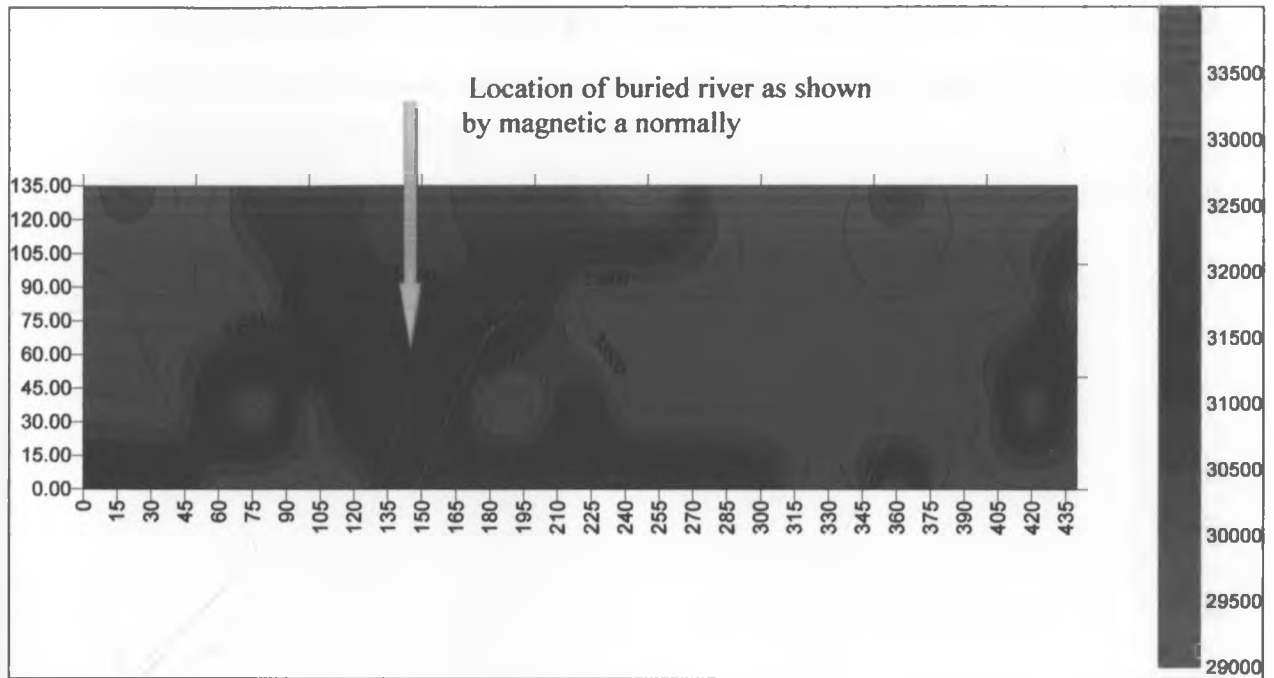

Fig 6.3: The map shows the distribution of the total magnetic anomaly in Kabatini well field. Note the low total magnetic a normally in middle showing the position of the buried river.

6.2 Concluding remarks

The research did not only pave way for a clear picture of the hydrogeological knowledge of Kabatini in other to create awareness on the productive and prolific aquifer for sustainable groundwater supply but act as guides to both the government and individuals especially those involved in groundwater development on the areas and depths boreholes could be sited and drilled for sustainable water supply. It has been ascertained that Kabatini area has got a river channel that is oriented N- S geometrically as seen in figures 5.26, 5.27, 5.28, 5.29, and 5.30. It is also noted that the underground river channel traversing Kabatini area, feeds the kabatini aquifer as indicated by vertical electrical sounding and electrical resistivity tomography. The depth of the river channel and the thickness of the Kabatini aquifer exceed 165m. The bottom layers of stations {(1W, 0), (0, 0), (1E, 0), (2E, 0)}, {(1W, 1S), (1E, 1S), (2E, 1S)}, {(1W, 2S), (1E, 2S), (2E, 2S)},{(1W, 3S), (0,3S), (1E, 3S), (2E, 3S)}, on fig 4.2a have very low resistivity values indicating that the depth of the aquifer extends beyond these layers (165m). It is also noted

that the river channel occurs on the eastern part of the study area as proved by all the methods used in this research.

6.3 Recommendation

The following are the recommendations made from this study;

I.   Drilling of the boreholes in Kabatini area should be deeper than 60 m from the surface since the channels that contain water occur at this depth and extends beyond the depth of 165m for the better yield.

II.   Future research work should be carried out using Vertical electrical sounding and other geophysical methods that could cover deeper and a more wide area.

References

Abd El-Rahman, A. and Khaled, M.A., 2005: Geophysical Exploration for Groundwater Possibilities in Wadi El-Rahba, Eastern Desert, Egypt, *Geophysical Society Journal,* 3(1), pp 99-108.

Al-Abaseiry, A., Abdel Rahman and Ezz El-Deen, M.M., 2005: Geophysical Exploration for Groundwater Potientialities in Wadi El-Rahba, Eastern Desert, Egypt, *Geophysical SocietyJournal*, 3(1), pp 119-1128.

Alotaibi, A.M. and AlAmri, A.M., 2007: Ground Water Potentialities of Wadi Malakan-Southern Makkah AlMokadash City, Saudi Arabia, *Geophysical Society Journal*, 5(1), pp 101-116.

Baker, B.H., Mohr,P.A and Williams, L.A.J., 1972: Geology of the Eastern Rift system of Africa, Geological society of America, Special paper No. 136

Barongo J., 2007: Mawari Project (unpublished report), University of Nairobi.

Barritt, S., 1993: The African Magnetic Mapping Project. ITC Journal, 2, pp 122–131.

Becht, R., Fred Mwango, Fred A. Muno., 2005. Groundwater links within Rift Valley Lakes. 11th World Lakes Conference, Nairobi.

Bernard, J. and Valla, P. (1991) Groundwater exploration in fissured media with electric and VLF methods, *Geoexploration, No. 27*,pp 81-91.

Bonini, W. and Hickok, E., 1969: Seismic refraction method in ground-water exploration. Am. Inst. Min., Metallurg., Petr. Eng. Trans., Vol. 211, pp 485–488.

Carmichael, R. and Henry, G. J., 1977: Gravity exploration for groundwater and bedrock topography in glaciated areas. Geophysics, Vol. 42, pp 850–859

Choudhury, K., D.K. Saha and P. Chakraborty, 2001: Geophysical study for saline water intrusion in a coastal alluvial terrain, *J. Appl. Geophys.*, Vol.46, pp 189-200.

Clarke, M., Woodhall, D., Allen, D., and Darling, G., 1990: Geological, volcanological and hydrological controls of the occurrence of geothermal activity in the area surrounding Lake Naivasha. Technical report: Government of Kenya, Ministry of Energy/British Geological Survey.

Daniels F. and Alberty R.A., 1966: Physical Chemistry. John Wiley and Sons, Inc. deGroot-Hedlin, C. and Constable, S., 1990: Occam's inversion to generate smooth, two dimensional models form magnetotelluric data. Geophysics, No.55, pp 1613-1624

de Groot – Hedlin C. and Constable S.C. 1990. Occam's inversion to generate smooth, two dimensional model from magnetotelluric data. Geophysics 58, pp 1603 – 1628.

Dey, A. and Morrison, H. 1979: Resistivity modeling for arbitrary shaped two dimensional structures. Geophys. Prospect., 27:106–136.

Dey A. and Morrison H.F. 1979a: Resistivity modeling for arbitrary shaped two-dimensional structures. Geophysical Prospecting 27, 1020-1036.

Dey A. and Morrison H.F., 1979b. Resistivity modeling for arbitrarily shaped three dimensional shaped structures. Geophysics 44, 753-780.

Dey, A., and Morrison, H. F, 1979, Resistivity modeling for arbitrarily shaped three-dimensional structures: Geophysics, 44, 753-780.

Electrical imaging surveys for environmental and engineering studies; a practical guide to 2d and 3d surveys. www.geoelectrical.com. Visited on 17/2/2010

Elkheder, H.I., Shereef, M.R., El Galladi, A.A. and Pederson, L.B. 2004 Geoelectric Study on Quaternary Groundwater Aquifers in Northwest Sainai, Egypt, *Geophysical Society Journal*, 2 (1): pp. 69-74.

EL-Waheidi, M.M., F. Merlanti and M. Pavan, 1992: Geoelectrical resistivity survey of the central part ofAzraq Basin (Jordan) for identifying saltwater/freshwater interface, *J. Appl. Geophys.*, 29, 125-133.

Fitterman, D. and Stewart, M. 1986: Transient electromagnetic sounding for groundwater. Geophysics, 51(4):995–1005.

Frohlich, R.K. and W.E. Kelly., 1987: Estimates of specific yield with the geoelectric resistivity method in glacial aquifers, *J. Hydrol.*, 97, pp. 33-44.

Frohlich, R.K. and D. Urish 2002: The use of geoelectrics and test wells for the assessment of groundwater quality of a coastal industrial site, *J. Appl. Geophys.*, 50, pp. 261-278. Geological survey of Iran.

Griffiths, D. and Baker, R., 1993: Two-dimensional resistivity imaging and modelling in areas of complex geology. Journal of Applied Geophysics, 29, pp. 211–226.

Griffiths, D. and Turnbull, J.,1985: A multi-electrode array for resistivity surveying. First Break, 3(7), pp. 16–20.

Haggard, L, *Proton\ Precession Ferrous Metal Detector*, Practical Electronics, pp. 782-793, October, 1970

Hosny, M.M., EZZ El-Deen, Abdallah, A.A., Abdel Rahman and Barseim, M.S.M.,2005

Geoelectrical Study on the Groundwater Occurrence in the Area Southwest of Sidi Barrani, Northwestern Coast, Egypt, *Geophysical Society Journal,* 3(1), pp 109-118.

Ghosh, D.P., 1971: Inverse filter coefficient for the computation of apparent resistivity standard curves for a horizontal stratified earth , Geophysical prospecting 19, pp. 769 – 775.

Ibrahim, E.H., Shereef, M.R., El Galladi, A.A. and Pederson, L.B.,2004: Geoelectric Study on Quaternary Groundwater Aquifers in Northwest Sainai, Egypt, *Geophysical Society Journal,* 2(1), pp. 69-74.

Jackson, P.N., S.D. Taylor and P.N. Stanford 1978: Resistivity- porosity-particle shape relationships for marine sands, *Geophysics,* 43, pp.1250-1268.

Kaya, G.K. 2001: Investigation of groundwater contamination using electric and electromagnetic methods at an open waste-disposal site: a case study from Isparta, Turkey, *Environ. Geol.,* 40, pp.725-731

Keller G.V. and Frischknecht F.C.,1966: Electrical methods in geophysical prospecting. Pergamon Press Inc., Oxford.

Kelly, E.W. 1976: Geoelectric sounding for delineating ground water contamination, *Ground Water,* 14, pp.6-11.

Kessels, W., I. Flentge and H. Kolditz 1985: DC geoelectric sounding to determine water content in the salt mine (FRG), *Geophys. Prospect.,* 33, pp.456-446.

Koefoed O.,1979. Geosounding Principles 1 : Resistivity sounding measurements. Elsevier Science Publishing Company, Amsterdam.

Kossinski, W.K. and W.E. Kelly 1981: Geoelectricsounding for predicting Aquifer Properties, *Ground Water,* pp. 163-171.

Kuria Z.N,1999.Hydrogeology of lake Nakuru drainage basin using GIS data and electrical resistivity, MSc. Thesis, University of Nairobi.

LaBrecque, D.J., Miletto, M., Daily, W., Ramirez, A. and Owen, E., 1996. The effects of noise on Occam's inversion of resistivity tomography data. Geophysics, 61, pp. 538-548.

LaBrecque, D., Morelli, G., Daily, W., Ramirez, A., and Lundegard, P., 1999, Occam's inversion of 3Delectrical resistivity tomography, in Oristaglio M., and B. Spies, Eds., Three Dimensional Electromagnetics,: Soc. Expl.Geophys.

Loke, M. and Barker, R. 1996. Rapid least-squares inversion of apparent resistivity pseudosections by a quasi-newton method. Geophysical Prospecting, 44, pp. 131–152.

Loke, M.H., Dahlin, T., 1997. A combined Gauss –Newton and quasi-Newton inversion method for the interpretation of apparent resistivity pseudosections. Procs. 3rd Meeting of the European Association for Environmental and Engineering Geophysics, 8–
11 Sept. 1997, Aarhus, Denmark, pp. 139– 142.

Loke, M.H., 2000. Topographic modelling in resistivity imaging inversion. 62nd EAGE Conference & Technical Exhibition Extended Abstracts, D-2.

Mathu 2006, Mawari project (unpublished report), University of Nairobi

Matias, M.J.S. 2002: Squary array anisotropy measurements and resistivity sounding interpretation, *J. Appl. Geophys.*, pp 49. 185-194.

McCall, C.J.H., 1967, Geology of the Nakuru – Thomson's falls – lake Hannington area, Report No. 78 . Kenya Geol. Surv., Nairobi, Kenya.

Michel, R., Jean-Claude, P., Diouf, S., Beauvais, A., Dione, F.,and Dione, F. 1999: Electrical imaging of lateritic weathering mantles over granitic and metamorphic basement of eastern Senegal, West uppercaseAfrica. Journal of Applied Geophysics, 41, pp. 335–344.

Mousa, D.A. 2003: The role of 1-D sounding and 2-D resistivity inversions in delineating the near-surface lithologic variations in Tushka area, south of Egypt, *Geophysical Society Journal*, 1, pp. 57-64.
Nabidi, I. K.2002: Development of 3-D conceptual hydrogeological model for Lake Naivasha area. Msc. Thesis, WREM. Enschede, ITC.

Nigm, A.A., Elterb, R. A., Nasr, F.E. and Thobaity, H.M. 2008 Contribution of Ground Magnetic and Resistivity Methods in Groundwater Assessment in Wadi Bany Omair. Holy Makkah Area, Saudi Arabia, Egyptian, *Geophysical Society Journal*, 6(1): 67-79.

Nowroozi, A., Horrocks, B. and Henderson, P., 1999: Saltwater intrusion into the freshwater aquifer in the eastern shore of Virginia: a reconnaissance electrical resistivity survey, *J. Applied Geophysics*, 42, pp. 1-22.

Olivar, A., de Lime, L. and Sharma, M.M., 1990: A grain conductivity approach to shaly sandstones. Geophysics, 55, pp. 1347-1356.

Onyere,S.M.,1997, Structural analysis of the drainage basin of Kenyan Rift Valley lakes within the Aberdare detachment using satellite data, GIS and field observation, PhD Thesis, Department of Geology , University of Nairobi.

Parasnis, D. 1997 *Principle of Applied Geophysics*, London: Chapman & Hall., 275 p.

Pastor, M. S. 2001. Geophysical study of the groundwater system south of lake Naivasha, Kenya, International Institute for Aerospace Survey and Earth Sciences, The Netherlands.
Res2DINV Manual, 2003. Geotomo Sofware, 5 CangkatMiden Loroung 6, Miden Heights, 11700 Gelugor, Penang,Malaysia (www.geoeletrical.com)

Serson, P.H., *A Simple Proton Precession Magnetometer*, Dominion Observatory, Ottawa, Canada, 1962
Smith, M. and Mosley, P. 1993, Crustal heterogeneity and basement influence on the development of the Kenya Rift, East Africa, Tectonics, Vol.12, No.2,pp. 592-606.

Sporry, R. 2001. Lecture material on Resistivity. Earth System Analysis
Department, ITC.

Stefanesco, S., C. Schlumberger, and M. Schlumberger. The distribution of electrical potential about a point electrode in an earth of horizontal, homogeneous, and isotropic beds. *J. Phys. Radium* 1, pp.130–141, 1930.
Taylor, K., Widmer, M., and Chesley, M. 1992. Use of transient electromagnetics to define local hydrogeology in an arid alluvial environment. Geophysics, 57(2), pp. 343–352.
Troisi, S., C. Fallicos, S. Straface and E. Migliari 2000: Application of kriging with external drift to estimate hydraulic conductivity from electrical resistively data in unconsolidated deposits near Montato Uffugo, Italy, *Hydrogeol. J.*, 8, pp. 356-367.

Van Overmeeren, R., 1989: Aquifer boundaries explored by geoelectrical measurements in thecoastal plain of Yemen, *A Case of Equivalence. Geophysics*, 54, pp. 38-48.

Vouillamoz, J.M., M. Descloitres, J. Bernard, P. Fourcassier and L. Romagny, 2002: Application of integrated magnetic resonance sounding and resistivity methods for borehole implementation. A case study in Cambodia, *J. Appl. Geophysics*, 50, pp. 67-81.

Waters, G.S. and Phillips, G., *A New Method of Measuring the Earth's Magnetic* Field, Geophys. Prospecting 1-9, 1956 Serson, P.H., U.S. Patent No. 3,070,745, 1962

Whitely R.,1973: "Electrode arrays in Resistivity and induced polarization prospecting a review" Bulleting of the Australian Society of Exploration Geophysics, pp. 1- 29.

Yadav, G.S. and H. Abolfazli ,1998: Geoelectric soundings and their relationship to hydraulic parameters in semiarid regions of Jalore, Northwestern India, *J. Appl. Geophys.*, 39, pp. 35-51.

Yechieli, Y., 2000: Fresh-saline ground water interface in the Western Dead Sea area, *Ground Water*, 38, pp. 615-623.

Young, M.E., R.G.M. De Bruijn and A. Salim al-Ismaily, 1998: Report: exploration of an alluvial aquifer in Oman by time-domain electromagnetic sounding, *Hydrogeol. J.*, 6, pp. 383-393.

Youssef, A.M.A., Abdellatief, T.A., El Mousa, S.E.D. and Tamamy, M.M.A., 2004 Geoelectrical Survey to Delineate the Extension of the Water Bearing Formations in Wadi Gharandal, Southwest Sainai, Egypt, *Geophysical Society Journal*, 2(1), pp.75-84.

Zohdy, A., Eaton, G., and Mabey, D.,1974, Application of surface geophysics to groundwater investigations,Techniques of Water-Resources Investigation of the United States Geological Survey, Book 2, D1.

Zohdy A. A. R., 1989. A new method for the automatic interpretation of Schlumberger and Wenner sounding curves; Geophysics, Vol. 54, No.2, pp245-253
Zohdy, A.A.R. 1969: Application of deep electrical soundings for groundwater exploration in Hawaii, *Geophysics*, pp.584-600.

Young, M.E., R.G.M. De Bruijin and A. Salim al-Ismaily, 1998: Report: exploration of an alluvial aquifer in Oman by time-domain electromagnetic sounding, *Hydrogeol. J.*, 6, pp. 383-393.

Youssef, A.M.A., Abdellatief, T.A., El Mousa, S.E.D. and Tamamy, M.M.A., 2004 Geoelectrical Survey to Delineate the Extension of the Water Bearing Formations in Wadi Gharandal, Southwest Sainai, Egypt, *Geophysical Society Journal*, 2(1), pp.75-84.

Zohdy, A., Eaton, G., and Mabey, D.,1974, Application of surface geophysics to groundwater investigations,Techniques of Water-Resources Investigation of the United States Geological Survey, Book 2, D1.

Zohdy A. A. R., 1989. A new method for the automatic interpretation of Schlumberger and Wenner sounding curves; Geophysics, Vol. 54, No.2, pp245-253
Zohdy, A.A.R. 1969: Application of deep electrical soundings for groundwater exploration in Hawaii, *Geophysics*, pp.584-600.